



# tecnología

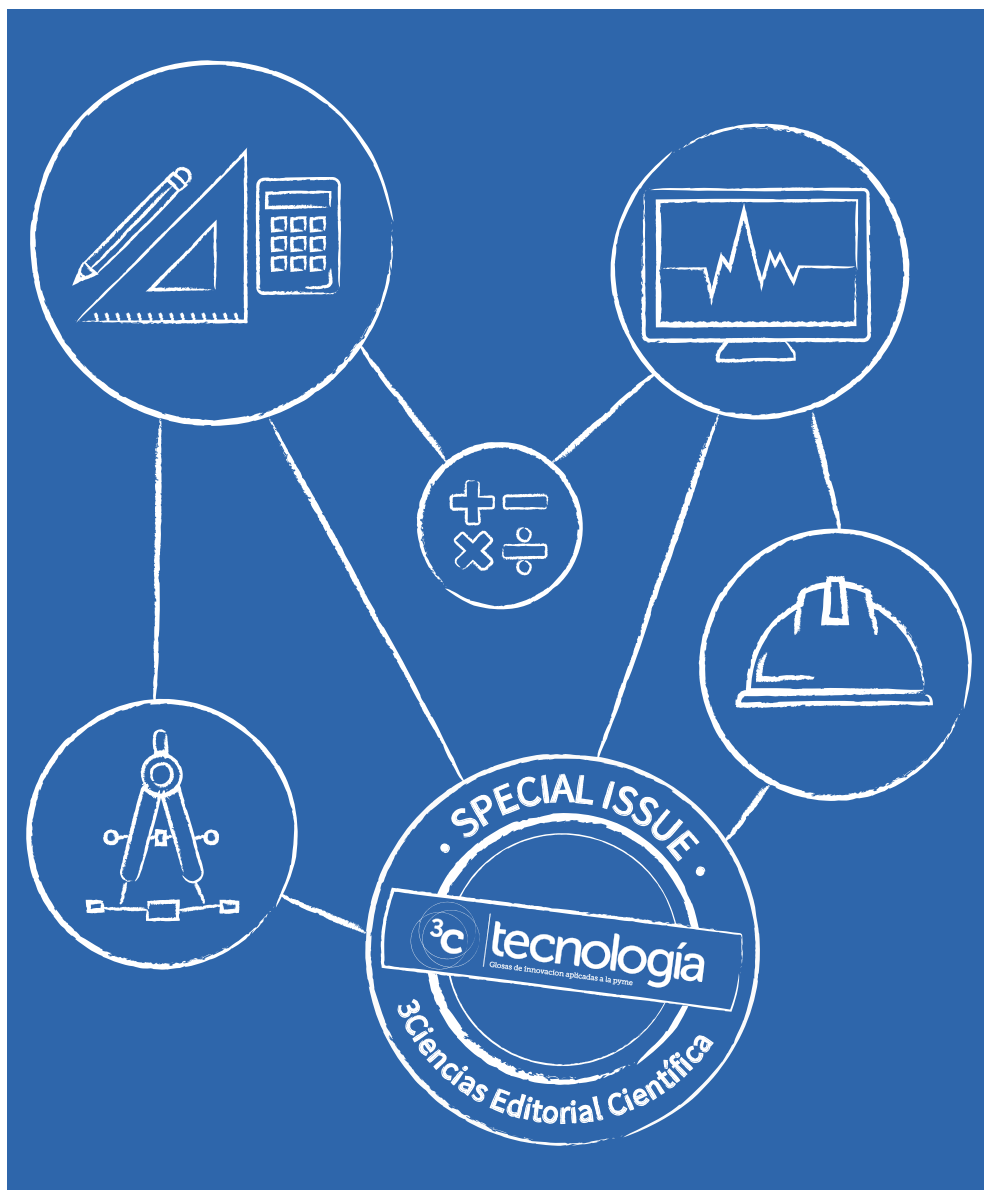
Glosas de innovación aplicadas a la pyme

Edición Especial  
Noviembre\_2020

Special Issue  
November 2020

ISSN: 2254 – 4143

## 6<sup>TH</sup> INTERNATIONAL CONFERENCE ON GREEN COMPUTING AND ENGINEERING TECHNOLOGIES



### **3C Tecnología. Glosas de innovación aplicadas a la pyme.**

Edición Especial. Noviembre 2020. *Special Issue. November 2020.*

Tirada nacional e internacional. *National and internacional circulation.*

Artículos revisados por el método de evaluación de pares de doble ciego.

*Articles reviewed by the double blind peer evaluation method.*

### **Special Issue on 6<sup>th</sup> International Conference on Green Computing and Engineering Technologies, 16-18 September 2020**

**Herzen State Pedagogical University of Russia, St Petersburg, Russia.**

#### **Guest Editors**

Prof. Geetam S. Tomar (Birla Institute of Applied Sciences, Bhimtal, India).

E-mail: [gstomar@ieec.org](mailto:gstomar@ieec.org) ORCID: <https://orcid.org/0000-0002-0246-1527>

Dr. Bishwajeet Pandey (Birla Institute of Applied Sciences, Bhimtal, India).

E-mail: [gyancity@gyancity.com](mailto:gyancity@gyancity.com) ORCID: <https://orcid.org/0000-0001-5593-8985>

Dr. Robin Singh (Birla Institute of Applied Sciences, Bhimtal, India).

E-mail: [robin@ieec.org](mailto:robin@ieec.org) ORCID: <https://orcid.org/0000-0002-6314-4736>

Prof Doris Esenarro Vargas (Federico Villarreal National University, Lima, Peru).

E-mail: [desenarro@unfv.edu.pe](mailto:desenarro@unfv.edu.pe) ORCID: <https://orcid.org/0000-0002-7186-9614>

ISSN: 2254 – 4143

Nº de Depósito Legal: A 268 – 2012

DOI: <https://doi.org/10.17993/3ctecno.2020.specialissue6>

Edita:

Área de Innovación y Desarrollo, S.L.

C/Alzamora 17, Alcoy, Alicante (España)

Tel: 965030572

[info@3ciencias.com](mailto:info@3ciencias.com) \_ [www.3ciencias.com](http://www.3ciencias.com)



Todos los derechos reservados. Se autoriza la reproducción total o parcial de los artículos citando la fuente y el autor. *This publication may be reproduced by mentioning the source and the authors.*

Copyright © Área de Innovación y Desarrollo, S.L.



## CONSEJO EDITORIAL EDITORIAL BOARD

---

Director	Víctor Gisbert Soler
Editores adjuntos	María J. Vilaplana Aparicio Maria Vela Garcia
Editores asociados	David Juárez Varón F. Javier Cárcel Carrasco

## CONSEJO DE REDACCIÓN DRAFTING BOARD

---

- Dr. David Juárez Varón. *Universidad Politécnica de Valencia (España)*  
Dr. Martín León Santiesteban. *Universidad Autónoma de Occidente (México)*  
Dr. F. Javier Cárcel Carrasco. *Universidad Politécnica de Valencia (España)*  
Dr. Alberto Rodríguez Rodríguez. *Universidad Estatal del Sur de Manabí (Ecuador)*

## CONSEJO ASESOR ADVISORY BOARD

---

- Dra. Ana Isabel Pérez Molina. *Universidad Politécnica de Valencia (España)*  
Dr. Julio C. Pino Tarragó. *Universidad Estatal del Sur de Manabí (Ecuador)*  
Dr. Jorge Francisco Bernal Peralta. *Universidad de Tarapacá (Chile)*  
Dr. Roberth O. Zambrano Santos. *Instituto Tecnológico Superior de Portoviejo (Ecuador)*  
Dr. Sebastián Sánchez Castillo. *Universidad de Valencia (España)*  
Dra. Sonia P. Ubillús Saltos. *Instituto Tecnológico Superior de Portoviejo (Ecuador)*  
Dr. Jorge Alejandro Silva Rodríguez de San Miguel. *Instituto Politécnico Nacional (México)*



## CONSEJO EDITORIAL EDITORIAL BOARD

---

Área textil	Dr. Josep Valldeperas Morell <i>Universitat Politècnica de Catalunya (España)</i>
Área financiera	Dr. Juan Ángel Lafuente Luengo <i>Universidad Jaime I (España)</i>
Organización de empresas y RRHH	Dr. Francisco Llopis Vañó <i>Universidad de Alicante (España)</i>
Estadística; Investigación operativa	Dra. Elena Pérez Bernabeu <i>Universidad Politécnica de Valencia (España)</i>
Economía y empresariales	Dr. José Joaquín García Gómez <i>Universidad de Almería (España)</i>
Sociología y Ciencias Políticas	Dr. Rodrigo Martínez Béjar <i>Universidad de Murcia (España)</i>
Derecho	Dra. María del Carmen Pastor Sempere <i>Universidad de Alicante (España)</i>
Ingeniería y Tecnología	Dr. David Juárez Varón <i>Universidad Politécnica de Valencia (España)</i>
Tecnologías de la Información y la Comunicación	Dr. Manuel Llorca Alcón <i>Universidad Politécnica de Valencia (España)</i>
Ciencias de la salud	Dra. Mar Arlandis Domingo <i>Hospital San Juan de Alicante (España)</i>

# POLÍTICA EDITORIAL

## OBJETIVO EDITORIAL

---

La Editorial científica 3Ciencias pretende transmitir a la sociedad ideas y proyectos innovadores, plasmados, o bien en artículos originales sometidos a revisión por expertos, o bien en los libros publicados con la más alta calidad científica y técnica.

## COBERTURA TEMÁTICA

---

3C Tecnología es una revista de carácter científico-social en la que se difunden trabajos originales que abarcan la Arquitectura y los diferentes campos de la Ingeniería, como puede ser Ingeniería Mecánica, Industrial, Informática, Eléctrica, Agronómica, Naval, Física, Química, Civil, Electrónica, Forestal, Aeronáutica y de las Telecomunicaciones.

## NUESTRO PÚBLICO

---

- Personal investigador.
- Doctorandos.
- Profesores de universidad.
- Oficinas de transferencia de resultados de investigación (OTRI).
- Empresas que desarrollan labor investigadora y quieran publicar alguno de sus estudios.

# AIMS AND SCOPE

## PUBLISHING GOAL

---

3C Ciencias wants to transmit to society innovative projects and ideas. This goal is reached through the publication of original articles which are subjected to peer review or through the publication of scientific books.

## THEMATIC COVERAGE

---

3C Tecnología is a scientific-social journal in which original works that cover Architecture and the different fields of Engineering are disseminated, such as Mechanical, Industrial, Computer, Electrical, Agronomic, Naval, Physics, Chemistry, Civil, Electronics, Forestry, Aeronautics and Telecommunications.

## OUR TARGET

---

- Research staff.
- PhD students.
- Professors.
- Research Results Transfer Office.
- Companies that develop research and want to publish some of their works.

# NORMAS DE PUBLICACIÓN

3C Tecnología es una revista arbitrada que utiliza el sistema de revisión por pares de doble ciego (*double-blind peer review*), donde expertos externos en la materia sobre la que trata un trabajo lo evalúan, siempre manteniendo el anonimato, tanto de los autores como de los revisores. La revista sigue las normas de publicación de la APA (American Psychological Association) para su indización en las principales bases de datos internacionales.

Cada número de la revista se edita en versión electrónica (e-ISSN: 2254 – 4143), identificándose cada trabajo con su respectivo código DOI (Digital Object Identifier System).

## PRESENTACIÓN TRABAJOS

---

Los artículos se presentarán en tipo de letra Baskerville, cuerpo 11, justificados y sin tabuladores. Han de tener formato Word. La extensión será de no más de 6.000 palabras de texto, incluidas referencias.

Los trabajos deben ser enviados exclusivamente por plataforma de gestión de manuscritos OJS:

<https://ojs.3ciencias.com/>

Toda la información, así como las plantillas a las que deben ceñirse los trabajos se encuentran en:

<https://www.3ciencias.com/revista/informacion-para-autores/>

<https://www.3ciencias.com/normas-de-publicacion/plantillas/>

# SUBMISSION GUIDELINES

3C Tecnología is an arbitrated journal that uses the double-blind peer review system, where external experts in the field on which a paper deals evaluate it, always maintaining the anonymity of both the authors and of the reviewers. The journal follows the standards of publication of the APA (American Psychological Association) for indexing in the main international databases.

Each issue of the journal is published in electronic version (e-ISSN: 2254 – 4143), each work being identified with its respective DOI (Digital Object Identifier System) code.

## PRESENTATION WORK

---

The papers will be presented in Baskerville typeface, body 11, justified and without tabs. They must have Word format. The extension will be no more than 6.000 words of text, including references. Papers must be submitted exclusively by OJS manuscript management platform:

<https://ojs.3ciencias.com/>

All the information, as well as the templates to which the works must adhere, can be found at:

<https://www.3ciencias.com/en/journals/infromation-for-authors/>

<https://www.3ciencias.com/en/regulations/templates/>

## ESTRUCTURA

---

Los trabajos originales tenderán a respetar la siguiente estructura: introducción, métodos, resultados, discusión/conclusiones, notas, agradecimientos y referencias bibliográficas.

Es obligatoria la inclusión de referencias, mientras que notas y agradecimientos son opcionales. Se valorará la correcta citación conforme a la 7.ª edición de las normas APA.

## RESPONSABILIDADES ÉTICAS

---

No se acepta material previamente publicado (deben ser trabajos inéditos). En la lista de autores firmantes deben figurar única y exclusivamente aquellas personas que hayan contribuido intelectualmente (autoría), con un máximo de 4 autores por trabajo. No se aceptan artículos que no cumplan estrictamente las normas.

## INFORMACIÓN ESTADÍSTICA SOBRE TASAS DE ACEPTACIÓN E INTERNACIONALIZACIÓN

---

- Número de trabajos aceptados publicados: 11.
- Nivel de aceptación de manuscritos en este número: 68,75%.
- Nivel de rechazo de manuscritos: 31,25%.
- Internacionalización de autores: 6 países (Rusia, Perú, Ecuador, Arabia Saudita, Alemania y Pakistán).

Normas de publicación:

<https://www.3ciencias.com/normas-de-publicacion/instrucciones/>

## STRUCTURE

---

The original works will tend to respect the following structure: introduction, methods, results, discussion/conclusions, notes, acknowledgments and bibliographical references. The inclusion of references is mandatory, while notes and acknowledgments are optional. The correct citation will be assessed according to the 7th edition of the APA standards.

## ETHICAL RESPONSIBILITIES

---

Previously published material is not accepted (they must be unpublished works). The list of signatory authors should include only and exclusively those who have contributed intellectually (authorship), with a maximum of 4 authors per work. Articles that do not strictly comply with the standards are not accepted.

## STATISTICAL INFORMATION ON ACCEPTANCE AND INTERNATIONALIZATION FEES

---

- Number of accepted papers published: 11.
- Level of acceptance of manuscripts in this number: 68,75%.
- Level of rejection of manuscripts: 31,25%.
- Internationalization of authors: 6 countries (Russia, Peru, Ecuador, Saudi Arabia, Germany and Pakistan).

Guidelines for authors:

<https://www.3ciencias.com/en/regulations/instructions/>

## INDEXACIONES INDEXATIONS

---





## INDEXACIONES INDEXATIONS

---



# /SUMARIO/ /SUMMARY/

Prologue	
Geetam S. Tomar, Bishwajeet Pandey, Robin Singh y Doris Esenarro Vargas	17
Superimposed anatomical structures in augmented reality	
Vladimir Ivanov , Nikolay Kalakutskiy, Alexander Klygach y Sergey Strelkov	21
The balanced scorecard (BSC) as a support to the CMMI-DEV constellation SCAMPI for the recognition of the maturity of the software process	
Oswaldo Alfaro Bernedo, Doris Esenarro, Ciro Rodriguez y Maria Rene Alfaro	33
Roadside vertical solar-wind energy tower	
Mirsad Hyder Shah y Gasim Othman Alandjani	51
Design and construction of Savonius rotor	
Mirsad Hyder Shah y Sameer Ali Alsibiani	65
Augmented reality based gesture detection & object creation system using XCode & ARKit	
Sallar Khan, Syed Abbas Ali, Muhammad Nadeem y Raj Chawla	79
Multiple faults detection and identification of three phase induction motor using advanced signal processing techniques	
Majid Hussain, Rana Rizwan Ahmed, Imtiaz Hussain Kalwar y Tayab Din Memon	93
An automated system for traffic sign recognition using convolutional neural network	
Sanam Narejo, Shah Nawaz Talpur, Madeha Memon y Amna Rahoo	119
Acceptability in the optimal formulation of chrysin with partial replacement of pituca flour	
Pervis Paredes, Doris Esenarro, Jannina J. Bernabe y Wilber Quispe	137
Yield of tocosh flour in two potato varieties ( <i>solanum tuberosum</i> ) and their characteristics	
Jorge Jave Nakayo, Verónica Espinel Pino, Jorge Luis López Bulnes y Violeta Vega Ventosilla	149
Vulnerability of the soils of Metropolitan Lima and their relationship with urban sustainability	
Raúl Méndez Gutiérrez, Doris Esenarro Vargas, Pedro Amaya Pingo y Ciro Rodríguez Rodríguez	161
Microbial biodegradation of polyethylene of low density, under controlled thermal conditions in air lift bio-reactor	
Alexandra Milagros Hermoza Rojas, Jorge Jave Nakayo, Jorge Luis López Bulnes y Vicenta Irene Tafur Anzualdo	179

# /PROLOGUE/

## PROLOGUE

**Geetam S. Tomar**

Birla Institute of Applied Sciences, Bhimtal, (India).

E-mail: [gstomar@ieee.org](mailto:gstomar@ieee.org) ORCID: <https://orcid.org/0000-0002-0246-1527>

**Bishwajeet Pandey**

Birla Institute of Applied Sciences, Bhimtal, (India).

E-mail: [gyancity@gyancity.com](mailto:gyancity@gyancity.com) ORCID: <https://orcid.org/0000-0001-5593-8985>

**Robin Singh**

Birla Institute of Applied Sciences, Bhimtal, (India).

E-mail: [robin@ieee.org](mailto:robin@ieee.org) ORCID: <https://orcid.org/0000-0002-6314-4736>

**Doris Esenarro Vargas**

Federico Villarreal National University, Lima, (Peru).

E-mail: [desenarro@unfv.edu.pe](mailto:desenarro@unfv.edu.pe) ORCID: <https://orcid.org/0000-0002-7186-9614>

In this special issue of 3C Tecnología, we are publishing only 11 papers of the *6th International Conference on Green Computing and Engineering Technologies*, which was held on 16-18 September 2020 in Herzen State Pedagogical University of Russia, St Petersburg, Russia. Although, we have received 374 papers and 72 papers are accepted and published in conference proceedings. Due to the high-quality standards of our guest editorial board of 3C Tecnología, we shortlisted only 11 papers out of 72 and invited extended versions from the author and we are publishing the following 11 papers in the October Special Issue of 3C Tecnología.

In the first paper, Ivanov *et al.* (2020), considers an approach to visualization of human body structure using augmented reality. This approach will be a boon for doctors. This research is going to revolutionize the process of surgery in the healthcare industry. This paper discusses a project to develop a technology for using augmented reality in planning and performing surgery. The capabilities of the technology, as well as the prospects for its use, are highlighted.

In the second paper, Alfaro *et al.* (2020), are establishing the degree to which influence exerted by technology called Balanced Scorecard (BSC) as a support to the software development. This research also deals with the standardization of CMMI appraisal method,

Systemic Approach to conceive the problem comprehensively, and level of maturity of the software process. There is a 26.4% improvement in performance obtained by this research methodology.

In the third paper, Shah and Alandjani (2020), highlights the major dependency of the USA on Fossil Fuels and Nuclear power. This research deals with another approach to the global clean energy crisis. This approach said instead of finding new energy sources, we should become energy efficient. Road power generation is a new technology where the wasted energy of a moving vehicle can be extracted and converted to useful work done. This paper presents such a technology which when employed at the corner of a road can send power directly to the grid or run streetlights depending on the mode of operation.

In the fourth paper, Shah and Alsibiani (2020) highlighted the ongoing research in renewable energy sources in this century. It is often said that wind energy is an unreliable source of energy. But, Shah and Alsibiani (2020) insist that it is not unreasonable if placed at places where wind currents are smooth. Savonius rotor as Vertical Axis Wind Turbine (VAWT) is used as a standalone power generation device because of its low cost, low cut-in speed and the fact that it can accept wind from any direction. According to the study conducted, the voltage output recorded at 5.4 m/s wind speed was 19.1 Volts.

In the fifth paper, Khan *et al.* (2020) investigated one of the emerging areas of research called Augmented Reality (AR). In this research, they successfully deployed an IOS application which can detect live gestures of our hand movements and then creating 3D models with the help of their hand gestures.

In the sixth paper, Hussain *et al.* (2020) have proposed the multiple fault detection and identification system for three-phase induction motors using current signature analysis method (CSAM). The simulated system in MATLAB/SIMULINK and simulation is performed based on the healthy and unhealthy conditions of the motor. Comparative analysis between FFT and STFT, shows STFT as a promising approach.

In the seventh paper, Narejo, Talpur, Memon, and Rahoo (2020) applied CNN (Convolutional Neural Network) for traffic sign recognition especially for railway drivers. This paper explores the system to help the driver recognize road signs to avoid road accidents. In this

paper, they implement the traffic sign recognition by using CNN, the CNN is trained by using the dataset of 43 different classes of traffic signs along with TensorFlow library. They are getting results with 95% accuracy.

In the eighth paper, Paredes *et al.* (2020) investigate the acceptability of chrysin with the partial replacement of pituca flour based on intake of protein. They used quasi-experimental design and food ingredients mainly wheat flour, pituca flour, margarine, white sugar and yeast in their research. MINITAB and SPSS programs used by researchers for evaluation of data and samples taken.

In the ninth paper, Nakayo *et al.* (2020) investigate to demonstrate the yield of the flour of tocosh of two varieties of potato (*solanum tuberosum*) canchán and native variety of “calamarca. The raw material was acquired in the district of Paucartambo province of Pasco department of Pasco, to 2880 msnm, for the experimental study the two varieties of potatoes were placed using as technique a pool with a water current with varied times, where the microorganisms act and increase their activity related to the acidity.

In the tenth paper, Gutiérrez *et al.* (2020) discusses a great influence on the physical security of the urban infrastructure and the citizens of our capital city, that is why it is necessary to apply prevention strategies since our city is located in a very vulnerable area to seismic events, mainly huaycos, floods and landslides, settlements, landslides and other superficial mass movements, so it is necessary to have knowledge of the causes and effects of these phenomena, the different types and carrying capacity of soils in the districts of Metropolitan Lima, in order to contribute to the knowledge of the degree of vulnerability in which urban areas, marginal urban areas, human settlements are exposed.

In the eleventh paper, Rojas *et al.* (2020) identify new mechanisms that serve as tools for the mitigation of plastic contamination through the biodegradation of low density polyethylene using microorganisms of the species *Pseudomona aeruginosa* (bacteria) and *Aspergillus brasiliensis* (fungus) under controlled thermal conditions in an airlift bioreactor. The methods used were 2 samples of LDPE with concentrations of 50 mg/L and 2 samples of 100 mg/L deposited in an airlift bioreactor under controlled thermal conditions with a duration of 7 days.

/01/



# SUPERIMPOSED ANATOMICAL STRUCTURES IN AUGMENTED REALITY

---

**Vladimir Ivanov**

Herzen State Pedagogical University of Russia,  
Saint-Petersburg, (Russia).

E-mail: [voliva@rambler.ru](mailto:voliva@rambler.ru) ORCID: <https://orcid.org/0000-0001-8194-2718>

**Nikolay Kalakutskiy**

Pavlov First State Medical University of St. Petersburg,  
Saint-Petersburg, (Russia).

E-mail: [kalakutsky@yandex.ru](mailto:kalakutsky@yandex.ru) ORCID: <https://orcid.org/0000-0002-6851-5073>

**Alexander Klygach**

Herzen State Pedagogical University of Russia,  
Saint-Petersburg, (Russia).

E-mail: [voolf00@yandex.ru](mailto:voolf00@yandex.ru) ORCID: <https://orcid.org/0000-0002-2984-0201>

**Sergey Strelkov**

Herzen State Pedagogical University of Russia,  
Saint-Petersburg, (Russia).

E-mail: [sergin3d2d@gmail.com](mailto:sergin3d2d@gmail.com) ORCID: <https://orcid.org/0000-0002-4830-5407>

**Recepción:** 07/08/2020 **Aceptación:** 29/09/2020 **Publicación:** 13/11/2020

## Citación sugerida Suggested citation

Ivanov, V., Kalakutskiy, N., Klygach, A., y Strelkov, S. (2020). Superimposed anatomical structures in augmented reality. *3C Tecnología. Glosas de innovación aplicadas a la pyme. Edición Especial, Noviembre 2020*, 21-31. <https://doi.org/10.17993/3ctecno.2020.specialissue6.21-31>

## ABSTRACT

The paper considers an approach to visualization of anatomical structures using augmented reality, which allows for more accurate planning of operations and reduces the degree of surgical intervention.

To achieve this goal, a technology was developed using a frame with a volumetric optical marker, which allows you to correlate a virtual 3D model with the patient. As a result, it was possible to achieve an accurate positioning of the 3D model and obtain a reliable visualization of the location of internal anatomical structures. At the same time, the parallel application of spatial mapping technology allows you to fix the 3D model at a certain point in space and, in case of loss of marker tracking, save the correct location of the 3D model, taking into account that the patient is in a stationary state.

This approach can be effectively applied in surgery, if it is possible to fix the skeleton relative to any bone structure. Options for surgical intervention can be different, starting with the installation of prostheses, ending with the removal of cancerous tumors. The article discusses a project to develop a technology for using augmented reality in planning and conducting maxillofacial surgery. The capabilities of the technology, as well as the prospects for its use, are highlighted.

## KEYWORDS

Medicine, Surgery, Maxillofacial surgery, Augmented reality, Markers, 3D graphics, Visualization.

# 1. INTRODUCTION

Worldwide, the modern standard for jaw cancer surgery is the simultaneous reconstruction of a defect with a vascular graft. To reduce the risk of intra- and postoperative complications, improve the postoperative quality of life of patients and increase the accuracy of operations, much attention is paid to their careful preoperative planning (Hartman, Spauwen, & Jansen, 2002). The complexity of planning reconstructive operations in oncology lies in the need to combine data from different studies to simultaneously visualize several body tissues (bones, blood vessels, nerves, soft tissues) in order to increase the objectivity of determining the boundaries of the resection, optimizing the choice of a vascularized graft and determining donor and recipient vessels. All the above tasks correspond to an offline “map” of the patient, used in the developed augmented reality program, which is compiled on the basis of CT or MRI data and can be supplemented by ultrasound, dopplerography, angiography, etc.

Augmented Reality (AR) is a combination of virtual reality and with the “offline map” of a patient and allows the user to interact in real time between various material and virtual objects, as if they exist in a single environment (Bartella *et al.*, 2019). Using this feature, we can increase the productivity and quality of services in many areas, especially in head and neck surgery. The proposed solution will help the doctor easily see where the internal anatomical structures are located during the operation. We offer an advanced solution for tracking optical markers with spatial imaging based on patient CT data. The surgeon during the operation through glasses sees a 3D visualization of the received data, due to which he less looks at the monitor with the data of diagnostic tests and constantly monitors the state of the surgical wound, which reduces the risk of intraoperative complications, including bleeding, which leads to an increase in the accuracy of surgery, reducing its duration and reducing the risk of complications. Also, this project can be widely used for educational purposes.

Currently, many scientific papers on the use of augmented reality in various fields of medicine have been published: neurosurgery, cardiology, urology, plastic surgery, including dentistry and maxillofacial surgery (Ayoub & Pulijala, 2019; Elmi-Terander *et al.*, 2020; Kim, Kim, & Kim, 2017; Kwon, Park, & Han, 2018). However, most of them are descriptions

of individual clinical cases or their series, which certainly does not have a very high class of evidence (Bosc *et al.*, 2019). Available literature reviews also note the lack of clinical trial results for a more objective assessment of this method. Therefore, the goal of our work is to conduct a multicenter randomized clinical trial in the treatment of patients with jaw cancer, which shows their resection with simultaneous plastic surgery of the defect with a vascularized bone graft with microtechnology. A feature of basic research is their careful planning, strict adherence to the research protocol, good statistical analysis of the data obtained, as well as a unified scale for assessing the data obtained (calibrated investigator) and their analysis by an uninvolved specialist, to reduce the likelihood of bias on the part of the scientist when interpreting the data, compliance All of the above conditions will allow you to perform a high-class evidence study, the results of which will be useful for the development of modern science.

On the basis of the Department of Maxillofacial and Reconstructive Surgery of the First St. Petersburg Medical University named after Acad. I.P. Pavlova reconstructive plastic surgery to eliminate jaw defects due to malignant and benign neoplasms, post-traumatic defects and deformations of various genesis with the help of vascularized bone and soft-tissue flaps with microsurgical technique has been carried out for more than 30 years by a team led by professor N.V. Kalakutsky During this time, vast clinical experience has been accumulated in the treatment of this group of patients, which will facilitate the introduction of new technologies and improve the quality of the study.

According to the example of the following clinical case of using augmented reality technology in dentistry, within the framework of the planned study, it is supposed to be used when performing a jaw resection for cancer with simultaneous plastic surgery of the defect with a bone graft with microtechnology.

## 2. METHODOLOGY

### 2.1. MEDICAL CASE

For the first case, we took a patient who has a small hollow cluster of cells that is grouped together - a cyst in the left nasal sinus (Figure 1), which was recommended for removal. It also has a complex and uneven shape. Therefore, to help the doctor better understand

where he is during planning and work, we have developed a visual solution with the display of anatomical structures on top of what the doctor sees.



**Figure 1.** Cyst in left sinus marked in red.

## 2.2. OVERLAY 3D MODELS OF THE SKULL IN THE REAL WORLD

For the selected task, Augmented Reality is the optimal visual solution.

Augmented Reality (AR) presents information in the right context of the real world. To do this, the system must know where the user is and what he is looking at. Usually the user observes an object through a display that displays a camera image along with augmented reality. Thus, in practice, the system needs to determine the location and orientation of the camera relative to the object. In the case of Hololens glasses, it is almost the same. To do this, use a separate built-in camera, and as a display - two holographic projectors.

In AR technology, tracking markers are used for display on the display and in the camera - AR codes that help align the 3d model from the user's point of view. In our problem, when an object should be viewed from different sides, we used a special marker called cuboid, where on each side there is a unique AR code. The Hololens camera has a limited resolution of 720p and a low dynamic range compared to modern cameras. This causes problems

with accurate tracking. To improve this, we have added the wrong organic structure, which provides additional tracking capabilities.

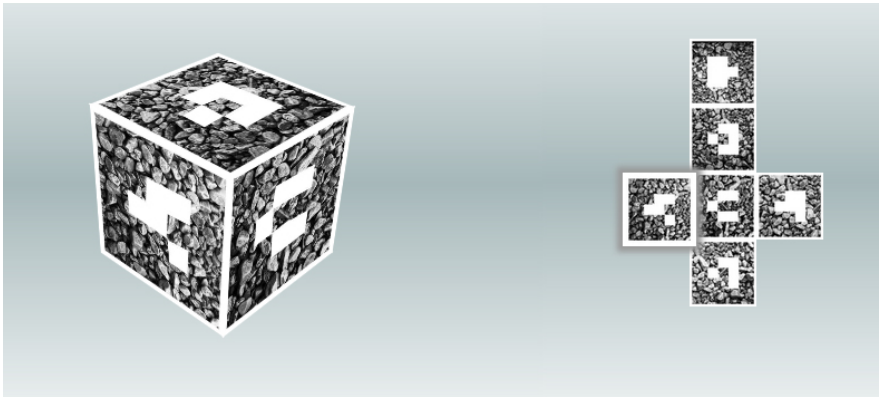


**Figure 2.** Type of marker.

In addition to the problem of aligning the object with the camera, our case is complicated by the fact that the marker must be fixed on the person's head, strictly in a certain position and with a certain orientation. For this task, we built a 3D model of the head from CT data using the Materialize Mimics software. Then we designated the areas where the marker will align and fix. Based on the selected areas, a three-dimensional wireframe model was built with a platform for attaching a marker. The frame was made in such a way that it could be easily put on and fixed in the correct position (Figure 3). Finally, it was printed on a 3D printer (Figure 4), and the marker was attached at a predetermined location.

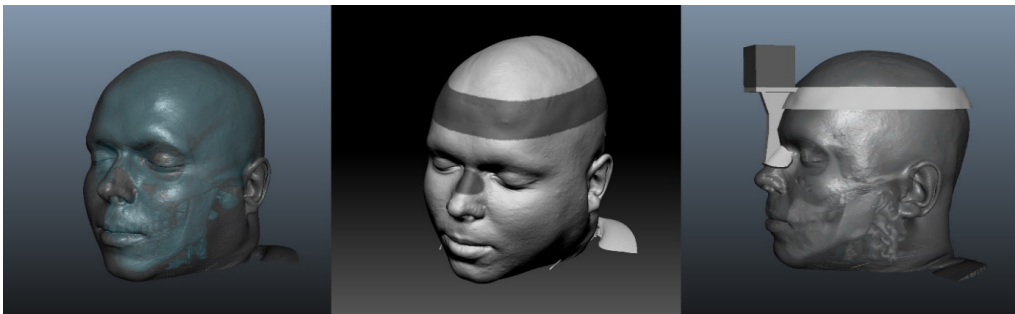


**Figure 3.** Left image - A constructed model of the face and skull based on CT data; in the middle are designated areas for fixing the frame, on the right is the model of the frame with a zone for the marker on top.



**Figure 4.** Printed frame.

After that, using the same CT dataset, we extracted a model of the patient's skull and cysts using Mimics. In the case of a cyst, it was isolated by CT by the doctor in layers, because such structures are clearly not readable on CT, and the program cannot automatically detect them. These two models were exported to Unity for further development under Hololens glasses (Figure 5).

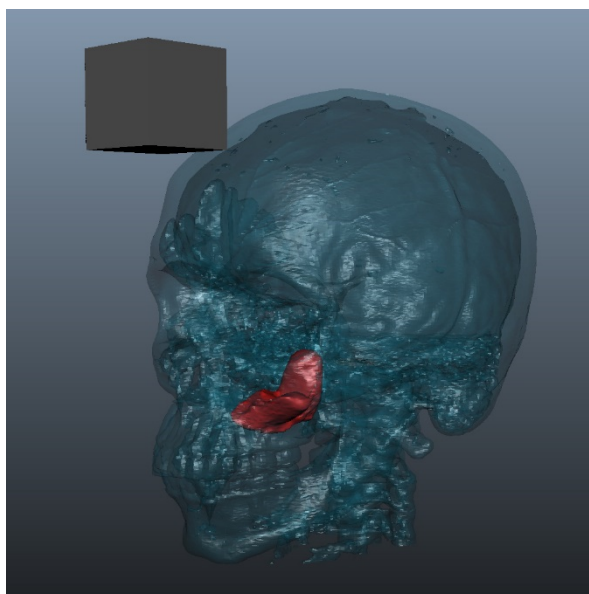


**Figure 5.** 3D model of a skull and cyst for augmented reality. The cube determines the size and position of the marker.

## 3. RESULTS

### 3.1. APPLICATION DEVELOPMENT FOR HOLOLENS

We developed the application using the Unity environment, which has special tools for HoloLens. There are also additional modules for Unity that expand the capabilities. One of them is Vuforia, designed for augmented reality using marker tracking.

In addition, a simple user interface was added using a gesture that the glasses recognize - a click to hide the skull and a click and drag to change the opacity when viewing the hologram.

To improve tracking performance, we also used a feature called spatial mapping, which is available in HoloLens. Spatial mapping provides additional information about the position and orientation of glasses in the environment with high accuracy.

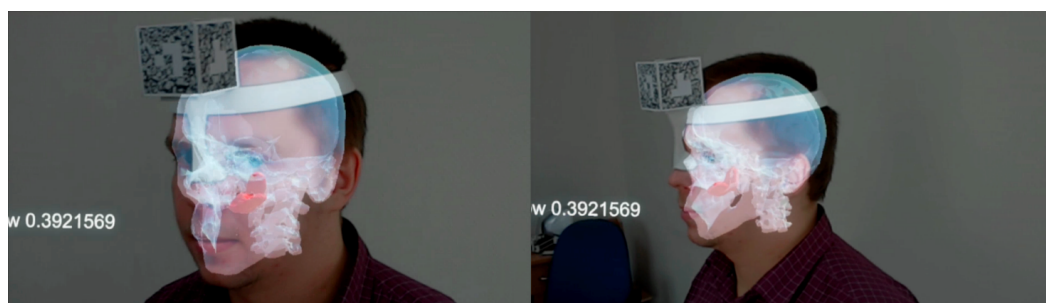


**Figure 6.** View of the skull and cyst through the HoloLens glasses.



**Figure 7.** View of an isolated cyst through HoloLens glasses.



## 4. CONCLUSIONS

The proposed approach using holographic representation of anatomical structures can be potentially used in surgery planning and during a procedure with some restrictions. Currently, marker based solutions on HoloLens devices have few limitations, such as low resolution cameras that are sensitive to lighting conditions and insufficient computing power of glasses. This causes a delay between 100-500 milliseconds and produces an error threshold in hologram positioning between 1-5mm. Such problems can be solved by upgrading hardware in the future glasses releases and possibly by switching to a geometry tracking solution, where markers can be represented by geometrical objects with any shape.

## REFERENCES

- Ayoub, A., & Pulijala, Y.** (2019). The application of virtual reality and augmented reality in Oral & Maxillofacial Surgery. *BMC Oral Health*, 19(1), 238. <https://doi.org/10.1186/s12903-019-0937-8>
- Bartella, A. K., Kamal, M., Scholl, I., Schiffer, S., Steegmann, J., Ketelsen, D., Hölzle, F. & Lethaus, B.** (2019). Virtual reality in preoperative imaging in maxillofacial surgery: implementation of “the next level”? *British Journal of Oral and Maxillofacial Surgery*, 57(7), 644-648. <https://doi.org/10.1016/j.bjoms.2019.02.014>
- Bosc, R., Fitoussi, A., Hersant, B., Dao, T. H., & Meningaud, J. P.** (2019). Intraoperative augmented reality with heads-up displays in maxillofacial surgery: a systematic review of the literature and a classification of relevant technologies. *Int J Oral Maxillofac Surg*, 48(1), 132-139. <https://doi.org/10.1016/j.ijom.2018.09.010>
- Elmi-Terander, A., Burström, G., Nachabé, R., Fagerlund, M., Ståhl, F., Charalampidis, A., Edström, E., & Gerdhem, P.** (2020). Augmented reality navigation with intraoperative 3D imaging vs fluoroscopy-assisted free-hand surgery for spine fixation surgery: a matched-control study comparing accuracy. *Scientific Reports*, 10(1), 707. <https://doi.org/10.1038/s41598-020-57693-5>

- Hartman, E. H., Spauwen, P. H., & Jansen, J. A.** (2002). Donor-site complications in vascularized bone flap surgery. *Journal of Investigative Surgery*, 15(4), 185-197. <https://doi.org/10.1080/08941930290085967>
- Kim, Y., Kim, H., & Kim, Y. O.** (2017). Virtual Reality and Augmented Reality in Plastic Surgery: A Review. *Archives of Plastic Surgery*, 44(3), 179-187. <https://doi.org/10.5999/aps.2017.44.3.179>
- Kwon, H. B., Park, Y. S., & Han, J. S.** (2018). Augmented reality in dentistry: a current perspective. *Acta Odontologica Scandinavica*, 76(7), 497-503. <https://doi.org/10.1080/0016357.2018.1441437>



/02/

# THE BALANCED SCORECARD (BSC) AS A SUPPORT TO THE CMMI-DEV CONSTELLATION SCAMPI FOR THE RECOGNITION OF THE MATURITY OF THE SOFTWARE PROCESS

---

**Oswaldo Alfaro Bernedo**

National University Federico Villarreal, (Perú).

E-mail: [oalfaro@unfv.edu.pe](mailto:oalfaro@unfv.edu.pe) ORCID: <https://orcid.org/0000-0002-9803-5986>

**Doris Esenarro**

National University Federico Villarreal, (Perú).

E-mail: [desenarro@unfv.edu.pe](mailto:desenarro@unfv.edu.pe) ORCID: <https://orcid.org/0000-0002-7186-9614>

**Ciro Rodriguez**

National University Mayor de San Marcos, (Perú).

E-mail: [crodriguezro@unmsm.edu.pe](mailto:crodriguezro@unmsm.edu.pe) ORCID: <https://orcid.org/0000-0003-2112-1349>

**Maria Rene Alfaro**

National University Federico Villarreal, (Perú).

E-mail: [mralfaro@unfv.edu.pe](mailto:mralfaro@unfv.edu.pe) ORCID: <https://orcid.org/0000-0003-4601-6748>

**Recepción:** 01/09/2020 **Aceptación:** 07/10/2020 **Publicación:** 13/11/2020

## **Citación sugerida Suggested citation**

Alfaro, O., Esenarro, D., Rodriguez, C., y Rene, M. (2020). The balanced scorecard (BSC) as a support to the CMMI-DEV constellation SCAMPI for the recognition of the maturity of the software process. *3C Tecnología. Glosas de innovación aplicadas a la pyme. Edición Especial, Noviembre 2020*, 33-49. <https://doi.org/10.17993/3ctecno.2020.specialissue6.33-49>

## ABSTRACT

This research tries to establish the degree of influence exerted by the design and use of a Balanced Scorecard (BSC), as a support to the Standard CMMI Appraisal Method for Process Improvement SCAMPI of the CMMI-DEV constellation, in recognition of the level of maturity of the software process, due to the efficiency and effectiveness provided by its application in practical life. In addition, it uses the Systemic Approach to conceive the problem comprehensively, under a holistic perspective, covering the relationships of each element within the system and its relationships with external agents; the applied methodology consists in the collection, tabulation, and analysis of the antecedents that have been obtained for its direct validation during development, that is, the management of cause-effect variables, where the independent or experimental variable is of interest to the researcher because the variable that is hypothesized (X), is one of the causes that produce the supposed effect. As a result of the effectiveness of the SCAMPI evaluation process, going from 72.7% to 92.7%; This is equivalent to a 26.4% improvement in performance, increasing from 10.9 correct evaluations to 13.9 for conducting such evaluations.

## KEYWORDS

Balanced scorecard, Support, Constellation, SCAMPI, Maturity of the software.

# 1. INTRODUCTION

In its research to help organizations develop and maintain quality products and services, the Software Engineering Institute (SEI) has found several dimensions that an organization can focus on to improve its business. Also, it illustrates the three fundamental dimensions on which organizations usually focus: people, procedures and methods, and tools and equipment. This virtuous circle involving these components is key to achieving a quality product (2GC Active Management, 2019).

Software, understood in its duality of process and product, is inherently problematic; such complexity is manifested in many aspects, the most relevant being: the fact of being intangible, difficulty in delimiting the scope or domain, diversity of languages to express it in semantic and notational form, frequent changes in business rules that attempt against its functional validity and, consequently, the predominance of accelerated product obsolescence, etc.

The CMMI has two structures of Representations, the same ones that give rise to two different types of evaluations. Figure 1 illustrates the structure of the Representations Continuous. The differences between the structures of Figure 1 and the Staged representation are subtle but significant. The staged picture uses maturity levels to characterize the overall state of the organization’s processes concerning the model. In contrast, the continuous representation uses capability levels to characterize the state of the organization’s processes concerning an individual process area. This dimension (the capability/maturity dimension) of CMMI is used for benchmarking and assessment activities, as well as to guide an organization’s improvement efforts (Álvarez, 2016).

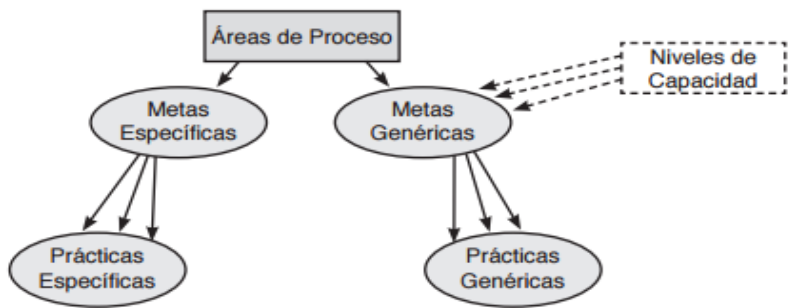


**Figure 1.** Continuous representation.

As show in Figure 1, capacity levels refer to the achievement of process improvement in an organization in individual process areas. These levels are a means of incrementally improving the processes that correspond to a given process area.

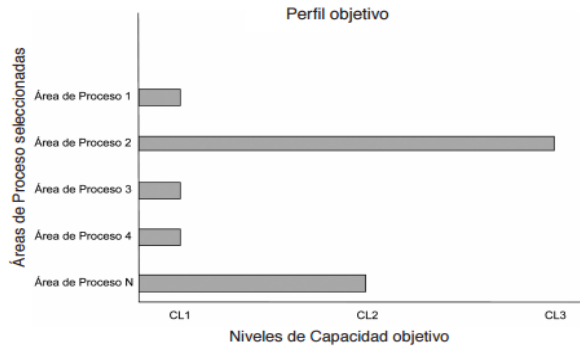


**Figure 2.** The four levels of capability are numbered from 0 to 3.

Maturity levels, on the other hand, refer to the achievement of process improvement in an organization in multiple process areas. These levels are a means of improving processes for a given set of process areas (i.e., maturity level). As illustrated in the Figure 2, the five maturity levels are numbered from 1 to 5.

There is a dependency or causal relationship between Strategic Planning and the BSC, i.e., the formulation of the strategic plan is the primary input of the latter, so when designing and operating the BSC, this condition should not be lost sight of. In this regard, the structure of the strategic plan under the BSC approach has the following structure (De Flander, 2018):

- a) **Institutional:** where the values, role, and scope of the institution are stated; the philosophy of the institution; the expectations of related agents or interest groups.
- b) **Strategic Management:** a segment in which the Mission, Vision, and General Strategic Objectives and Specific Strategic Objectives for the established time horizon are formally expressed.
- c) **Related strategies:** the set of actions to be deployed to achieve the formulated objectives.
- d) **Management indicators:** sets of metrics to measure the institution's functional performance.



The following table shows in a structured way the perspectives, general objectives, specific objectives, and corresponding indicators that are part of a corporate strategic plan.

The BSC is configured in four hierarchically aligned perspectives under a causal alignment. This structure responds to the logic of the so-called strategic map, which in turn is constituted by the causal relationship of the strategic objectives derived from the institutional strategic plan. The perspectives considered are financial, commercial, internal processes, and learning; each one of them, in turn, is made up of strategic objectives, indicators, and goals.

The BSC is used as a strategic management model, a communication tool, and, in its best implementations, an organizational change tool. This management model is based on a basic principle stated as “you can only manage what you can measure” (Lamé, Jouini & Stal-Le Cardinal, 2019).

The BSC is a tool that translates strategy into action. BSC is a performance planning and management model that places strategy at the center of the process. The applicability of the BSC has no limits of any nature because being a comprehensive management measurement system can be adapted to any organization, for tangible or intangible processes, for large or small organizations, public or private.

There is a wide variety of software tools to implement and automate the operation of this important strategic management tool. However, there is one that, taking the institutional strategic plan as a reference base, allows move towards management by indicators. This is the case of Sixtina BSC, whose flexibility, robustness, and user-friendliness allow for relatively easy incorporation of the designed strategic matrix into the strategic plan.

The software organizes the management indicators in a structured manner. The highest hierarchy is General Compliance, then Critical Factor, then Indicator, and finally, Data. This structure is causal, i.e., the sequencing starts from the Learning perspective, then Internal processes, Customers, and Financial. The person responsible for designing the BSC assigns the weighted weights to each of the management indicators.

The BSC dashboard shows in the second column, the performance status of each indicator in the chromatic form: green means satisfactory, yellow is equivalent to alert, and red indicates deficient. The next column shows the actual value of each indicator; this

information is extracted from the database of the institution's information system; then it shows the measure of the expression of each indicator, corresponding points for general compliance, critical factor, and indicator; instead, for data, it corresponds to the measure corresponding to its nature. The columns follow it for the date, operation (maximize, minimize or stabilize), perspectives already indicated, the person responsible for the results achieved by each indicator; the weighted weight (%) in determining the formula for the compound indicators, the trend, the target value defined, the deviation observed between the actual value and the target, the origin of the data (formula, manual, database, Excel) and finally the frequency of recording the information (daily, weekly, monthly or annual) (Catchpole *et al.*, 2017).

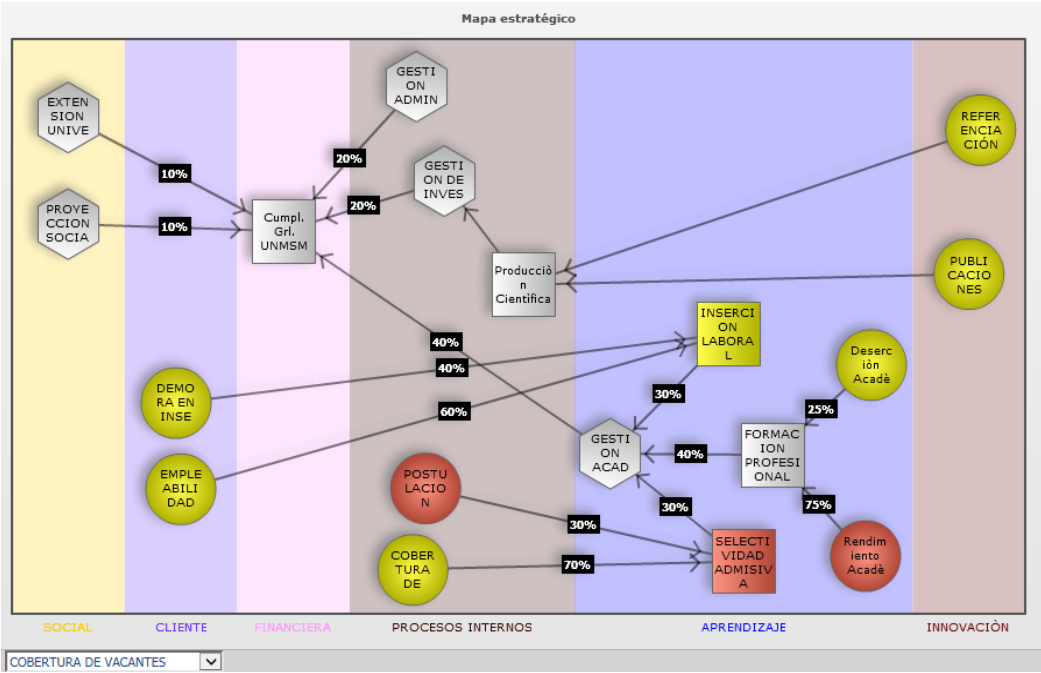


Figure 3. BSCS strategic Map.

Figure 3 shows the strategic map corresponding to the BSC scorecard, whose purpose is to articulate in a systemic, causal, hierarchical, transversal, and weighted way all the management indicators. This view is very important for the stakeholders because, in one single view, the interaction of the indicator system can be understood.



**Figure 4.** Homogenization of heterogeneous indicators.

The calculation and color representation of each of the indicators in the BSC control panel is shown in Figure 4. The sequence is bottom-up, i.e., based on data of a heterogeneous nature, quantity, orientation, and weighting, using the corresponding formula, the resulting indicators of a homogeneous nature are determined in units of measurement (points) and orientation (maximize). To determine the values of the critical factors and general compliance, the same procedure is followed as above (Institute and Faculty of Actuaries, 2019).

**Table 1.** Parameterization and import of information in BSC Sixtina.

SERIES	DETAIL	DATA			GENERAL COMPLIANCE, CRITICAL FACTOR OR INDICATOR
REAL	Operation	Maximize	Minimize	Stabilize	Maximize
	Capture	excel import - databases			formula (rank/average index children)
	Magnitude	original size			score (0 to 10)
ALARM	Operation	Maximize	Minimize	Stabilize	Maximize
	Capture	excel - manual			excel – manual
	Magnitude	original size			score (0 to 10)
OBJECTIVE	Operation	Maximize	Minimize	Stabilize	Maximize
	Capture	excel - manual			excel - manual
	Magnitude	original size			score (0 to 10)

**Maximize**

Fees		
0		Max
Deficiency	Alarm	Target

Minimize

Fees		
0		Max
Target	Alarm	Deficiency

Stabilize

Fees				
0				Max
Default default	Lower alarm	Target	Higher alarm	Deficiency due to excess

Table 1 is a summary of the information processing for the construction of the BSC control panel content. For each series (actual, alarm or target), depending on the type of indicator, operations are performed (maximize, minimize or stabilize) as appropriate; information capture is defined (import from Excel or database, Excel or manual); also, the magnitude (points or original magnitude of the data) is established. Likewise, the dimensions for the three operation options of the indicators and their corresponding color are defined.

Since the CMMI, SCAMPI, and BSC models have been characterized integrally, by the research objective, it has been possible to establish an analogy between the SCAMPI evaluation process and the BSC control panel. As shown in Table 2, it is possible to equate the hierarchical levels of maturity assessment of SCAMPI and the performance of the management indicators of the Sixtina BSC scorecard.

Table 2. Equivalences between SCAMPI model and Sistine BSC.

SCAMPI Maturity Assessment Model	BSC control panel model
Maturity level	General compliance
Process area	Critical factor
Goals	Indicator
Internship	Fact

The convenience of applying the BSC as a tool to facilitate the SCAMPI evaluation of the CMMI-DEV constellation, oriented to the recognition of the software process maturity level, is supported by the following reasons.

## 2. METHOD

This research work is based on the Scientific Research Method due to the efficiency and effectiveness provided by its application in practical life. Furthermore, it uses the Systemic Approach to conceive the problem integrally, under a holistic perspective, covering the relations of each element within the system and its relations with external agents.

Consequently, the project is following a proven method of collecting, tabulating, and analyzing the background that has been obtained and proving its validity directly in the field in which the research fact is being presented (Borchert, Schirmeier & Spinczyk, 2017).

The design of the Experimental Research has been selected, that is to say, the handling of variables of the cause-effect type, where the independent or experimental variable is of interest to the researcher because the variable that is hypothesized (X) is one of the causes that produce the supposed effect (Denicolai & Previtali, 2020).

The design is quasi experimental, allows the use of pre-tests and post-tests to analyze the evolution of the effect of the “pilot” implementation before and after the experimental treatment so that the subtype of Research design used is: “Post-test design and control group”, whose general model is shown below:

<b>RG1</b>	<b>X</b>	<b>O1</b>
<b>RG2</b>	<b>–</b>	<b>O2</b>

Where:

**RG1** = Experimental Group (formed randomly by software process evaluations for recognition of maturity levels using the BSC)

**RG2** = Control group (formed randomly by software process evaluations for recognition of maturity levels in the absence of the stimulus)

**X** = Stimulation (El Balanced ScoreCard)

**–** = Absence of Stimulus

**O1, O2** = Measurement of maturity level indicators

This design includes two groups, one receiving the experimental treatment (Experimental Group) and the other not (Control Group). That is, the manipulation of the independent variable reaches only two levels (presence and absence).

- Materials:
  - CMMI-DEV Constellation
  - SCAMPI model
  - Software development processes
  - Balanced Score Card Software
- Procedure:
  1. Business processes that have been automated through software development processes are identified.
  2. The development constellation of the CMMI model is characterized.
  3. Requests for evaluation of CMMI-DEV maturity levels are received.
  4. The evaluation team is constituted, designating the leader.
  5. The Balanced Score Card logic model applied to the SCAMPI model is built.
  6. An evaluation or audit is carried out to recognize the level of maturity required.
  7. The results of the evaluations are compared
  8. The results are interpreted.
  9. The hypotheses are verified.

### 3. RESULTS

By the objective of the research, the hypothesis, the design, and the procedure that has been applied in this investigation, initially, a company has been characterized as a prototype, which constitutes the control group to which the BSC was not applied in the SCAMPI evaluation process, for the recognition of the level of maturity of the software process implemented in that organization, that is, maintaining its original conditions of structure and operation. Then, the prototype was made for a SCAMPI evaluation of maturity level 2, using the BSC, whose software corresponds to Sixtina BSC. Specifically, the following procedure has been followed. (Brocklesby, 2016).

1. The MWC-SCAMPI metamodel logic has been constructed to understand the scope and reach of the entities included in this integral process. This model has been designed with a view to the subsequent generation of the physical database (PIIDB), necessary to import the information from the Sistine BSC.

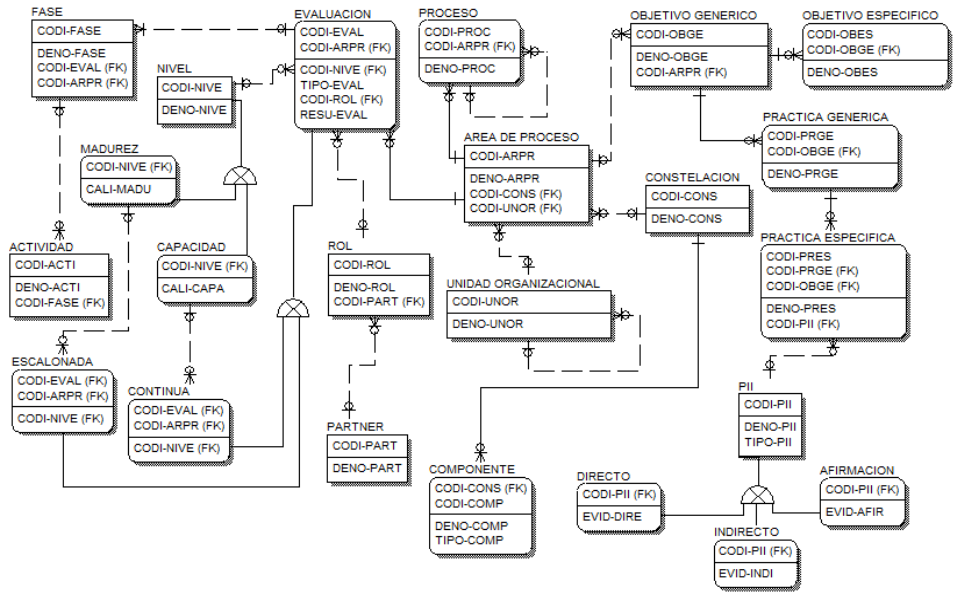


Figure 5. Logical metamodel CMMI SCAMPI.

Figure 5 shows all the entities, relationships, and attributes that are most prominent in this metamodel. Recursive relationships and sub-entities are also identified.

- 1) Advanced engineering has been carried out for the generation of the database (PIIDB) corresponding to the entity-relationship model designed in the previous point.
- 2) The equivalence between the components of the CMMI-SCAMPI model and the BSC Sixtina control panel has been established, as shown in the following table. It shows the relevance of establishing similar and, therefore, comparable hierarchies at the corresponding levels.

This analogy constitutes the full support to the proposal of this research project to use the Balanced Scorecard (BSC), as a support to the SCAMPI of the CMMI-DEV constellation, in recognition of the maturity level of the software process.

- 1) Using the software BSC Sixtina under the web environment, the SCAMPI evaluation model of the CMMI development constellation (DEV) has been characterized.
- 2) In the same BSC board, the evaluation corresponding to maturity level 2 for the Process and Product Quality Assurance (PPAQ) process area, its four goals, as well as its 15 practices, has been carried out. I am applying for the SCAMPI protocol. With the information recorded in the database, the information has been contrasted, and the software has produced the color results observed, and, applying the decision rule of the SCAMPI protocol, the requested maturity level has not been reached as (Brocklesby, 2016) in an applied situation.
- 3) By way of simulation, the results of the research efficiency indicator have been measured. This metric expresses the time spent in carrying out a SCAMPI assessment, for maturity level 2, both for the control group (in the conventional form) and for the experimental group (using the BSC)

**Table 3.** Efficiency for the Control Group.

EVALUATION	DURATION (DAYS)		EFFICIENCY
	ESTIMATE	REAL	
1	12	15	80.0%
2	10	14	71.4%
3	9	12	75.0%
4	10	15	66.7%
5	12	14	85.7%
6	10	15	66.7%
7	8	12	66.7%
8	14	18	77.8%
9	12	16	75.0%
10	14	16	87.5%
AVERAGE	11.10	14.70	75.2%
DEVIATION			0.08



**Table 4.** Efficiency for the Experimental Group.

EVALUATION	DURATION (DAYS)		EFFICIENCY
	ESTIMATE	REAL	
1	12	12	100.0%
2	10	11	90.9%
3	9	9	100.0%
4	10	15	66.7%
5	12	11	109.1%
6	10	11	90.9%
7	8	8	100.0%
8	14	15	93.3%
9	12	13	92.3%
10	14	13	107.7%
AVERAGE	11.10	11.80	95.1%
DEVIATION			0.12

- 4) There is a substantial increase in the efficiency of the SCAMPI evaluation process, from 75.2% to 95.1%; this is equivalent to a 26.4% improvement in performance, decreasing from 14.7 days to 11.8 days for such evaluation.

**Table 5.** Efficiency for the Control Group.

EVALUATION	PRACTICES		EFFICACY
	EVALUATED	ACCEPTED	
1	15	11	73.3%
2	15	10	66.7%
3	15	9	60.0%
4	15	13	86.7%
5	15	11	73.3%
6	15	11	73.3%
7	15	9	60.0%
8	15	12	80.0%
9	15	12	80.0%
10	15	11	73.3%
AVERAGE	15.00	10.90	72.7%
DEVIATION			0.09

- 5) Also, by way of simulation, the results of the research effectiveness indicator have been measured. This metric expresses the degree of accuracy used in carrying

out a SCAMPI assessment, for maturity level 2, for both the control group (in a conventional form) and the experimental group (using the BSC).

**Table 6.** Efficiency for the Experimental Group.

EVALUATION	PRACTICES		EFFICACY
	EVALUATED	ACCEPTED	
1	15	14	93.3%
2	15	14	93.3%
3	15	15	100.0%
4	15	13	86.7%
5	15	14	93.3%
6	15	13	86.7%
7	15	13	86.7%
8	15	14	93.3%
9	15	14	93.3%
10	15	15	100.0%
AVERAGE	15.00	13.90	92.7%
DEVIATION			0.05

There was a substantial increase in the effectiveness of the SCAMPI evaluation process as we can compare in tables 5 and 6, from 72.7% to 92.7%; this is equivalent to a 26.4% improvement in performance, increasing from 10.9 correct evaluations to 13.9 for conducting such evaluations.

4. CONCLUSIONS

The BSC is a powerful tool insofar as it is applied to follow up on performance reports. Using the software BSC Sixtina under the web environment, the SCAMPI evaluation model of the CMMI development constellation (DEV) has been characterized.

As a result of the effectiveness of the SCAMPI evaluation process, going from 72.7% to 92.7%; This is equivalent to a 26.4% improvement in performance, increasing from 10.9 correct evaluations to 13.9 for conducting such evaluations.

## REFERENCES

- 2GC Active Management.** (2019). *Balanced Scorecard Usage Survey 2018*. Retrieved on August 30, 2019, from: [https://2gc.eu/media/resource\\_files\\_survey\\_reports/2018\\_Survey\\_Document\\_10\\_Final-compressed.pdf](https://2gc.eu/media/resource_files_survey_reports/2018_Survey_Document_10_Final-compressed.pdf)
- Álvarez, I.** (2016). *FORBES*. Retrieved on August 12, 2019, from: <https://forbes.es/listas/3865/las-diez-mejores-firmas-de-consultoria/>
- Borchert, C., Schirmeier, H., & Spinczyk, O.** (2017). Generic soft-error detection and correction for concurrent data structures. *IEEE Transactions on Dependable and Secure Computing*, 14(1), 22–36. <https://ieeexplore.ieee.org/document/7097670>
- Brocklesby, J.** (2016). The what, the why, and the how of operational behavioral research—An invitation to potential skeptics. *European Journal of Operational Research*, 249(3), 796–805. <https://doi.org/10.1016/j.ejor.2015.09.034>
- Catchpole, K., Neyens, D.M., Abernathy, J., Allison, D., Joseph, A., & Reeves, S.T.** (2017). Framework for direct observation of performance and safety in healthcare. *BMJ Quality & Safety*, 26(12), 1015–1021. <https://doi.org/10.1136/bmjqs-2016-006407>
- De Flander, J.** (2018). *Strategy Execution - The Definitive Guide - Jeroen De Flander*. Retrieved on August 24, 2019, from: <https://jeroen-de-flander.com/strategy-execution/>
- Denicolai, S., & Previtali, P.** (2020) Precision Medicine: Implications for value chains and business models in life sciences. *Technological Forecasting and Social Change*, 151, page 119767. <https://doi.org/10.1016/j.techfore.2019.119767>
- Institute and Faculty of Actuaries.** (2019, October 7). *RSS and IFOA publish new ethical guidance in data science*. <https://www.actuaries.org.uk/news-and-insights/news/rss-and-ifo-a-publish-new-ethical-guidance-data-science>
- Lamé, G., Jouini, O., & Stal-Le Cardinal, J.** (2019) Combining Soft Systems Methodology, ethnographic observation, and discrete-event simulation: A case study in cancer care. *Journal of the Operational Research Society*, 71(10). <https://doi.org/10.1080/01605682.2019.1610339>

**Ubalde, R., Rodriguez, C., Petrlik, I., Esenarro, D., Lezama, P., & Sotomayor, J.**  
(2020). Quality model for Peruvian microenterprises of a software product Factory.  
*Test Engineering and Management*, 83, 13434.



/03/

# ROADSIDE VERTICAL SOLAR-WIND ENERGY TOWER

---

**Mirsad Hyder Shah**

Student, Technische Universitat Dortmund.  
Dortmund, (Germany).

E-mail: [Itsmirsadhyder@yahoo.com](mailto:Itsmirsadhyder@yahoo.com) ORCID: <https://orcid.org/0000-0003-2476-5887>

**Gasim Othman Alandjani**

Assistant Professor, Computer Science and Engineering Department. Yanbu University College, Yanbu  
Industrial City, (Kingdom of Saudi Arabia).

E-mail: [Alandjanig@rcyci.edu.sa](mailto:Alandjanig@rcyci.edu.sa) ORCID: <https://orcid.org/0000-0003-0321-7013>

**Recepción:** 01/09/2020 **Aceptación:** 29/09/2020 **Publicación:** 13/11/2020

## **Citación sugerida Suggested citation**

Hyder, M., y Othman, G. (2020). Roadside vertical solar-wind energy tower. *3C Tecnología. Glosas de innovación aplicadas a la pyme. Edición Especial, Noviembre 2020*, 51-63. <https://doi.org/10.17993/3ctecno.2020.specialissue6.51-63>

## ABSTRACT

Fossil fuels and Nuclear power is responsible for about 82% of the current Energy Production in the US. While a small part is still being met by renewable energy sources, engineers are working hard on finding new sources of Energy. Another approach to the global clean energy crisis is that instead of looking for a new energy source, we should become Energy Efficient. Road power generation is a new technology where the wasted energy of a moving vehicle can be extracted and converted to useful work done. This paper presents such a technology which when employed at the corner of a road can send power directly to the grid or run streetlights depending on the mode of operation. This is done by constructing a Savonius Wind Turbine and then converting the wasted wind energy produced by a moving vehicle. In addition, a solar panel can also be placed on the top of the turbine and produce more energy. A microcontroller decides how Energy is to be sent to the grid or stored to be used for street lighting load. While the power production may vary depending on the traffic and conditions of the city, the S-rotor and solar panel have a maximum voltage of 19.1 V and 19.65 V respectively.

## KEYWORDS

Savonius rotor, Inverter, Solar Panel, Wind turbine, Road Power generation, Charge Controller.



## 1. INTRODUCTION

The need of alternate energy sources is not a debate but a necessity in this modern era. The demand of clean and affordable energy sources led to the breakthrough of renewable energy sources (Shah, Alandjani, & Asghar, 2020). Such is the scope of renewable energy sources that Road Power Generation (RPG) Technologies are being researched upon. One of the technologies involves extracting the wind gushes produced by nearby vehicles. The rotor design is a challenging design and many different types of rotors can be employed.

## 2. METHODOLOGY AND RESEARCH

This paper discusses an experimental work done to harness the wind energy produced by moving vehicles on a road and extracting the solar potential with a solar panel along with it. This is achieved by designing a Savonius wind turbine and placing a mono-crystalline solar panel together. The system takes input from both renewable energy sources and voltage sensors provide voltage values to the Arduino. This Microcontroller is programmed with a code which will be discussed later. The extracted voltages are sent to a nearby grid in the day and at night are used to power streetlights.

When the solar panel is operational, the voltages are sent to the MPPT (Maximum Power Point Tracking). This MPPT is connected to a reference battery which powers it. The MPPT stabilizes the voltages from the solar panel and charges the main battery. The power from the battery is then provided to the inverter which then converts DC to AC and sends it to the grid or streetlight as necessary.

When the wind turbine extracts the wasted wind potential from nearby vehicles, power is generated by the PMDC generator. The voltages from the PMDC generator are provided to the Buck/Boost converter which are either bucked or boosted depending on the situation. This DC power will then charge the battery and converted to AC by the inverter for any load.

The Vertical solar wind energy tower is a power generation unit which harnesses the wind potential of moving vehicles and the solar potential of the sun. It has the following parts:

## 2.1. SOLAR PANEL

After careful observation and survey of the site where the power generation unit is to be installed; it was decided that a mono crystalline solar panel will be used. Since the selection of a solar panel depends upon heat tolerance and since the average temperature in Karachi usually remains in between 27-30°C, the choice made was the best available.

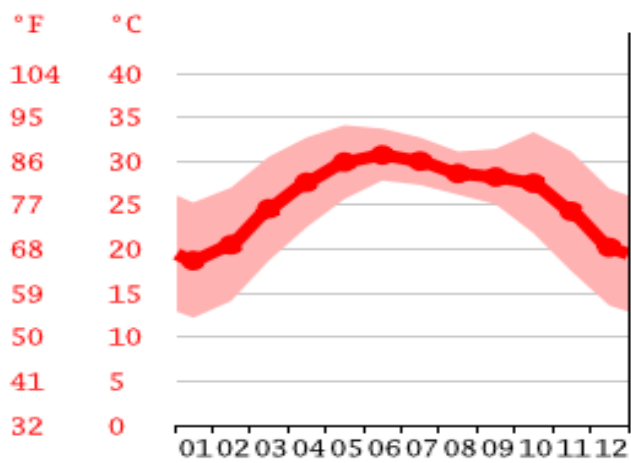


**Figure 1.** Graph of average temperatures in Karachi. **Source:** (Climate-Data.Org, n.d.).

## 2.2. S- ROTOR

A detailed discussion on the design and construction of Savonius rotor has been discussed in Shah and Alsibiani (2020).

## 2.3. INVERTER

An inverter is a circuit that changes DC to AC. The following components were used in its construction:

- IC CD4047, Transistor 2N3904, eight tip 35C transistors, Diodes, Transformer, Capacitors and Resistors.

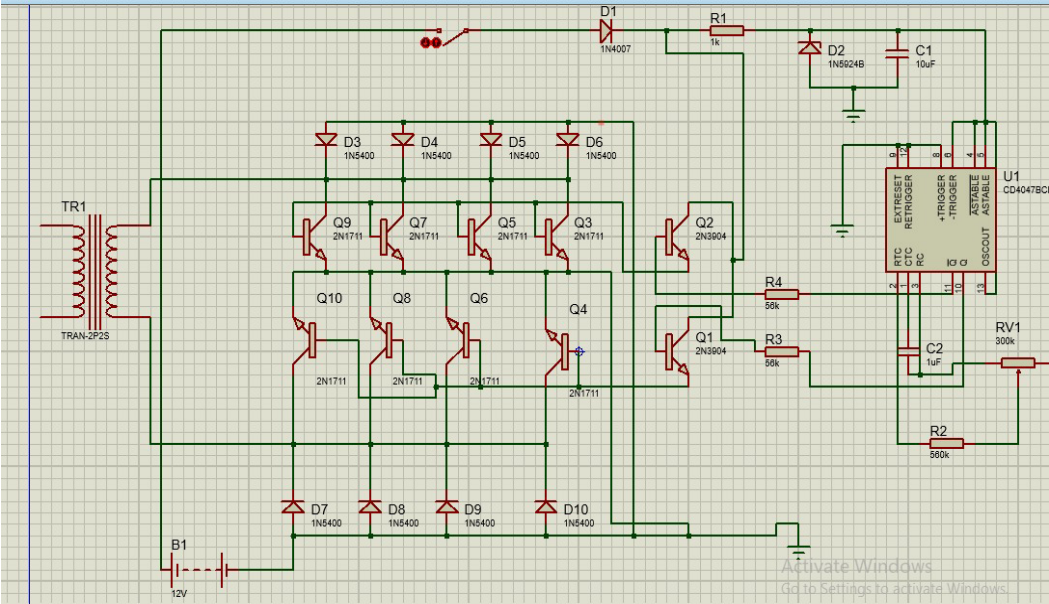


Figure 2. Simulation of an Inverter.

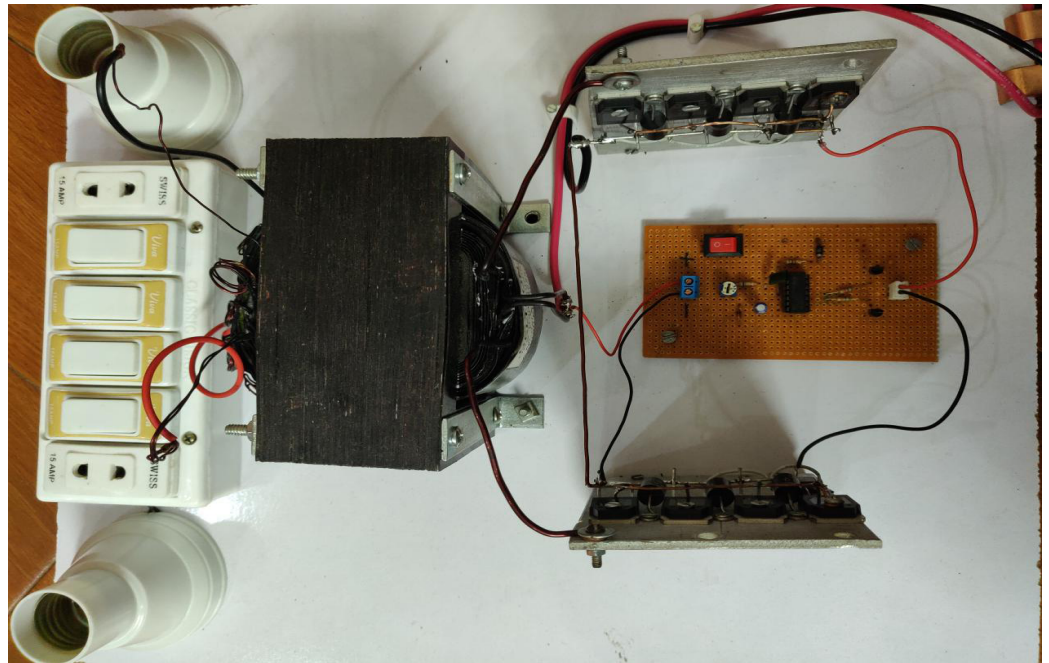


Figure 3. Inverter Hardware.

## 2.4. GENERATOR

A generator is required to convert the rotational motion of the wind turbine into Electrical Energy. The specifications of the Generator are as follows:

- Rated Power: 1hp
- Rated Speed: 1650 RPM
- Rated Voltage: 18 VDC
- Pole: 2-4
- Current: 4.8 Amp



**Figure 4.** PMDC Generator.

## 2.5. CHARGE CONTROLLER

A charge controller is needed since the voltages produced by the generator are unstable. To stabilize/buck/boost the voltages the charge controller is needed. The function of the Charge controller over here is to supply constant output while the input is varying due to different wind speeds generated by vehicles. It consists of the following components:

- NE555 timer, IC7805, Diodes, Relay, Resistors, Transistor 2N2222 NPN, Capacitors

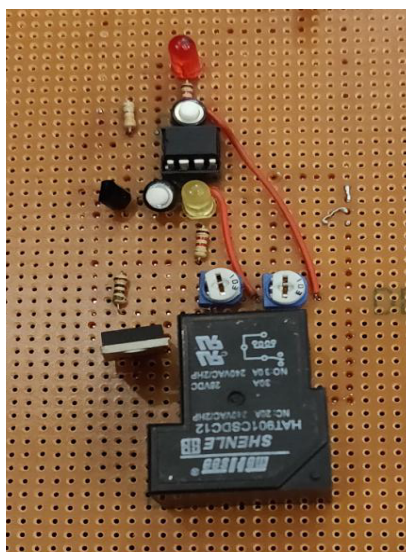


**Figure 5.** Hardware of Charge Controller.

## 2.6. MICROCONTROLLER

Since the integration of both the power sources has not been carried out, only one source of energy can be stored in the battery, while the other must be sent to the grid for sale. For this obstacle the microcontroller is programmed with a basic code whose Algorithm is discussed below:

- From the time 9:00 A.M to 5 P.M the power output of solar panel is sent directly to the grid, while the output of the wind turbine is stored into the battery.
- If the weather is cloudy, the solar panel will not be able to extract any power from the sun and hence a message will be sent to the grid notifying no power output per hour.
- In the meantime, the wind turbine captures the gushes of wind from nearby vehicles and will store its power into a battery.
- At 6 P.M the nearby streetlights will be powered from all the wind energy collected in the 12 Hours of its operation.
- At 6 A.M, all the remaining power of the battery is sent to the grid for sale.

## 3. BLOCK DIAGRAM OF UNIT

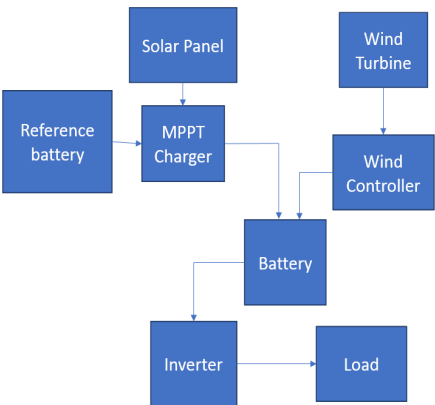


**Figure 6.** Block Diagram of System.



**Figure 7.** Hardware of System.

## 4. CALCULATIONS

The power of a wind turbine can be calculated by:

$$P = \frac{1}{2} \times \rho \times A \times v^3 \times C_p$$

$$N = \frac{60}{2\pi} \times \omega$$

Torque:

$$T_s = \frac{P}{\omega}$$

Over Lap Ratio:

$$\beta = \frac{e}{D}$$

Swept Area:

$$\text{Swept Area} = \text{Height} \times \text{Diameter}$$

Height of the turbine is 1.24m

Diameter of the turbine is 0.375m

$$\text{Swept Area} = A = 1.24 \times 0.375$$

$$A = 0.465 \text{ m}^2$$

Over Lap Ratio:

$$\beta = \frac{e}{D}$$

Overlap distance is 0.0381m

Diameter of the turbine is 0.375m

$$\beta = \frac{0.0381}{0.375}$$

$$\beta = 0.1016$$

Aspect Ratio:

$$\alpha = \frac{H}{D}$$

$$\alpha = \frac{1.24}{0.375}$$

$$\alpha = 3.3066$$

Rotational Speed:

$$N = \frac{60}{2\pi} \times \omega$$

Where,

$$\omega = 20.49 \text{ rad} / \text{s}$$

$$N = \frac{60}{2\pi} \times 20.49$$

$$N = 199.93 \text{ rpm}$$

Power

$$P = \frac{1}{2} \times \rho \times A \times v^3 \times C_p$$

sWhere,

$\rho$  = density of air = 1.225

A = swept area

v = wind speed

$C_p$  = coefficient of power

$$P = \frac{1}{2} \times 1.225 \times 0.465 \times 4.5^3 \times 0.21$$

$$P = 5.4502 \text{ Watts}$$

## 5. RESULTS

The results of the project have been discussed below:

In Figure 8, the resultant waveform of a square wave was obtained. The square wave inverter converts solar DC power to AC power. This type of inverter is simpler in design and more efficient than a sine wave inverter.

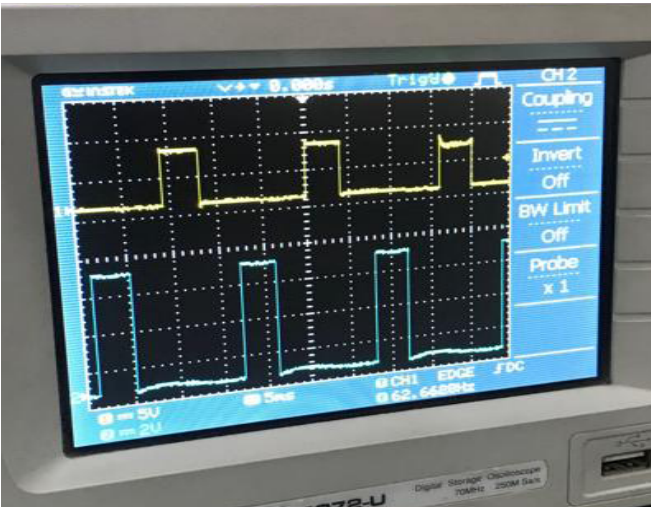


**Figure 8.** Waveform of Oscillation of Inverter.

In Table 1, the results for the wind turbine have been shown. The velocity of the wind was measured using an anemometer which was placed right in front of the rotor. The wind made the rotor move as intended. However, the maximum wind velocity that could be simulated was 5.4 m/s. On the Beaufort Scale, such a wind speed has a Beaufort number of 3 and is considered as a Gentle Breeze only. But due to the rotor being lightweight it was easily rotated, and enough Revolutions were generated.

**Table 1.** Results of Wind Turbine.

WIND SPEED m/s	RPM	VOLTAGES
4.1	200	14.91V
4.5	241	17.0V
4.9	253	18.17V
5.1	265	18.64V
5.4	302	19.1V

In the Table 2, the results of the solar panel are discussed. By placing the solar panel throughout the day and measuring the solar panel output using a multimeter following



open source voltages were obtained. Since the panel was directed at a 90 degree angle at the peak hour (12:00 p.m.), the maximum voltage output of 19.65V was obtained.

**Table 2.** Results of Solar Panel.

TIME	VOLTAGE
8:00 a.m.	10V
10:00 a.m.	15.46V
12:00 p.m.	19.65V
14:00 p.m.	19.34V
17:00 p.m.	14.62V
20:00 p.m.	0.0V

Since the weather and traffic may vary and affect the power output, only the results which are definite have been discussed in this paper. In addition both the Energy sources do not have a common storage system and may be lethal if constructed in the wrong way.

## 6. CONCLUSION

This paper discusses the construction of a Road Power Generation unit, which when placed along a roadside can be considered as a green energy source. The mechanical system consists of a Savonius Rotor which captures the wasted energy produced by a moving vehicle and converts it into useful work done. Moreover, a solar panel converts the light energy from the sun to generate electricity through the Photovoltaic Effect. The project demanded designing and manufacturing of a wind turbine with solar energy tower. A wind turbine is essentially a vertical axis wind turbine specifically of the Savonius type. Research has been going on VAWT in order to study their performance parameters and introduce them in the market as a competitor to the conventional horizontal axis wind turbine (Menet, 2004). Furthermore, RPG units are the future of smart cities.

## REFERENCES

**Al-Kayiem, H. H., Bhayo, B. A., & Assadi, M.** (2016). Comparative critique on the design parameters and their effect on the performance of S-rotors. *Renewable Energy*, 99, 1306-1317. <https://www.infona.pl/resource/bwmetal.element.elsevier-ecfe7f09-5a99-3d0f-b5da-d7693769036a>

**Climate-Data.Org** (n.d.). <https://en.climate-data.org/asia/pakistan/sindh/karachi-992367/>

**Menet, J. L.** (2004). A double-step Savonius rotor for local production of electricity: a design study. *Renewable energy*, 29(11), 1843-1862. [https://econpapers.repec.org/article/eereenene/v\\_3a29\\_3ay\\_3a2004\\_3ai\\_3a11\\_3ap\\_3a1843-1862.htm](https://econpapers.repec.org/article/eereenene/v_3a29_3ay_3a2004_3ai_3a11_3ap_3a1843-1862.htm)

**Shah, M. H., & Alsibiani, S. A.** (2020). Design and construction of Savonius Rotor. *3C Tecnología. Glosas de innovación aplicadas a la pyme* (October, Special Issue).

**Shah, M. H., Alandjani, G. O., & Ashgar, M.** (2020). Energy harvesting using kinetic energy of vehicles. *3C Tecnología. Glosas de innovación aplicadas a la pyme*, 9(2), 113-126. <http://doi.org/10.17993/3ctecno/2020.v9n2e34.113-126>



/04/

# DESIGN AND CONSTRUCTION OF SAVONIUS ROTOR

---

**Mirsad Hyder Shah**

Student, Technische Universitat Dortmund.  
Dortmund, (Germany).

E-mail: [Itsmirsadhyder@yahoo.com](mailto:Itsmirsadhyder@yahoo.com) ORCID: <https://orcid.org/0000-0003-2476-5887>

**Sameer Ali Alsibiani**

MD. Yanbu University College,  
Yanbu Industrial City, (Kingdom of Saudi Arabia).

E-mail: [Alsibianis@rcyci.edu.sa](mailto:Alsibianis@rcyci.edu.sa) ORCID: <https://orcid.org/0000-0003-1918-5175>

**Recepción:** 04/09/2020 **Aceptación:** 07/10/2020 **Publicación:** 13/11/2020

## **Citación sugerida Suggested citation**

Hyder, M., y Ali, S. (2020). Design and construction of Savonius rotor. *3C Tecnología. Glosas de innovación aplicadas a la pyme. Edición Especial, Noviembre 2020*, 65-77. <https://doi.org/10.17993/3ctecno.2020.specialissue6.65-77>

## ABSTRACT

Renewable energy sources have been researched for more than a century now. Wind energy; which is often characterized as an unreliable source of energy, is not unreliable if placed at places with smooth wind currents. Savonius rotor as Vertical Axis Wind Turbine (VAWT) can be used as a standalone power generation device because of its low cost, low cut-in speed and the fact that it can accept wind from any direction. S-Rotors when compared to other types of rotors have a lower Power Coefficient but factors like Overlap ratio, Aspect Ratio, Number of Blades and Blade shapes can affect its efficiency. This paper discusses the Design and construction of a Savonius wind turbine by studying how the factors above influence the rotor's performance. Finally, a Single-stage, Two blade conventional Savonius rotor with an Overlap Ratio of 0.1 and Aspect Ratio of 3.3 has been constructed and discussed below. Studies for choosing the best material have also been conducted and PolyVinyl Chloride (PVC) has been selected to prepare the blades from. According to the study conducted, the voltage output recorded at 5.4 m/s wind speed was 19.1 Volts.

## KEYWORDS

Savonius Rotor, Wind Turbine, S-Rotor, HAWT, VAWT.

# 1. INTRODUCTION

Wind turbines are classified into two categories: HAWT and VAWT. This classification refers to the position of rotor axis relative to wind direction. The Savonius rotor is thus used as vertical axis wind turbine like the other Darrieus rotor. S-Rotors or Savonius rotors have been employed as VAWT widely in the previous decades. The main reasons for which S- rotors are employed in residential areas are because they are self-starting, produce low noise and can accept wind energy from any directions. S-Rotors are also employed at places with low wind potential and where HAWTs cannot run. Since the  $C_p$  (Power Coefficient) of an S-Rotor is poor in large wind turbines, design parameters are altered as to improve the power coefficient by reducing the size of the rotor itself (Al-Kayiem, Bhayo, & Assadi, 2016).

The S-rotor was invented by Finnish engineer S. J. Savonius in 1925. As discussed earlier, S-Rotors are generally preferred over D-rotor because of low cut-in speeds and high torque, but their  $C_p$  is poor when compared with other wind turbines. In 1919, German physicist Albert Betz put forth what is known as the Betz theory. According to him, the theoretical maximum efficiency for a wind turbine is 59.3%. This value is generally known as the Betz limit for wind turbines (Al-Kayiem *et al.*, 2016).

Because of their superiority over other wind turbines, S-Rotors have been used to harness energy for various purposes; mainly power generation, to meet electricity demands (Al-Kayiem *et al.*, 2016).

## 2. RESEARCH DESIGN AND CONSTRUCTION

### 2.1. BLADES SHAFT AND COUPLING OF WIND TURBINE

For the design of blades and the selection of material for the wind turbine, following factors were taken into consideration:

- The blades of the windmill should not break if winds with high current cross the surface.
- The material should not decompose over time and not prone to rusting in harsh environment.

- The material should be easily accessible.
- The cost of the material should be low cost.
- The blades should be durable in the long run.

Considering all the reasons mentioned above, Polyvinyl Chloride (PVC) was the best choice available. After cutting the PVC to achieve the desired design the edges were smoothened with sandpaper.

**Table 1.** Parameters and Values of Blades Shaft and Coupling.

PARAMETERS	VALUES
Diameter of turbine	0.375 m
Volume of Blade	0.0395 m <sup>3</sup>
Diameter of Single Blade	0.203 m
Overlap distance	0.0381 m
Density of PVC	1467 kg/m <sup>3</sup>
Mass of PVC	3.8 kg
Blade angle	180°
Shaft Height	1.34 m
Shaft Diameter	0.036 m
Coupling Height	0.058 m
Bush size	0.02 m

The blades were weld to a shaft at an angle of 90 degrees, this enabled the blades to be rotated by wind currents. The shaft had to be strong enough to withstand strong gushes of wind and considering the work of Menet (2004); the shaft was made out of PVC.



**Figure 1.** AutoCAD vs Hardware of Blades and Shaft.



## 2.2. BASE OF WIND TURBINE

For the construction of the base, mild steel bars were welded together to provide stability to the whole design. For maximum stability a four legged stand base was proposed and implemented.

**Table 2.** Parameters and values of base height and diameter.

PARAMETERS	VALUES
Base Height	0.36 m
Base Diameter	0.56 m



**Figure 2.** AutoCAD vs Hardware of Base of Turbine.

## 3. IMPORTANT DESIGN PARAMETERS OF SAVNOIUS ROTORS

- Overlap Ratio.
- Aspect Ratio.
- Number of Blades.
- Number of Stages.
- Blade Shapes.

### 3.1. OVERLAP RATIO

The overlap ratio is ratio of the overlap distance (the distance by which the inner edge of the blade overlaps the inner edge of the adjacent blade) by the diameter of the entire turbine. As shown below in figure (Al-Kayiem *et al.*, 2016).

$$\text{Overlap Ratio} = \beta = \frac{e}{D}$$

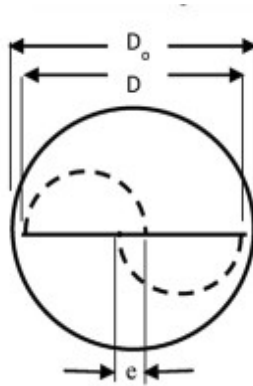


**Figure 3.** S-Rotor with Overlap ratio. **Source:** (Al-Kayiem *et al.*, 2016).

### 3.2. ASPECT RATIO

Aspect Ratio is the ratio of Rotor's height  $H$  to its Diameter  $D$ ;

$$\text{Aspect Ratio} = \frac{H}{D}$$

Increasing Aspect ratio increases performance and angular speed of the rotor. Aspect ratio is adjusted to meet the torque and RPM requirements of the generator, which will produce electricity (Al-Kayiem *et al.*, 2016).

Blackwell, Sheldahl, and Feltz (1978), experimentally concluded that increasing aspect ratio increased the power coefficient (while keeping all other parameters constant).

### 3.3. NUMBER OF BLADES

With an increase in the number of blades the power coefficient decreases. This decrease is due to the fact that, as the number of blades is increased, more wind is deflected by a blade from entering into the concave side of its adjacent blades (Al-Kayiem *et al.*, 2016).

Al-Kayiem *et al.* (2016) in his work concluded that S-Rotors indeed do perform better at low wind currents. It is also compared and concluded that two blades perform better than

three blades as more drag is wasted in the three-blade system. The  $C_p$  of two blade design is much better than a three-blade system.

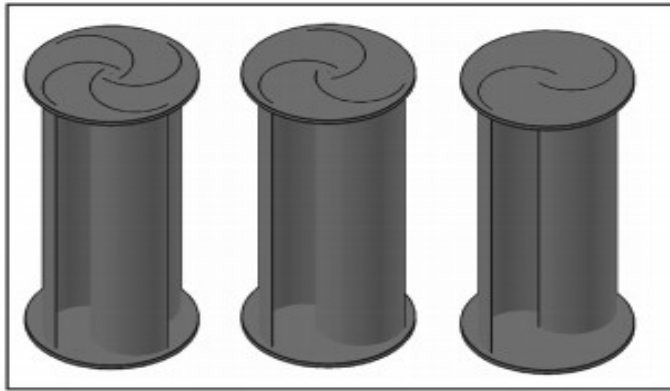


**Figure 4.** S-Rotor with various number of blades. **Source:** (Al-Kayiem *et al.*, 2016)

### 3.4. NUMBER OF STAGES

Number of stages mean one or more stages of an S-Rotor in a single design. This means that the wind currents will have more area to sweep through and better torque uniformity around 360 degrees. This eliminates the dead zones left by rotor's blades that are not rotating. Note that the stages of an S-Rotor are shifted at a specific phase shift angle.

In his paper, Al-Kayiem *et al.* (2016), debated that a Double staged S-Rotor may produce the best power coefficient as compared to a single or three staged S-Rotor. This explains the hypothesis that as the stages of an S-Rotor are increased it means if one of the stages of S-Rotor is rotating it must carry the inertia of the other stages since they are not producing any torque.

Saha, Thotla, and Maity (2008), in his experimental work, concluded that a single staged rotor gave a  $C_p$  of 0.18, a two-staged rotor gave a power coefficient of 0.29, while the three-staged demonstrated a  $C_p$  of only 0.23.

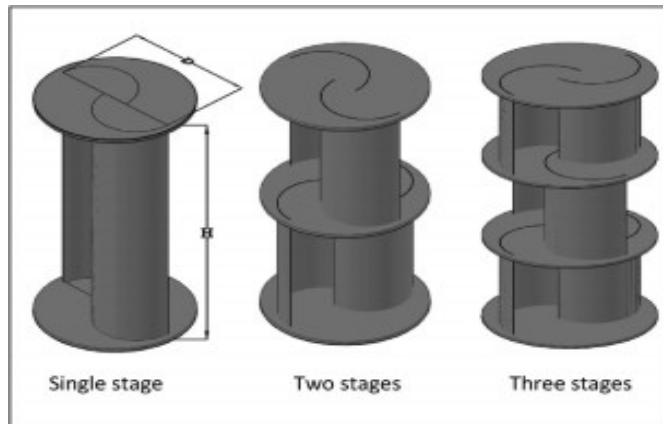


**Figure 5.** Single and Multistage S-rotors. **Source:** (Al-Kayiem *et al.*, 2016).

### 3.5. BLADE SHAPES

Although S-Rotors are generally similar S-shaped rotors, there have been few attempts to modify the blade shape in order to increase its aerodynamic property in order to increase the  $C_p$ .

Muscoloa and Molfinob (2014) simulated five different S-type VAWTs, including a simple S-Roto. In the four wind rotors, two were new models and two were proposed by Kyozuka (2008). The rotor named Bronzinus, performed the best and produced the highest power coefficient. But if the tip speed was crossed  $C_p$  of the wind rotor proposed by Menet (2004) was found to be superior.

## 4. FINAL DESIGN OF ROTOR AND ASSEMBLY

The Rotor assembly consisted of the following parts:

- Base:

The base was made up of mild steel. The purpose of the base was to hold the rotor in its place and provide a suitable height above the ground for the blades to face the wind. The PMDC motor was coupled under the base as well. To provide maximum strength Mild steel bars were welded in an L-shaped arrangement.

- Bearing & Bearing Housing:

The purpose of the bearing was to support the shaft and lessen the friction for the shaft to rotate. The bearing housing protects the bearing from any damage and restricts the movement of the shaft.

- Motor Housing:

Motor housing consists of two horizontal plates made of Mild Steel which will have the motor sandwiched in the between. The top end of the motor was secured to the assembly by screws.

- Rotor Shaft:

The rotor shaft was made up of PVC. Due to its high strength, Polyvinyl Chloride was chosen to withstand bending forces exerted by the rotating blades. The shaft had to be strong enough to withstand strong gushes of wind and considering the work of Menet (2004); the shaft was made out of PVC.

5. RESULTS

The parameters and values for the final design have been presented in Table 3. As the factors discussed above have been carefully considered such that the power coefficient of the rotor never drops. According to Al-Kayiem *et al.* (2016), the average Power Coefficient of an S-rotors under open flow conditions ranges from 0.037 to 0.37. However, the Power Coefficient of S-rotors with external flow guides can reach up to 0.52.

**Table 3.** Parameters and values of Final Design.

PARAMETERS	VALUES
Model type	Two blade conventional Savonius rotor
Height	1.25 m
Diameter	0.375 m
Area	0.456 m <sup>2</sup>
Aspect ratio	3.3
Overlap ratio	0.1
Number of stages	1
Number of Blades	2
Design of Blade	Conventional Blade

In the Figure 6, the AutoCAD drawing and the actual hardware are shown. As the Savonius rotor has a conventional blade design and it is a two blade system. Furthermore, it uses minimal area and takes only 0.456 m<sup>2</sup> of area. The factors affecting the power coefficient of the S-rotor have also been calculated and presented.



**Figure 6.** AutoCAD vs Hardware of S-rotor.

In Table 4, the results for the wind turbine have been shown. The velocity of the wind was measured using an anemometer which was placed right in front of the rotor. The wind made the rotor move as intended. However, the maximum wind velocity that could be simulated was 5.4 m/s. On the Beaufort Scale, such a wind speed has a Beaufort number of 3 and is considered as a Gentle Breeze only. But due to the rotor being lightweight it was easily rotated, and enough Revolutions were generated. At a windspeed of 5.4 m/s, the generator under the S-Rotor generated 19.1 Volts.

**Table 4.** Results of Wind Turbine.

WIND SPEED m/s	RPM	VOLTAGES
4.1	200	14.91V
4.5	241	17.0V
4.9	253	18.17V
5.1	265	18.64V
5.4	302	19.1V

## 6. CONCLUSION

This paper presented a study in which S-rotors have been employed as a power generation unit. The design and construction of a Savonius rotor has been carried out in this paper and S-rotors have been proved to be used in power generation units. S-Rotors are generally highly affected by varying geometric parameters and blade shapes. S-rotors produce high starting torques and low cut-in speeds. Furthermore, factors such as Overlap Ratio, Aspect ratio, number of blades and number of stages have been briefly discussed in this paper. It is also concluded that by increasing/decreasing the factors discussed above, the Power Coefficient of the wind turbine varies. For the design of blades and the selection of material for the wind turbine, Poly Vinyl Chloride (PVC) was chosen as the best material available. It was chosen mainly because of its low cost and durability. Furthermore, choosing the suitable Aspect and Overlap ratio is a difficult task but from the work of Blackwell *et al.* (1978) it can be inferred that keeping the Overlap ratio to a minimal and increasing the Overlap ratio; increased the power coefficient of the Savonius Rotor. Finally, for a better power coefficient, the authors predict a two blade two stage rotor will do a better job for conventional wind turbines but will prove ineffective if the wind currents are equally distributed from the top to the bottom on the whole blade design.

## REFERENCES

- Al-Kayiem, H. H., Bhayo, B. A., & Assadi, M.** (2016). Comparative critique on the design parameters and their effect on the performance of S-rotors. *Renewable Energy*, 99, 1306-1317. <https://doi.org/10.1016/j.renene.2016.07.015>
- Blackwell, B. F., Sheldahl, R. E., & Feltz, L. V.** (1978). Wind tunnel performance data for two-and three-bucket Savonius rotors. *Journal of Energy*, 2(3), 160-164. <https://pdfs.semanticscholar.org/9c43/b666ff48d4396dc6a42cb27eb9f6a6563c21.pdf>
- Kyozuka, Y.** (2008). An experimental study on the Darrieus-Savonius turbine for the tidal current power generation. *Journal of Fluid Science and Technology*, 3(3), 439-449. <https://doi.org/10.1299/jfst.3.439>

- Menet, J. L.** (2004). A double-step Savonius rotor for local production of electricity: a design study. *Renewable energy*, 29(11), 1843-1862. <https://doi.org/10.1016/j.renene.2004.02.011>
- Muscoloa, G. G., & Molfinob, R.** (2014). From Savonius to Bronzinus: a comparison among vertical wind turbines. *Energy Procedia*, 50, 10-18. <https://doi.org/10.1016/j.egypro.2014.06.002>
- Saha, U. K., Thotla, S., & Maity, D.** (2008). Optimum design configuration of Savonius rotor through wind tunnel experiments. *Journal of Wind Engineering and Industrial Aerodynamics*, 96(8-9), 1359-1375. <https://doi.org/10.1016/j.jweia.2008.03.005>





/05/

# AUGMENTED REALITY BASED GESTURE DETECTION & OBJECT CREATION SYSTEM USING XCODE & ARKIT

---

**Sallar Khan**

Sir Syed University of Engineering and Technology, Karachi, (Pakistan).  
E-mail: [Sallarkhan\\_92@yahoo.com](mailto:Sallarkhan_92@yahoo.com) ORCID: <https://orcid.org/0000-0001-8988-3388>

**Syed Abbas Ali**

N.E.D University of Engineering and Technology, Karachi, (Pakistan).  
E-mail: [saaj.research@gmail.com](mailto:saaj.research@gmail.com) ORCID: <https://orcid.org/0000-0001-6014-1559>

**Muhammad Nadeem**

Sir Syed University of Engineering and Technology, Karachi, (Pakistan).  
E-mail: [mnadeem79@gmail.com](mailto:mnadeem79@gmail.com) ORCID: <https://orcid.org/0000-0002-9271-5008>

**Raj Chawla**

Sir Syed University of Engineering and Technology, Karachi, (Pakistan).  
E-mail: [rajchawlas72@gmail.com](mailto:rajchawlas72@gmail.com) ORCID: <https://orcid.org/0000-0003-1289-3849>

**Recepción:** 04/09/2020 **Aceptación:** 29/09/2020 **Publicación:** 13/11/2020

## **Citación sugerida Suggested citation**

Khan, S., Abbas, S., y Chawla, R. (2020). Augmented reality based gesture detection & object creation system using XCode & ARKit. *3C Tecnología. Glosas de innovación aplicadas a la pyme. Edición Especial, Noviembre 2020*, 79-91. <https://doi.org/10.17993/3ctecno.2020.specialissue6.79-91>

## ABSTRACT

In this modern era of mobile applications, Augmented Reality (AR) is becoming one of the emerging areas of implementation for researchers around the globe. While live gesture detection and 3D model creation still need more attention from researchers. In this paper, we present an interactive AR character that directly interacts with real objects. The interactive AR character automatically determines how to behave and to control real objects. This current research presents three studies that test the social psychological effects of Augmented Reality. In this research, we are using Apple's IDE for native iOS development on swift, XCode for UI design and architectural functionalities of our application. We used the ARKIT library to import all the necessary functions and classes to manipulate and use according to our needs. Finally, we successfully deployed an IOS application which can detect live gestures of our hand movements and then create 3D models with the help of our hand gestures.

## KEYWORDS

Augmented Reality, Hand Gestures, 3D Model Creation, IOS Application, Apple, XCode, ARKit.

# 1. INTRODUCTION

Augmented Reality (AR) is a grand vision where the digital domain blends with the physical world. Information not only follows a person, but also her very gaze: looking at an object is enough to retrieve and display relevant information, amplifying her intelligence. Though research on AR has advanced over the last several decades, AR technology has yet to reach the mass-market. The minimum requirement for AR is a display, a camera for tracking, and a processing unit. These are also the components of camera phones, predicted to account for more than 80 percent of total worldwide mobile phone sales by 2010.

The average person learns better by observing and listening something than by simply reading something. We will be using this specific property of the human mind to accelerate learning. Although there are thousands of videos on the internet about almost every field of life but they're mostly from the perspective of video makers. By combining AR with learning and practicing we will provide immersive learning experience to our users in a way that the information settles in the long-term memory, with control over their interaction with the object they experiment as the way they want it. AR being the in the top 5 technologies of 2019 is momentous for the upcoming future as users incline towards augmented virtual experiences. With AR users can experience and interact with things that would be physically inaccessible or inconvenient otherwise. Our product will cater to users from students to professionals belonging to diversified fields of life and practice. The ability to touch and interact with augmented models in real time space is a new to the industry of Augmented Reality and our app is one of a kind with its ability to utilize real world spaces and objects to detect and write with our bare hands or using any object, from your ordinary pen, to any object with a pointed end. Users can write and then save their work to resume or view later.

# 2. RELATED WORK

This research describes experiences with development of an AR application for augmentation of an industrial robot. The paper focuses on the description of the application requirements and prototype implementation (Löfvendahl, 2014). Another application is Robotic Modeling Assistant (RoMA), an interactive fabrication system providing a fast,

precise, hands-on and in-situ modeling experience. As a designer creates a new model using RoMA AR CAD editor, features are constructed concurrently by a 3D printing robotic arm sharing the same design volume.

The partially printed physical model then serves as a tangible reference for the designer as she adds new elements to her design. RoMA's proxemics-inspired handshake mechanism between the designer and the 3D printing robotic arm allows the designer to quickly interrupt printing to access a printed area or to indicate that the robot can take full control of the model to finish printing. RoMA lets users integrate real-world constraints into a design rapidly, allowing them to create well-proportioned tangible artifacts or to extend existing objects. We conclude by presenting the strengths and limitations of our current design (Peng *et al.*, 2018).

An app that is based on usage of AR in historical recreation as well as it elaborates previous work that has been done in this area and gives knowledge about technologies that allows creating application for AR oriented historical site. This app will showcase various ancient artifacts and heritage sites across the world showing how important history is how we can learn from the immaculate and genius architecture and solutions of the past that those people came up with much lesser resources (Desai, 2018).

An Augmented Reality application for mobile devices that promoted and supports the learning of geometric figures. The application is named AGeRA, consists of a geometry book and software capable of reading special markers inserted into the book's content. When this book is placed in front of the camera of a mobile device, 3D objects, sounds, animations, and other interactive elements leap from book pages making learning more immersive and interesting. Tests were made with teachers and students and showed good acceptance of the application to support the teaching of geometry (Neto, 2013).

An android based app has been developed in Indonesia help the Indonesian students to learn Batik. Pre-test and post-test are administered to check whether the application is improving the spatial intelligence of the students. This android based application was based on Augmented Reality Batik Ikonik (ARtikon) Joyful. First registration to the app is required by logging in with matching usernames and password. After successfully logging in the

camera will be activated. All the 2D and the 3D objects will reflect in the Batik patterns by this app while the object will remain unidentified if the object is in 2D (Widiaty *et al.*, 2017).

KUFSGT a school of Global tourism at Kyoto University of Foreign studies collaborated with MAVR, an immersive learning group in Japan, for augmented learning environments. With the help of AREiantation, application which simplifies the workflow of AR contents so in seconds the idea can be prototyped. On the open campus they created an area for the activities they call ARVR experience zone. These activities included KUFSGO and MY HOMETOWN PROJECT (Hawkinson, 2019). An application was developed in India that scans the menu of any restaurant to provide ratings to each dish on the menu by the help of OCR. These rating were given by the sentiment analysis over the reviews provided by the customers. For a better experience, these menus have an AR system that projects the rating for the dishes (Wang, Chen, & Lang, 2015).

A researcher developed an innovation by the implementation of Augmented Reality technology in natural sciences learning of elementary school. The method that was used in this research was the method based on the Ball and George theory, which contained ten stages: Research and information collecting, Planning, Develop preliminary form of product, Preliminary field testing, Main product revision, Main field testing, Operational product revision, Operational field testing, Final product version and Dissemination and implementation (Fakhrudin, 2018).

A research was conducted; the purpose of this research was to calculate the impact of Augmented Reality mobile applications on the learning motivation of health science students of University of Cape Town. The ACRS (attention, relevance, confidence and satisfaction) model measured the impact of Augmented Reality on a student's motivation, and the Instructional Materials Motivation Survey guided the way to design the research instrument. A total of 78 participants used the Augmented Reality mobile application, and the result showed that satisfaction, attention and confidence factors were significantly increased. However, the decrease in relevance factor was proved to be insignificant (Khan *et al.*, 2019).

A new software system is developed by Brown University researchers that turns cell phones into Augmented Reality portals, enabling users to place virtual building blocks, furniture

and other objects into real-world backdrops, and use their hands to manipulate those objects as if they were here. The developers are hoping the new system that can be a tool for artists, designers, game developers and others to experiment with Augmented Reality (AR). The team will present at the ACM Symposium on User Interface Software and Technology (UIST 2019) in New Orleans. The source code for Android is freely available for download on the researchers' website, and iPhone code will follow soon (Brown University, 2019).

Physics education applications AR, which has been developed extensively in recent years, have a lot of restrictions in terms of accuracy and performance. The purpose of our research is to develop a real-time simulation system for physics education that is based on parallel processing. In this research, we present a video see-through AR (Augmented Reality) system that includes an environment recognizer using a depth image of Microsoft's Kinect V2 and a real-time soft body simulator based on parallel processing using GPU (Graphic Processing Unit). Soft body simulation can provide more realistic simulation results than rigid body simulation, so it can be more effective in systems for physics education. We have designed and implemented a system that provides the physical deformation and movement of 3D volumetric objects and uses them in education. We plan to use the stand-alone AR device including one or more cameras to improve the system in the future (Sung *et al.*, 2019).

Mobile devices are becoming a common target for Augmented Reality applications, especially for showing contextual information in buildings or construction sites. A prerequisite of contextual information display is the localization of objects and the device in the real world. In this research, we will present our approach to the problems of mobile indoor localization with a building model. The approach does not use external sensors or input. Accurate external sensors such as stationary cameras are expensive and difficult to set up and maintain. Relying on already existing external sources may also prove to be difficult, as especially inside buildings, Internet connections can be unreliable and GPS signals can be inaccurate. Therefore, we try to find a localization solution for Augmented Reality devices that can accurately localize itself only with data from internal sensors and preexisting information about the building. If a building has an accurate model of its geometry, we can use modern spatial mapping techniques and point-cloud matching to find a mapping between local device coordinates and global model coordinates. We use normal analysis and 2D template matching on an inverse distance map to determine



this mapping. The proposed algorithm is designed to have a high speed and efficiency, as mobile devices are constrained by hardware limitations. We show an implementation of the algorithm on the Microsoft HoloLens, test the localization accuracy, and use cases for the technology (Herbers & König, 2019).

Industrial Augmented Reality (AR) applications demand high on the visual consistency of virtual-real registration. To present, the marker-based registration method is most popular because it is fast, persistent, and convenient to obtain the registration matrix. The registration matrix should multiply an  $o$  set matrix that describes the transformation between the attaching position and the initial position of the marker relative to the object.

However, the  $o$  set matrix is usually measured, calculated, and set manually, which is not accurate and convenient. This paper proposes an accurate and automatic marker object of set matrix calibration method. First, the normal direction of the target object is obtained by searching and matching the top surface of the CAD model. Then, the spatial translation is estimated by aligning the projected and the imaged top surface. Finally, all six parameters of the  $o$  set matrix are iteratively optimized using a 3D image alignment framework. Experiments were performed on the publicity monocular rigid 3D tracking dataset and an automobile gearbox.

The average translation and rotation errors of the optimized  $o$  set matrix are 2.10 mm and 1.56 degree respectively. The results validate that the proposed method is accurate and automatic, which contributes to a universal  $o$  set matrix calibration tool for marker-based industrial AR applications (Yin *et al.*, 2019).

This current research presents three studies that test the social psychological effects of Augmented Reality.

Study 1 examined participants' task performance in the presence of embodied agents and replicated the typical pattern of social facilitation and inhibition. Participants performed a simple task better, but a hard task worse, in the presence of an agent compared to when participants complete the tasks alone. Study 2 examined nonverbal behavior. Participants meet an agent. Participants wearing the headset never sat directly on the agent when given the choice of two seats, and while approaching, most of the participants chose the

rotation direction to avoid turning their heads away from the agent. A separate group of participants chose a seat after removing the Augmented Reality headset, and the majority still avoided the seat previously occupied by the agent. Study 3 examined the social costs of using an Augmented Reality headset with others who are not using a headset. Participants talked in dyads, and Augmented Reality users reported less social connection to their partner compared to those not using Augmented Reality. Overall, these studies provide evidence suggesting that task performance, nonverbal behavior, and social connectedness are significantly affected by the presence or absence of virtual content (Miller *et al.*, 2019). In the research field of Augmented Reality (AR), applications using interactive characters have been developed as the form of giving users information such as LEGO assembly guidance and explanation about historical artifacts. Even though these characters respond to interaction with users, they could not create substantial effects or changes in a real space. Therefore, this limitation makes users reduce their coexistence with the AR characters.

In this paper, we present an interactive AR character that directly interacts with real objects. The interactive AR character automatically determines how to behave and to control these objects. At first, we make working space populated by AR characters that has a real object with which the AR character can interact. As an interactive AR character, we implement ARMate, which presents realistic responses according to changes of real objects manipulated by a user in real time. We develop ToyCart as a physical object that includes hardware devices for movement, and ARMate can control ToyCart. Finally, we expect that our AR character can increase coexistence through real object-based interaction (Kang & Woo, 2011).

### 3. METHODOLOGY

#### 3.1. XCODE

Using apple's IDE for native iOS development on swift, we used XCode to design the UI and architectural functionalities of our application. We used the ARKIT library to import all the necessary functions and classes to manipulate and use according to our needs. We then designed the UI of the application based on the Apple's modern iOS design language. The progression of development of our app was divided into 2 phases, first being the UI/

UX of the application, and second being the main programming and functionality of the application.

As the application is based on iOS and developed on XCode, we used the following libraries to construct our application.

### 3.2. ARKIT

Apple's AR Kit is a powerful library and tool that enables us to use already written code according to our functionality needs and modify it accordingly. Using the camera on iPhone or iPad it can detect live people in the real environment and track their motions and movements. We used this feature to track the hand or object movement that will enable us to draw and write in real time using the front or back camera of the device using our hands or objects. AR Kit also enabled us to make anything 3D after drawing it in 2D on any surface using its animation tools. ARKit is based on two main features, the camera in a location for a 3D space and the second main feature is the detection of horizontal plane. To make it possible the camera of your phone assumes that it is in an actual 3D space and placing some 3D object will pinpoint in real 3D space. Then the ARKit detects the horizontal surface and places the object on top of it. So how the ARKit can perform this? This is done through a simple technique known as Visual Inertial Odometry (VIO). In 3D space, to track the location of the device with the help of motion sensors fused with camera frames, this technique is known as VIO. By detecting the edge points in the image with high contrast we can track the motion of the camera frames.

It estimates where the device is in the 3D space, by detecting how much of these points relatively moved to each other from one frame to another frame. This is the sole reason why ARKit couldn't work with a white wall in the background or when the device is moving too fast to detect the 3D space which causes to create blurred images. We can create a new ARKit project from New > Project > Augmented Reality App. It is more accessible to begin the AR tutorial with the official Apple ARKit sample, which make plane detection more feasible.

## 4. RESULTS

By successfully integrating everything together, this is the result of our AR application. Firstly as seen below the yellow box detects your fingers or any other pointing object and then starts tracking it:

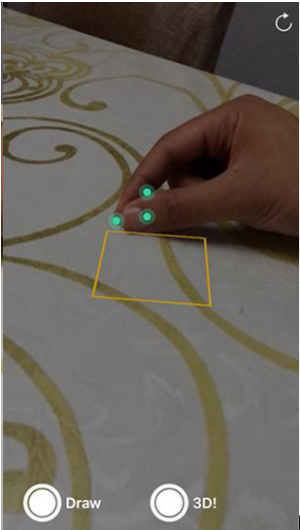


**Figure 1.** Tracking process of hand and its gestures.

After successfully track locking the finger/object, a red dot appears which will act as a pen to draw on the surface below:

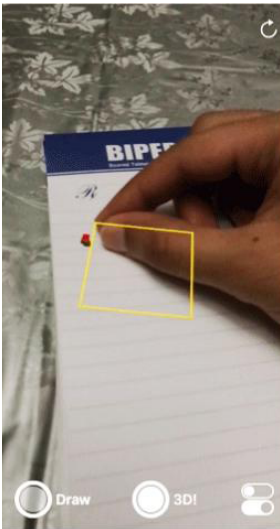


**Figure 2.** Implementation of drawing with the help of hand gestures.

Result of this can be seen below as after successfully tracking and drawing:

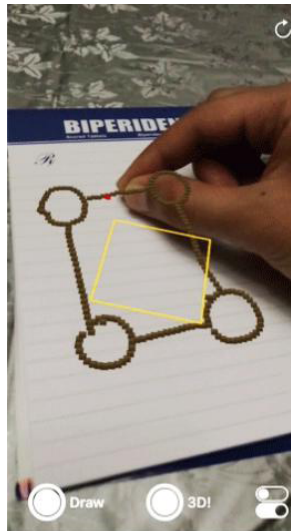


**Figure 3.** The desired 3D model is drawn successfully.

## 5. CONCLUSION

AR is one of the fastest future technologies that will soon become a huge part of our everyday lives, and with huge conglomerates adopting it such as Google, Apple, Facebook, it will soon be a must with everything.

Keeping that in mind, and the fact that immersive learning is so much of a better experience than the more traditional forms of learning such as text and video, it is bound to get attention and appreciation for the awe factor it cases. Technology has come a long way and not to use it to its full potential would be a waste of all the hard work put in by scientists and engineers to bring that innovation to the table of everyday common man so he can rejoice life and maybe one step at a time make it easier and convenient for him.

## REFERENCES

**Brown University.** (2019). *New augmented reality system lets smartphone users get hands-on with virtual objects.* ScienceDaily. <https://www.sciencedaily.com/releases/2019/10/191016153703.htm>

- Desai, N.** (2018). Recreation of history using augmented reality. *ACCENTS Transactions on Image Processing and Computer Vision*, 4(10), 1–5. <https://doi.org/10.19101/tpcv.2017.39019>
- Fakhrudin, A.** (2018). The Implementation of Augmented Reality Technology in Teaching Natural Sciences to Improve Elementary Students' Learning Achievement. *Al-Ta Lim Journal*, 25(1), 13. <https://doi.org/10.15548/jt.v25i1.374>
- Hawkinson, E.** (2019). *Student Designs in Augmented Tourism*. <https://medium.com/ready-teacher-one/student-designs-in-augmented-tourism-bc168bc5f7f>
- Herbers, P., & König, M.** (2019). Indoor localization for augmented reality devices using BIM, point clouds, and template matching. *Applied Sciences (Switzerland)*, 9(20). <https://doi.org/10.3390/app9204260>
- Kang, C., & Woo, W.** (2011). ARMate: An Interactive AR Character Responding to Real Objects. In Chang M., Hwang WY., Chen MP., Müller W. (eds) *Edutainment Technologies. Educational Games and Virtual Reality/Augmented Reality Applications*. Edutainment 2011. Lecture Notes in Computer Science, vol. 6872. Springer, Berlin, Heidelberg. [https://doi.org/10.1007/978-3-642-23456-9\\_3](https://doi.org/10.1007/978-3-642-23456-9_3)
- Khan, T., Johnston, K., & Ophoff, J.** (2019). The Impact of an Augmented Reality Application on Learning Motivation of Students. *Advances in Human-Computer Interaction*, Article ID 7208494. <https://doi.org/10.1155/2019/7208494>
- Löfvendahl, B.** (2014). *Augmented Reality Applications for Industrial Robots*. Umeå University. Department of Applied Physics and Electronics. <https://www.diva-portal.org/smash/get/diva2:706980/FULLTEXT01.pdf>
- Miller, M. R., Jun, H., Herrera, F., Villa, J. Y., Welch, G., & Bailenson, J. N.** (2019). Social interaction in augmented reality. *PLoS ONE*, 14(5), 1–27. <https://doi.org/10.1371/journal.pone.0216290>
- Neto, F. M. M.** (2013). Technology platform innovations and forthcoming trends in ubiquitous learning. In *Technology Platform Innovations and Forthcoming Trends in Ubiquitous Learning* <https://doi.org/10.4018/978-1-4666-4542-4>

- Peng, H., Briggs, J., Wang, C. Y., Guo, K., Kider, J., Mueller, S., Baudisch, P., & Guimbretière, F.** (2018). Roma: Interactive fabrication with augmented reality and a Robotic 3D printer. *Conference on Human Factors in Computing Systems - Proceedings, 2018* (April). <https://doi.org/10.1145/3173574.3174153>
- Sung, N. J., Ma, J., Choi, Y. J., & Hong, M.** (2019). Real-time augmented reality physics simulator for education. *Applied Sciences (Switzerland)*, 9(19), 2019. <https://doi.org/10.3390/app9194019>
- Wang, C. Y., Chen, Y., & Lang, Z.** (2015). Restaurant Menu Expert A digital image processing pipeline to increase the accuracy of the state-of-the-art OCR algorithm. [https://web.stanford.edu/class/ee368/Project\\_Autumn\\_1516/Reports/Wang\\_Cheng\\_Lang.pdf](https://web.stanford.edu/class/ee368/Project_Autumn_1516/Reports/Wang_Cheng_Lang.pdf)
- Widiaty, I., Riza, L. S., Danuwijaya, A. A., Hurriyati, R., & Mubaroq, S. R.** (2017). Mobile-based augmented reality for learning 3-dimensional spatial Batik-based objects. *Journal of Engineering Science and Technology*, 12(Special Issue 10), 12–22. [https://www.researchgate.net/publication/336603527\\_EDUCATIONAL\\_DIGITAL\\_MEDIA\\_FOR\\_TRADITIONAL\\_FOOD\\_OF\\_KAMPUNG\\_ADAT\\_CIREUNDEU\\_AN\\_ETHNOPEDAGOGY\\_PERSPECTIVE](https://www.researchgate.net/publication/336603527_EDUCATIONAL_DIGITAL_MEDIA_FOR_TRADITIONAL_FOOD_OF_KAMPUNG_ADAT_CIREUNDEU_AN_ETHNOPEDAGOGY_PERSPECTIVE)
- Yin, X., Fan, X., Yang, X., Qiu, S., & Zhang, Z.** (2019). An automatic marker-object offset calibration method for precise 3D augmented reality registration in industrial applications. *Applied Sciences (Switzerland)*, 9(20). <https://doi.org/10.3390/app9204464>

/06/



# MULTIPLE FAULTS DETECTION AND IDENTIFICATION OF THREE PHASE INDUCTION MOTOR USING ADVANCED SIGNAL PROCESSING TECHNIQUES

---

**Majid Hussain**

PhD Scholar IICT, Mehran University of Engineering and Technology.  
Jamshoro, (Pakistan).

E-mail: [majidhussain@quest.edu.pk](mailto:majidhussain@quest.edu.pk) ORCID: <https://orcid.org/0000-0002-5581-1260>

**Rana Rizwan Ahmed**

Department of Electronic Engineering, Mehran University of Engineering and Technology.  
Jamshoro, (Pakistan).

E-mail: [rizwan.ese@gmail.com](mailto:rizwan.ese@gmail.com) ORCID: <https://orcid.org/0000-0001-7449-3715>

**Imtiaz Hussain Kalwar**

Department of Electrical Engineering, DHA SUFFA University.  
Karachi, (Pakistan).

E-mail: [imtiaz.hussain@dsu.edu.pk](mailto:imtiaz.hussain@dsu.edu.pk) ORCID: <https://orcid.org/0000-0002-7947-9178>

**Tayab Din Memon**

NCRA CMS Lab, Mehran University of Engineering and Technology.  
Jamshoro, (Pakistan).

E-mail: [tayabdin82@gmail.com](mailto:tayabdin82@gmail.com) ORCID: <https://orcid.org/0000-0001-8122-5647>

**Recepción:** 07/09/2020 **Aceptación:** 02/10/2020 **Publicación:** 13/11/2020

## **Citación sugerida Suggested citation**

Hyder, M., y Ali, S. (2020). Multiple faults detection and identification of three phase induction motor using advanced signal processing techniques. *3C Tecnología. Glosas de innovación aplicadas a la pyme. Edición Especial, Noviembre 2020*, 93-117. <https://doi.org/10.17993/3ctecno.2020.specialissue6.93-117>

## ABSTRACT

In this paper, we have presented the multiple fault detection and identification system for three-phase induction motor. Fast Fourier Transform (FFT) is the most used signal processing technique that offers good frequency information but failing in providing time information and handling multiple faults identification with their occurrence time. FFT also fails to detect non-stationary condition of the signal and unable to convey sudden changes, start and end of the events, drifts and trends. To obtain simultaneous time frequency information and to deal with non-stationary signals Short Time Fourier Transform (STFT) is considered optimal technique that can clearly provide time and frequency information both. In this research work, the multiple fault detection and identification system is presented by employing Short Time Fourier Transform (STFT) signal processing technique. The proposed model is designed using current signature analysis method (CSAM) for three major faults including three phase supply imbalance, single phasing condition and breakage of rotor bars. The system is simulated in MATLAB/SIMULINK and simulation is performed based on healthy and unhealthy conditions of the motor. Comparative analysis between FFT and STFT, shows STFT as a promising approach.

## KEYWORDS

Induction Motor, STFT, Matlab/Simulink, Current Signature Analysis, Power Supply Imbalance, Single Phasing, Broken Rotor Bar.

# 1. INTRODUCTION

An Induction motor is the main source of mechanical power in almost every industry including sugar, fertilizer, packing, agriculture lands, domestic and commercial water supply schemes, water filtration, RO plant, locomotives etc. Apparently, induction motors are widely accepted in industrial processes as well due to its robustness, cost effectiveness, capability to operate in rough environment and less error chance (Pandey, Zope, & Suralkar, 2012; Mortazavizadeh & Mousavi, 2014; Nandi, Toliyat, & Li, 2005; Soother & Daudpoto, 2019). However, like other motors induction motor also faces several faults due to its operating environment and usage conditions. Most of the faults are due to load variations and improper power supply arrangements (Nandi *et al.*, 2005; Soother, Daudpoto, & Shaikh, 2018).

There are many electrical and mechanical faults related to both stator and rotor. Most described faults in the literature related to the rotor are bearing faults, broken rotor and end rings faults, and air gap eccentricity faults (Nandi *et al.*, 2005; Mortazavizadeh & Mousavi, 2014). The faults related to the stator are imbalance in the supply phase voltages, under or over voltage, single phasing condition, reverse phase sequence and inter turn short circuit fault etc. (Nandi *et al.*, 2005; Mortazavizadeh & Mousavi, 2014).

Presently much work is reported in this area to find, isolate and identify different types of the faults and avoid plant shutdown i.e., health of the motor is diagnosed by monitoring certain parameters. The parameter may be the vibration, torque, flux, temperature, current etc. (Mortazavizadeh & Mousavi, 2014; El Bouchikhi, Choqueuse, & Benbouzid, 2015). The condition monitoring makes it possible to detect any abnormal behavior in the motor at an early stage so that any big loss can be avoided (Gao, Cecati, & Ding, 2015). After observing any abnormal condition, the necessary preventive maintenance strategies can be applied for the removal of faults Unlike corrective maintenance strategy in which correction applied after fault has gone through motor and motor operation is disturbed (Mal *et al.*, 2020; Ujjan *et al.*, 2020). In this case, motor may be seriously damaged and can cause unrecoverable loss to the plant.

Many researchers have been working in the field of condition monitoring for fault detection and identification using different fault diagnoses schemes including vibration, thermal,

chemical and electrical (Nandi *et al.*, 2005; Mortazavizadeh & Mousavi, 2014; Gao *et al.*, 2015). In vibration monitoring, faults are identified based on intensity of vibrations in healthy and unhealthy conditions. Vibration monitoring sometimes gives ambiguous result when there are fluctuations in the load so thermal monitoring is employed, in which temperature of the different sections of the machine is monitored and faults identified based on the sensors located at different sections on the motors. Thermal technique does not give good results when there are multiple faults in the motor and multiple temperature sensors requirement make it costly (Siddiqui *et al.*, 2014).

Another technique previously used for fault detection is Air-Gap Torque monitored. In this technique motor torque is measured and non-zero frequency of the torque describes the faulty situation of the machine. Its main drawback is that there is no specific mathematical model available for fault signature (Gao *et al.*, 2015). Stator power analyses is another useful technique used previously for unbalance fault detection in which spectral and AC components of the power signal are measured in all three phases. This technique fails to produce good results for low intensity faults (Sharma *et al.*, 2015).

Nowadays, most used technique for condition monitoring of the motor is Motor Current Signature Analyses (MCSA). In MCSA stator current is continuously acquired and after applying a signal processing technique at current signal the frequency spectrum gives the knowledge about the health of the motor (Benbouzid, 2000; Zhongming & Bin, 2000; Gao *et al.*, 2015). The signal processing technique to be applied depends upon the type of the fault to be detected and nature of the fault. Some types of faults are low intensity in nature. Sometimes only information about frequency component of the signal is desired and, in some cases, both time and frequency information are required. So, it depends upon the fault which signal processing technique will be suitable for it (Nandi *et al.*, 2005; Mortazavizadeh & Mousavi, 2014). The most common signal processing techniques employed are FFT, Short time Fourier Transform (STFT), wavelet transform (WT), Hilbert-Huang transform (HHT) and Wigner-Ville Distribution (WVD) (Gao *et al.*, 2015).

In Mehala and Dahiya (2008), Cusidó *et al.* (2008), and El Bouchikhi *et al.* (2015), authors have reported comparative study on different signal processing techniques and compared the results for broken rotor bar fault using FFT, STFT and wavelet transform. With variable

FFT does not provides better results and misses to provide useful information like start and end of the event, changes in load etc. So, a new algorithm is proposed by using STFT and WT to achieve better results. It is further reported that each technique has advantages and disadvantages that depends upon the application and constraint for example – performance, complexity, and desired results. It is not advisable to use STFT and WT for ordinary fault where only frequency information is needed. No doubt WT provides better results as compared to STFT but wavelet transform is complex in nature, as signal is divided into high and low frequency parts, therefore requires more calculations and computation time. It always remains an issue of selecting the basis for wavelets which matches with type of information is required. Interpreting the results of the wavelets also requires skill. STFT is the trade-off technique between FFT and WT. STFT provides better results for ordinary faults both in time and frequency domain with less effort. In Mirabbasi, Seifossadat, and Heidari (2009), authors have detected unbalance in supply voltages using FFT. In Liang *et al.* (2002), and Messaoudi and Sbita (2010), authors have detected unbalance supply fault and broken rotor bar fault using FFT. In Mehrjou *et al.* (2010), Shi *et al.* (2014), and Siddiqui and Giri (2012), wavelet transform is employed for broken rotor bar fault detection. In Da Silva, Povinelli, and Demerdash (2008), authors have used stator current envelope analyses for broken rotor bar fault and stator short circuit fault detection. In Çalış and Çakır (2008) zero crossing time technique for rotor bar fault is employed. In Haggag and Mageed (2013) authors have developed unity relation in which instantaneous voltage and its complement are squared in order to detect Single Phasing condition.

This research work presents the detection and identification of three types of motor faults using short time Fourier transform (STFT) namely a) Imbalance of supply Voltage b) Single Phasing of supply and c) broken rotor bars. It also presents the simultaneous detection of multiple faults.

Further this paper proceeds as follows. Section 2 describes possible reasons and impacts of faults in induction motor, Section 3 presents the simulation and mathematical model of induction motor with description of STFT, Section 4 presents comparative results of the proposed system in terms of FFT and STFT analysis, and Section 5 concludes the research.

## 2. CAUSES AND EFFECTS OF FAULTS OVER INDUCTION MOTOR

In subsequent sections causes and effects of the faults over induction motor performance and stator current are discussed in detail that is followed by system modeling and simulations.

### 2.1. IMBALANCE SUPPLY VOLTAGE

There are several reasons for the imbalance in the power supply voltages. In Pakistan imbalance voltage condition is frequently faced in domestic, industrial and especially agriculture sector. The induction motors in the agriculture lands are located very far from the electrical substation. So, a very long distribution line and poor arrangement of electrical equipment causes too much voltage fluctuations and sometimes single phasing condition occurs, which can destroy the motor permanently. So, motor with applied imbalance voltage or in single phasing condition must not run for longer time to avoid any damage. Single phasing is most serious condition that induction motor faces and it can permanently damage the motor. The reasons for single phasing may include blowing of Line fuse, supply terminal loosening, connection of motor from a distribution transformer located very far, distribution transformer phase opening, Power supply wiring conductors may face unequal impedance (Mirabbasi *et al.*, 2009; Lee, 1999).

The imbalance and single phasing condition cause several adverse effects on the performance of the induction motor. According to National Electrical Manufacturers Association (NEMA), for a better life of induction motor it should not be operated with more than 5% unbalance in the supply (Quispe, Gonzalez, & Aguado, 2004). Due to unbalance supply motor may experience negative and pulsating torque which may produce excessive noise. The imbalance will also increase the current imbalance in windings and temperature of the motor; this can reduce the life and efficiency of the motor.

### 2.2. EFFECT OF SUPPLY VOLTAGES ON STATOR CURRENT

The induction motor is operated at 3 phase supply with 50 Hz frequency. When motor is operating in normal condition the stator current spectrum will show only 50 Hz frequency. If any type of the fault occurs, it causes sidebands near the main frequency. The frequency

of the generated sidebands depends upon the type of the fault. Every specific fault will have its own current signature.

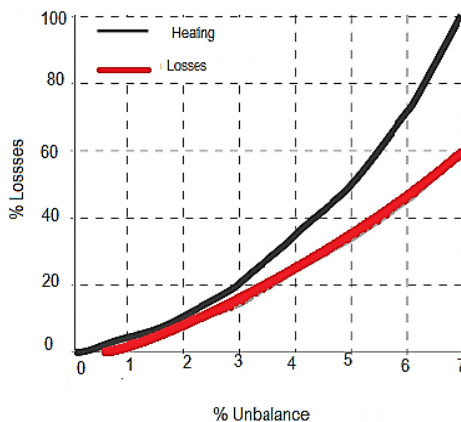


**Figure 1.** Increase in motor losses and heating due to unbalance voltage.

Figure 1 shows the impact of unbalance supply voltage on motor heating. The power supply unbalance fault will also introduce the sidebands frequencies upon occurrence of fault (Messaoudi & Sbita, 2010).

$$f_{unv} = (1 + 2k) f_s \quad (1)$$

where,  $k=1, 2, 3, \dots, N$ ,  $f_{unv}$  = unbalanced supply voltage,  $f_s$  = frequency of supply voltage

### 2.3. BROKEN ROTOR BAR FAULT

The rotor of Squirrel cage induction motor as shown in Figure 2 is constructed of usually copper bars instead of windings and permanently short circuited with end rings. So, under certain load conditions these bars and end rings are cracked.

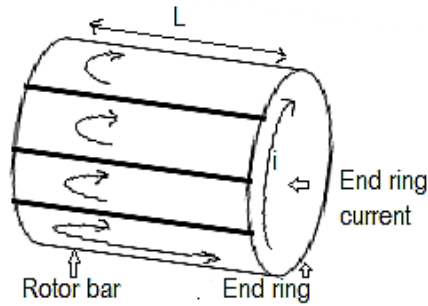


**Figure 2.** Rotor of induction motor.

Due to no. of reasons the cracks appear in the bars as well as at end rings. This may be due to thermal stress that causes overloading, magnetic stress caused by electromagnetic forces, due to electromagnetic force imbalance, vibration and noise cause stress on the Bars. Defect at manufacturing time causes residual stress. Dynamic stress as a result of shaft torque, centrifugal forces and cyclic stress has a negative impact on the rotor (Szabó, Dobai, & Biró, 2004).

Under normal condition, current distribution in the rotor bars is uniform according to the load applied. Upon breakage of the bars, the resistance of the bars is increased and causes uneven distribution in current loops made by end rings and bars. So, if load is changed during induction motor operation the current distribution is greatly affected (Liang *et al.*, 2014). This type of fault is load dependent.

## 2.4. EFFECT OF FAULTY BROKEN BARS

The change caused by broken rotor bars and end rings in the stator current will introduce new frequency components at the following frequencies (Messaoudi and Sbita, 2010):

$$f_{bb} = (1 \pm 2ks) f_s \quad (2)$$

where,  $k = 1, 2, 3, \dots, N$ ,  $f_{bb}$ : broken rotor bar frequency,  $f_s$ : electrical supply frequency,  $p$ : number of pole pairs,  $s$ : slip.



### 3. SYSTEM DESIGN AND IMPLEMENTATION

The scope of the research work is limited to the fault detection and identification. This is achieved by continuously monitoring three phase stator current as shown in Figure 3, which depicts the implementation of fault diagnoses system for three phase induction motor.

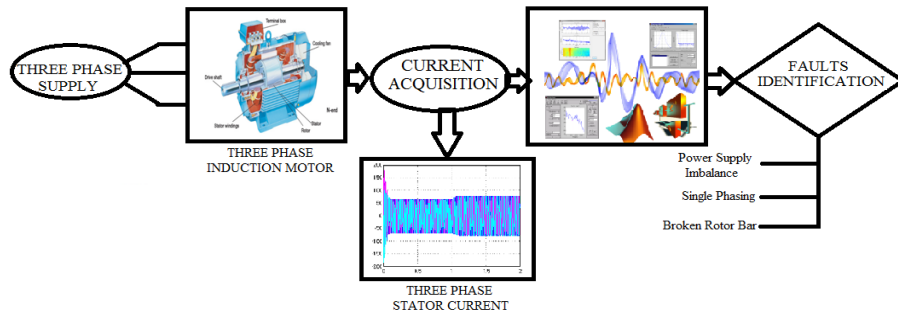


**Figure 3.** Multiple faults detection and identification system

Three phase supply is fed to the induction motor. Speed, Torque, and three phase stator current are the motor's outputs. As in MCSA, the individual phase stator current is taken as the monitoring parameter in order to detect the fault with its occurrence time. After acquiring the stator current STFT analysis is conducted on current signals and resulting spectrogram will convey the information about the condition of the motor. After analysis of the spectrogram the type and time of the fault can be detected and can be further decided whether motor should continue running or it may be stopped for necessary maintenance.

This section presents the Mathematical model of the induction motor including its simulation and describes STFT analysis in the following sub-sections.

#### 3.1. MATHEMATICAL MODEL OF THE INDUCTION MOTOR

The three-phase induction motor model is realized in Simulink using famous dq model that is explained in Simion, Livadaru, and Munteanu (2012), Robyns *et al.* (2012), and Batool and Ahmad (2013). According to this model the three phase quantities are converted to two phase dq model. The three phases, 120° electrically apart are converted into two phase voltage i.e. “d” and “q” as shown in Figure 4. The following assumptions are made while considering the two phase dq model:

- Uniform air gap with no saturation
- Stator windings are distributed sinusoidal.
- Inter bar current is zero

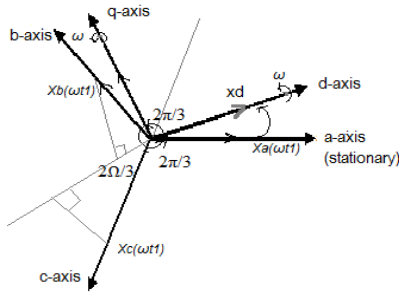


Figure 4. 'abc' to 'dq' conversion.

The equivalent circuit of three phase induction motor is given in Figure 5 with two phases d and q. All the related parameters are shown with labeling.

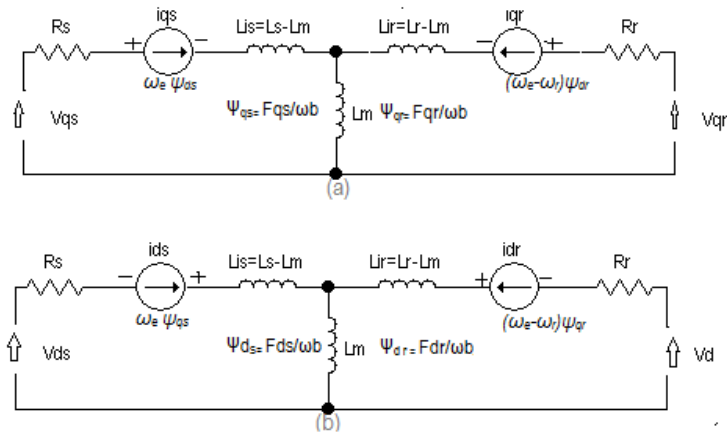


Figure 5. Induction Motor Equivalent circuit.

The following equations can be drawn from the equivalent circuit in order to develop a mathematical model in the Simulink.

$$\frac{dFqs}{dt} = W_b \left[ Vqs - \frac{We}{Wb} Fds + \frac{Rs}{Xls} (Fmq + Fqs) \right] \tag{3}$$

$$\frac{dFds}{dt} = W_b \left[ Vds + \frac{We}{Wb} Fqs + \frac{Rs}{Xls} (Fmd + Fds) \right] \quad (4)$$

$$\frac{dFqs}{dt} = W_b \left[ Vqs - \frac{We}{Wb} Fds + \frac{Rs}{Xls} (Fmq + Fqs) \right] \quad (5)$$

$$\frac{dFdr}{dt} = W_b \left[ Vdr + \frac{(We - Wr)}{Wb} Fqr + \frac{Rr}{Xlr} (Fmd - Fdr) \right] \quad (6)$$

$$Te = \frac{3}{2} \left( \frac{P}{2} \right) \frac{1}{Wb} (Fds * iqs - Fqs * ids) \quad (7)$$

$$Te - TL = J \left( \frac{2}{P} \right) \frac{dWr}{dt} \quad (8)$$

where,  $d$  : direct axis,  $q$  : quadrature axis,  $s$  : stator variable,  $r$  : rotor variable,  $F_{ij}$  is the flux linkage ( $i=q$  or  $d$  and  $j=s$  or  $r$ ),  $vqs$ ,  $lds$  :  $q$  and  $d$ -axis stator voltages,  $vqr$ ,  $ldr$  :  $q$  and  $d$ -axis rotor voltages,  $Fmq$ ,  $Fmd$  :  $q$  and  $d$  axis magnetizing flux linkages,  $Rr$  : rotor resistance,  $Rs$  : stator resistance,  $Xls$  : stator leakage reactance ( $w_e Lls$ ),  $Xlr$  : rotor leakage reactance ( $w_r Llr$ )

$$X_{ml} : \frac{1}{\frac{1}{x_m} + \frac{1}{x_{ls}} + \frac{1}{x_{lr}}}$$

$iqs$ ,  $ids$  :  $q$  and  $d$ -axis stator currents,

$iqr$ ,  $idr$  :  $q$  and  $d$ -axis rotor currents,

$P$  : number of poles,

$J$  : moment of inertia,

$Te$  : electrical output torque,

$TL$  : load torque,

$w_e$  : stator angular electrical frequency,

$w_b$  : motor angular electrical base frequency,

$w_r$  : rotor angular electrical speed.

Figure 6 represents Motor model developed by exploring Simulink Library using equations 03 to 08 (Ozpineci & Tolbert, 2003; Leedy, 2013). Three phases to two phase voltages are converted by abc-syn block and syn-abc block performs vice versa function. There are two inputs to the motor and three outputs. The inputs are three phase supply and the applied load. The outputs are three phase current, rotor speed and motor output torque.

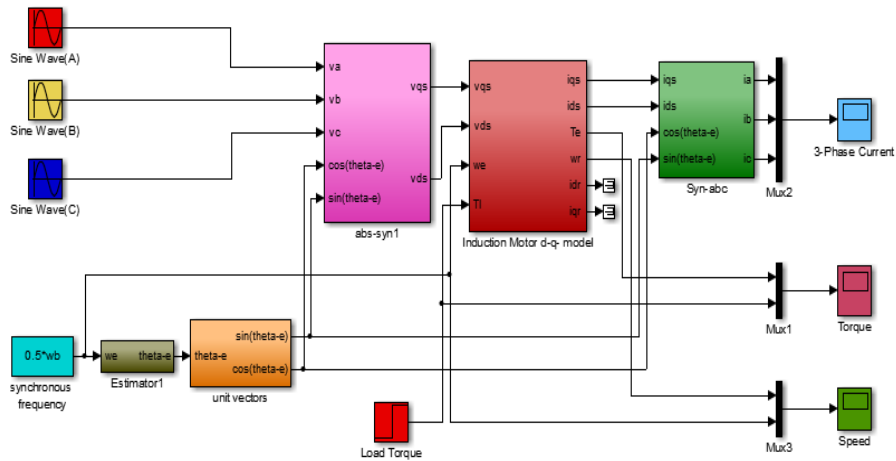


**Figure 6.** System Model in Matlab.

### 3.2. SHORT TIME FOURIER TRANSFORM

The STFT overcomes the drawback associated with the Fast Fourier Transform. The FFT performs the function of transformation from time to frequency domain. Usually the transformation is performed to extract the additional information from the signal. FFT is converting the signal from time to frequency completely misses out the time information (Polikar, 1994). In case of induction motor faults, the time information is important because some faults are severe and are not required to persist for long time. While there is some irregular behavior or any incipient fault which usually can be tolerated for certain time and the motor does not require the urgent maintenance. FFT fails to provide time information along with frequency information. By using STFT the simultaneous time and frequency information can be obtained. So, with time-frequency results both type and time of the fault can be identified. Mathematically STFT is expressed below:

$$\{x(t)\}(\tau, \omega) = X(\tau, \omega) \int_{-\infty}^{\infty} x(t) \omega(t - \tau) e^{-i\omega t} dt \quad (9)$$

where,  $X(\tau, \omega)$  is STFT output,  $x(t)$  is input signal,  $w(\tau)$  is the window function

The window function localizes the frequency contents in time. A window function “ $w_n$ ” has a tapering at its end to avoid unnatural irregularities present in the signal frequency contents. The window function is the trade-off between time and frequency. The time and frequency information depend upon the size and type of the window. Larger time window will result poor time resolution and vice versa.

Although there are different types of window that are used to localize time frequency representation, but Hamming, Hann and rectangular window are the most popular. In this research work Hamming window is used which resulted the useful information.

## 4. RESULTS AND DISCUSSIONS

This section presents the results obtained from mathematical model of the induction motor. Moreover, it describes each fault introduced in the model and their comparative analysis in terms of FFT and STFT spectrum. The system design, development and simulations are performed in MATABL/Simulink. The motor dq-model is implemented in Simulink and STFT is applied by exporting the parameters in command window. The supply to the motor is 220 V, 3-Phase, 50 Hz. The step function is used as load at different instants. The motor outputs include three phase current, Torque and speed of the rotor.

### 4.1. HEALTHY MOTOR CONDITION

Figures 7 to 9 give motor output parameters in healthy condition. The motor takes high starting current and then have normal current but when a load of 25 N/m is applied at 1 second the current is increased while rotor speed is decreased.

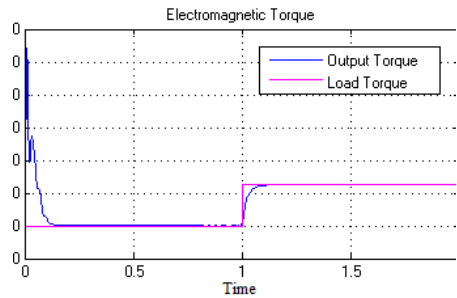


Figure 7. Motor output Torque.

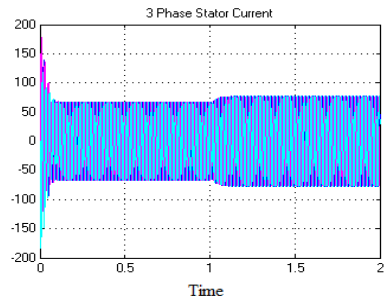


Figure 8. Three phase stator current.

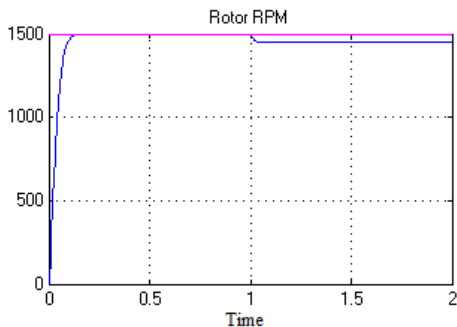


Figure 9. Motor RPM.

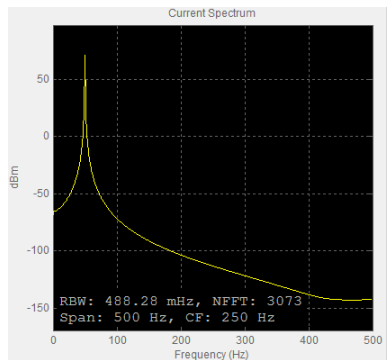


Figure 10. FFT Spectrum.

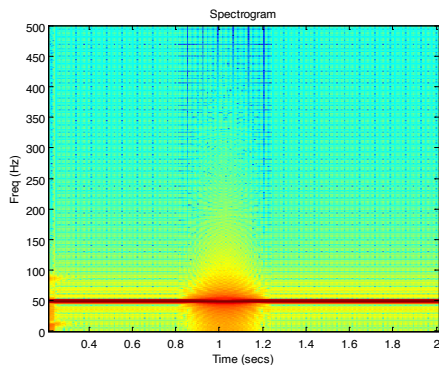


Figure 11. STFT showing abnormality at 1 second.

By taking FFT of stator current, the spectral contents can be seen at 50 Hz fundamental component which is the indication of healthy motor in Figure 10, FFT can compute perfect spectral contents but it fails to provide time information in addition to frequency information. To observe frequency and time simultaneously the STFT is computed as shown in Figure 11. Figure 11 shows changes at 1 second which is due to the change in

magnitude (load change) from lower to higher level which we are unable to identify using FFT. By having time domain signal, we can identify the time of any irregularity or event and in order to check that irregularity FFT can be computed but to explore simultaneous Time-Frequency information STFT can be the optimal choice.

4.2. FAULT 01 SIMULATION: POWER SUPPLY IMBALANCE

The 20 volts drop is simulated in Red Phase as power supply imbalance fault after 1 second and motor is simulated for 2 seconds which can be seen in time domain in Figure 12, having two irregularities, first at 0.5 second and second at 1 second. In order to check whether it is due to change in load or it is because of any fault, FFT is computed. The FFT shows a sideband is generated at 150 Hz in Figure 13, which indicates power supply imbalance fault as equation 1 but unable to determine when it occurred. In other words FFT fails to detect nonstationary condition of the signal. While computing STFT Figure 14, show a change in the load at 0.5 sec and a sideband is generated along with main frequency component at 1 sec. The color of the sideband generated is light because of the low magnitude of 150 Hz component.

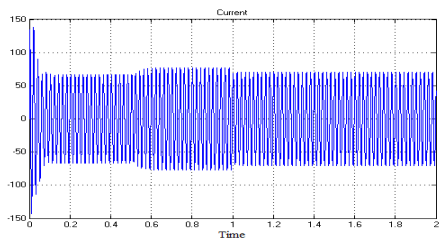


Figure 12. Sideband generated at 150 Hz.

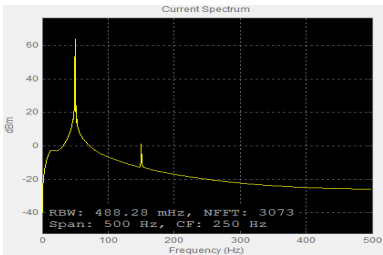


Figure 13. 20 Volt drop introduced after 1 second.

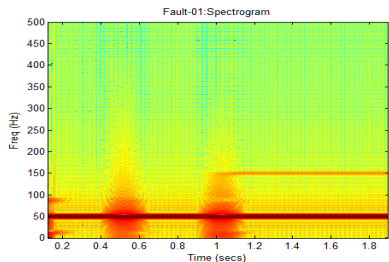


Figure 14. Power supply imbalance spectrogram.

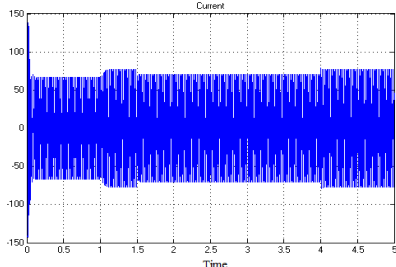
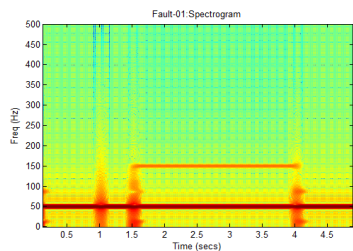
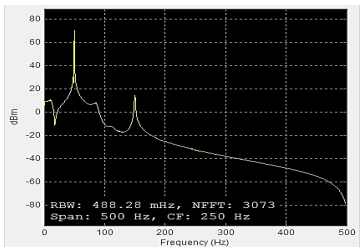


Figure 15. 20V drop between 1.5 to 4 seconds.

Again, the same 20 Volt drop in Red Phase is simulated between 1.5 to 4 seconds and can be seen in Figure 15, that time domain representation is unable to convey the information about irregularities at 1 sec, 1.5 sec and at 4 second. Computing FFT of red phase for same 20 V drop shown in Fig. 16 that a sideband is generated at 150 Hz frequency which is the indication of power supply imbalance fault but again we are unaware what happened at 1sec, 1.5 sec and at 4 sec instants. By analyzing the same fault by STFT Fig. 17, gives some idea about the time of load change and type of fault by looking 150 Hz sideband between 1.5 to 4 seconds.



**Figure 16.** FFT for 20V drop between 1,5 to 4 seconds. **Figure 17.** STFT for 20V drop between 1.5 to 4 seconds.

Figure 18 shows the 3-D spectrogram of the single fault i.e. imbalance in the supply phase voltages. It is showing all three parameters time frequency and magnitude of the signal, describing health and faulty portion of the signal. Similarly in Figure 19, power supply imbalance fault is detected between 01 to 03 seconds at no load condition.

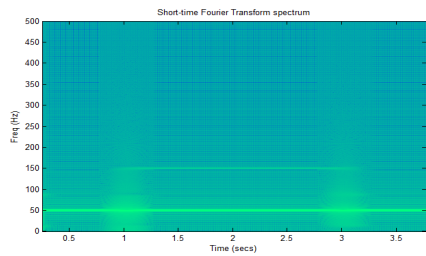
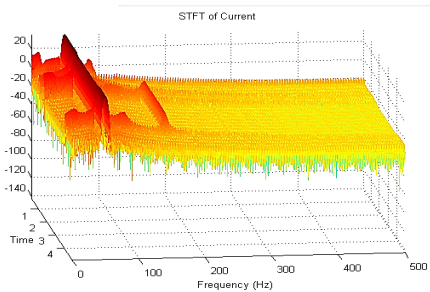


**Figure 18.** 3D spectrogram for imbalance of supply voltage. **Figure 19.** STFT for power imbalance fault between 1 to 3 seconds.

### 4.3. FAULT 02 SIMULATION: SINGLE PHASING CONDITION

Single phasing occurs if any phase among three phases of the supply is missing. Due to this condition current among the two phases increases drastically and can cause permanent



damage to induction motor. As in Figure 20, load is applied after 1sec and single phasing is introduced at 2 sec that causes huge increase in current. If in this condition motor is allowed to run it may be permanently damaged. By looking at Time domain representation we can not estimate what happened at '01' and '02' second. By computing FFT of the current signal in Figure 21 sidebands at 150,250 and 350 Hz are generated that is the clear indicatoin of single phasing condition according to relation (1). For having simultaneous time frequency information STFT is computed as shown in Figure 22, showing three side bands after 2 seconds. It is clear from Figure 22 that 50 Hz fundamental is dominant while 150,250 and 350 Hz has respectively decreasing contribution. Figure 23 shows 3D spectrogram for single phasing condition.

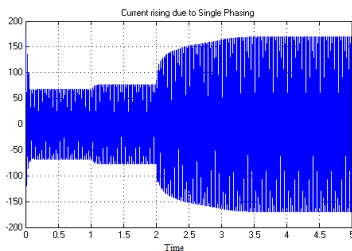


**Figure 20.** Irregularity at 1 and 2 seconds.

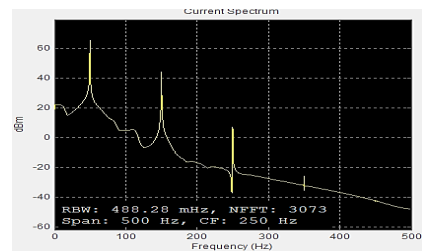


**Figure 21.** FFT for irregularity at 1 and 2 sec.

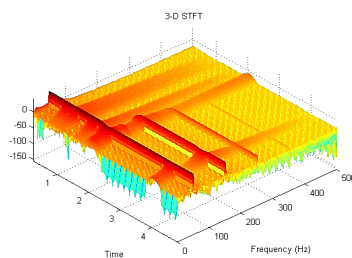


**Figure 22.** 3D Spectrogram for Figure 20.

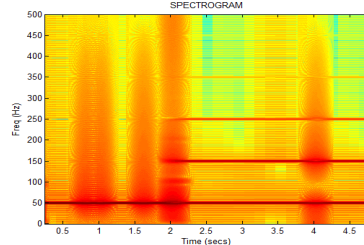


**Figure 23.** Irregularity identified by STFT.

#### 4.4. FAULT 03: BROKEN ROTOR BAR DETECTION

Figures 24-26 showing the diagrams for broken rotor bar fault in time, frequency and time-frequency domain respectively. The broken rotor bar fault is introduced by changing the resistance of the rotor circuit. Due to broken rotor bar two sidebands are generated at 36 Hz and 64 Hz according to equation (2). Figure 25 shows both sidebands are present for all times along with main frequency component. So broken rotor bar fault is present since start and remains all the time.

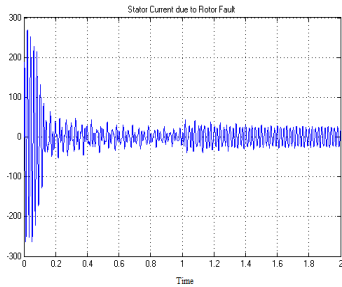


**Figure 24.** Broken rotor bar fault in time domain.

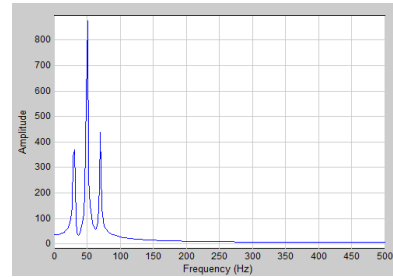


**Figure 25.** Broken rotor bar fault in frequency domain.

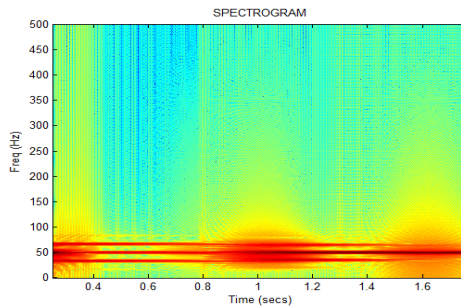


**Figure 26.** Broken rotor bar fault in time and frequency domsain.

## 4.5. MULTIPLE FAULT INDUCTION

When multiple faults are present in the motor then it is necessary to find out their occurrence time in order to know the nature of the fault so that it can be decided whether motor should continue to run, or it may be stopped. Figure 27 shows FFT spectrum for broken rotor bars and power supply imbalance faults together. Three side bands along with 50 Hz frequency component are generated. Two sidebands at 36 Hz and 64 Hz are due to the result of two broken bars and one sideband at 150 Hz frequency is the result of power supply imbalance fault but the time information of these faults is missing. Figure 28 shows the computation of STFT for these two faults. It is clear from the spectrogram that broken rotor bar fault is present all the time while power supply imbalance fault has occurred at 1.5 second instant. Similarly Figures 29 and 30 shows the six broken bars and power supply imbalance faults. Broken bar fault is present all the time and power supply imbalance fault exist between 1 to 3 seconds.

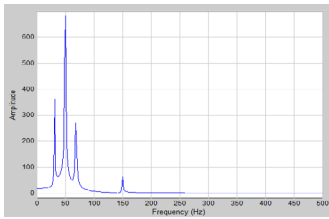


**Figure 27.** Two Broken Bars and Power Supply imbalance faults together.

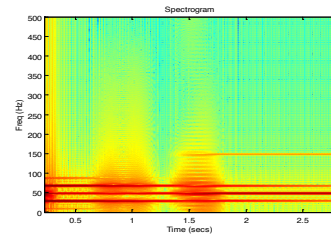


**Figure 28.** Spectrogram for Broken Bar and Power Supply imbalance faults together.

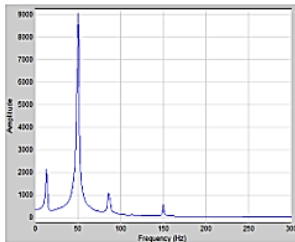


**Figure 29.** Six broken bars and 20 V drop fault.

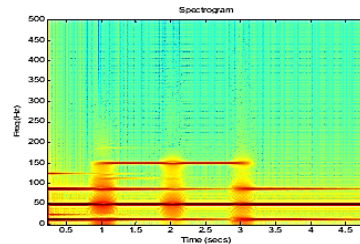


**Figure 30.** STFT for Six broken bars and 20 V drop fault.

## 5. CONCLUSION

Previously, a lot of research has been conducted on Induction motor fault diagnoses for single fault detection using multiple signal processing techniques. Very less work is reported on simultaneous multiple faults detection. In this paper, multiple faults with time information are successfully diagnosed in induction motor. Monitoring system efficiently detected imbalance of supply, single phasing and broken rotor bars occurring at different instants of time. This study can help to overcome the drawback of techniques which are unable to provide simultaneous time-frequency information of multiple faults. The short time Fourier transforms has accurately provided the desired results for multiple faults with their occurrence time. For more detailed information of the faults WT is better choice but for ordinary faults STFT provides optimal results and conveys enough time-frequency information with lesser efforts. In case of wavelet transform more calculations are required because of complex nature. By incorporating this research in the industries and agriculture fields, online health of the machine can be monitored. Upon having the knowledge of time and type of faults desired maintenance strategy can be applied thus saving enough time by avoiding costly downtime.

## ACKNOWLEDGMENT

The authors express their gratitude to Higher Education Commission (HEC), Pakistan and Ministry of planning and development Pakistan for providing funds for this research work as national laboratory on ‘Haptics and Human-Robotic, Condition Monitoring Systems Lab. This lab is part of the National Center of Robotics and Automation (NCRA). We are also thankful to MUET Jamshoro for providing lab facility to perform research work.

## REFERENCES

- Batool, M., & Ahmad, A.** (2013). Mathematical modeling and speed torque analysis of three phase squirrel cage induction motor using matlab simulink for electrical machines laboratory. *International Electrical Engineering Journal (IEEJ)*, 4(1), 880-889. <https://tarjomefa.com/wp-content/uploads/2016/09/5246-English.pdf>
- Benbouzid, M. E. H.** (2000). A review of induction motors signature analysis as a medium for faults detection. *IEEE Transactions on Industrial Electronics*, 47(5), 984-993. <https://ieeexplore.ieee.org/document/873206>
- Çalış, H., & Çakır, A.** (2008). Experimental study for sensorless broken bar detection in induction motors. *Journal of Energy Conversion & Management*, 49(4), 854-862. <https://doi.org/10.1016/j.enconman.2007.06.030>
- Cusidó, J., Romeral, L., Ortega, J. A., Rosero, J. A., & Espinosa, A. G.** (2008). Fault detection in induction machines using power spectral density in wavelet decomposition. *IEEE Transactions on Industrial Electronics*, 55(2), 633-643. <https://doi.org/10.1109/TIE.2007.911960>
- Da Silva, A. M., Povinelli, R. J., & Demerdash, N. A.** (2008). Induction machine broken bar and stator short-circuit fault diagnostics based on three-phase stator current envelopes. *IEEE Transactions on Industrial Electronics*, 55(3), 1310-1318. <https://doi.org/10.1109/TIE.2007.909060>

- El Bouchikhi, E. H., Choqueuse, V., & Benbouzid, M.** (2015). Induction machine diagnosis using stator current advanced signal processing. *International Journal on Energy Conversion*, 3(3), 76–87. <https://hal.archives-ouvertes.fr/hal-01249256/document>
- Gao, Z., Cecati, C., & Ding, S. X.** (2015). A survey of fault diagnosis and fault-tolerant techniques—Part I: Fault diagnosis with model-based and signal-based approaches. *IEEE Transactions on Industrial Electronics*, 62(6), 3757-3767. <https://doi.org/10.1109/TIE.2015.2417501>
- Haggag, S., & Mageed, H. M. A.** (2013). A new fault detection tool for single phasing of a three phase induction motor. *Proceedings of the World Congress on Engineering 2013*, Vol II, WCE 2013, July 3 - 5, 2013, London, U.K. [https://www.researchgate.net/publication/289698804\\_A\\_New\\_Fault\\_Detection\\_Tool\\_for\\_Single\\_Phasing\\_of\\_a\\_Three\\_Phase\\_Induction\\_Motor](https://www.researchgate.net/publication/289698804_A_New_Fault_Detection_Tool_for_Single_Phasing_of_a_Three_Phase_Induction_Motor)
- Lee, C.-Y.** (1999). Effects of unbalanced voltage on the operation performance of a three-phase induction motor. *IEEE Transactions on Energy Conversion*, 14(2), 202-208. <https://doi.org/10.1109/60.766984>
- Leedy, A. W.** (2013). Simulink/matlab dynamic induction motor model for use as a teaching and research tool. *International Journal of Soft Computing and Engineering (IJSCSE)*, 3(4), 102-107. <https://pdfs.semanticscholar.org/8005/18f68fac0e276d4b7be0ad0896e39d6714ee.pdf>
- Liang, B., Payne, B. S., Ball, A. D., & Iwnicki, S. D.** (2002). Simulation and fault detection of three-phase induction motors. *Journal of Mathematics and Computers in Simulation*, 61(1), 1-15. [https://doi.org/10.1016/S0378-4754\(02\)00064-2](https://doi.org/10.1016/S0378-4754(02)00064-2)
- Mal, K., Hussain, I., Chowdhry, B. S., & Memon, T. D.** (2020). Extended kalman filter for estimation of contact forces at wheel-rail interface. *3C Tecnología. Glosas de innovación aplicadas a la pyme. Edición Especial*, Abril 2020, 279-301. <http://doi.org/10.17993/3ctecno.2020.specialissue5.279-301>

- Mehala, N., & Dahiya, R.** (2008). A comparative study of FFT, STFT and wavelet techniques for induction machine fault diagnostic analysis. *Proceedings of the 7th WSEAS International Conference on COMPUTATIONAL INTELLIGENCE, MAN-MACHINE SYSTEMS and CYBERNETICS (CIMMACS ,08)*. <http://www.wseas.us/e-library/conferences/2008/cairo/CD-CIMMACS/CIMMACS34.pdf>
- Mehrjou, M. R., Mariun, N., Marhaban, M. H., & Misron, N.** (2010). Evaluation of fourier and wavelet analysis for efficient recognition of broken rotor bar in squirrel-cage induction machine. In *2010 IEEE International Conference on Power and Energy, Kuala Lumpur, Malaysia*. <https://doi.org/10.1109/PECON.2010.5697678>
- Messaoudi, M., & Sbita, L.** (2010). Multiple faults diagnosis in induction motor using the mcsa method. *International Journal of Signal & Processing*, 1(3), 190-195. [https://www.academia.edu/31924332/Multiple\\_Faults\\_Diagnosis\\_in\\_Induction\\_Motor\\_Using\\_the\\_MCSA\\_Method](https://www.academia.edu/31924332/Multiple_Faults_Diagnosis_in_Induction_Motor_Using_the_MCSA_Method)
- Mirabbasi, D., Seifossadat, G., & Heidari, M.** (2009). Effect of unbalanced voltage on operation of induction motors and its detection. In *2009 International Conference on Electrical and Electronics Engineering - ELECO 2009, Bursa, Turkey*. <https://doi.org/10.1109/ELECO.2009.5355288>
- Mortazavizadeh, S., & Mousavi, S.** (2014). A review on condition monitoring and diagnostic techniques of rotating electrical machines. *Physical Science International Journal*, 4(3), 310. <https://doi.org/10.9734/PSIJ/2014/4837>
- Nandi, S., Toliyat, H. A., & Li, X.** (2005). Condition monitoring and fault diagnosis of electrical motors—A review. *IEEE Transactions on Energy Conversion*, 20(4), 719-729. <https://doi.org/10.1109/TEC.2005.847955>
- Ozpineci, B., & Tolbert, L. M.** (2003). Simulink implementation of induction machine model-a modular approach. In *IEEE International Electric Machines and Drives Conference, 2003. IEMDC'03, Madison, WI, USA, USA*. <https://doi.org/10.1109/IEMDC.2003.1210317>

- Pandey, K., Zope, P., & Suralkar, S.** (2012). Review on fault diagnosis in three-phase induction motor. In *MEDHA-2012, Proceedings published by International Journal of Computer Applications (IJCA)*. <https://www.ijcaonline.org/proceedings/medha/number1/8680-1024>
- Polikar, R.** (1994). *The wavelet tutorial* (2nd ed.). Part I.
- Quispe, E., Gonzalez, G., & Aguado, J.** (2004). Influence of unbalanced and waveform voltage on the performance characteristics of three-phase induction motors. In *International Conference on Renewable Energies and Power Quality, Barcelona*. <http://www.icrepq.com/PONENCIAS/4.279.QUISPE.pdf>
- Robyns, B., Francois, B., Degobert, P., & Hautier, J. P.** (2012). Vector control of induction machines. In *Vector control of induction machines (pp. 75-121)*. Springer.
- Sharma, A., Chatterji, S., Mathew, L., & Khan, M. J.** (2015). A Review of Fault Diagnostic and Monitoring Schemes of Induction Motors. *International Journal for Research in Applied Science and Engineering Technology (IJRASET)*, 3(4). <http://behpouyan.ir/uploads/maghalat/861--57930db2-856c-47f1-bcf6-3453b9041dc8.PDF>
- Shi, P., Chen, Z., Vagapov, Y., Davydova, A., & Lupin, S.** (2014). Broken bar fault diagnosis for induction machines under load variation condition using discrete wavelet transform. *Proceedings of IEEE East-West Design & Test Symposium (EWDTS 2014), Kiev, Ukraine*. <https://doi.org/10.1109/EWDTS.2014.7027059>
- Siddiqui, K. M., & Giri, V.** (2012). Broken rotor bar fault detection in induction motors using wavelet transform. In *2012 International Conference on Computing, Electronics and Electrical Technologies (ICCEET), Kumaracoil, India*. <https://doi.org/10.1109/ICCEET.2012.6203753>
- Siddiqui, K. M., Sahay, K., & Giri, V.** (2014). Health monitoring and fault diagnosis in induction motor-a review. *International Journal of Advanced Research in Electrical, Electronics and Instrumentation Engineering*, 3(1), 6549-6565. <https://www.semanticscholar.org/paper/Health-Monitoring-and-Fault-Diagnosis-in-Induction-Siddiqui-Sahay/678e583567bce8a74397ab26ee677f3afc4d41bc>

- Simion, A., Livadaru, L., & Munteanu, A.** (2012). *Mathematical model of the three-phase induction machine for the study of steady-state and transient duty under balanced and unbalanced states*. <https://doi.org/10.5772/49983>
- Soother, D. K., & Daudpoto, J.** (2019). A brief review of condition monitoring techniques for the induction motor. *Transactions of the Canadian Society for Mechanical Engineering*, 43(4), 499-508. <https://doi.org/10.1139/tcsme-2018-0234>
- Soother, D. K., Daudpoto, J., & Shaikh, A.** (2018). Vibration measurement system for the low power induction motor. *Engineering Science And Technology International Research Journal*, 2(4), 53-57. [https://www.researchgate.net/publication/332672765\\_Vibration\\_measurement\\_system\\_for\\_the\\_low\\_power\\_induction\\_motor](https://www.researchgate.net/publication/332672765_Vibration_measurement_system_for_the_low_power_induction_motor)
- Szabó, L., Dobai, J. B., & Biró, K. A.** (2004). Rotor faults detection in squirrel-cage induction motors by current signature analysis. *Proceedings of the 2004 IEEE-TTTC - International Conference on Automation, Quality and Testing, Robotics, A&QTR 2004 (THETA 14)*, Cluj (Romania), Tome I., pp. 353-358. [https://www.academia.edu/20689627/Rotor\\_Faults\\_Detection\\_in\\_Squirrel\\_Cage\\_Induction\\_Motors\\_by\\_Current\\_Signature\\_Analysis](https://www.academia.edu/20689627/Rotor_Faults_Detection_in_Squirrel_Cage_Induction_Motors_by_Current_Signature_Analysis)
- Ujjan, S. M., Kalwar, I. H., Chowdhry, B. S., Memon, T. D., & Soother, D. K.** (2020). Adhesion level identification in wheel-rail contact using deep neural networks. *3C Tecnología. Glosas de innovación aplicadas a la pyme. Edición Especial*, Abril 2020, 217-231. <http://doi.org/10.17993/3ctecno.2020.specialissue5.217-231>
- Zhongming, Y., & Bin, W.** (2000). A review on induction motor online fault diagnosis. *Proceedings IPEMC 2000. Third International Power Electronics and Motion Control Conference (IEEE Cat. No.00EX435)*, Beijing, China, China. <http://doi.org/10.1109/IPEMC.2000.883050>





/07/

# AN AUTOMATED SYSTEM FOR TRAFFIC SIGN RECOGNITION USING CONVOLUTIONAL NEURAL NETWORK

---

**Sanam Narejo**

Department of Computer Systems Engineering, Mehran University of Engineering & Technology,  
Jamshoro, (Pakistan).

E-mail: [sanam.narejo@faculty.muet.edu.pk](mailto:sanam.narejo@faculty.muet.edu.pk) ORCID: <https://orcid.org/0000-0002-3537-8949>

**Shahnawaz Talpur**

Department of Computer Systems Engineering, Mehran University of Engineering & Technology,  
Jamshoro, (Pakistan).

E-mail: [shahnawaz.talpur@faculty.muet.edu.pk](mailto:shahnawaz.talpur@faculty.muet.edu.pk) ORCID: <https://orcid.org/0000-0002-2660-6145>

**Madeha Memon**

Department of Computer Systems Engineering, Mehran University of Engineering & Technology,  
Jamshoro, (Pakistan).

E-mail: [madeha.memon@gmail.com](mailto:madeha.memon@gmail.com) ORCID: <https://orcid.org/0000-0003-2147-0944>

**Amna Rahoo**

Department of Computer Systems Engineering, Mehran University of Engineering & Technology,  
Jamshoro, (Pakistan).

E-mail: [f16cs05@students.muet.edu.pk](mailto:f16cs05@students.muet.edu.pk) ORCID: <https://orcid.org/0000-0002-9376-6528>

**Recepción:** 13/11/2020 **Aceptación:** 13/11/2020 **Publicación:** 13/11/2020

## **Citación sugerida Suggested citation**

Narejo, S., Talpur, S., Memon, M., y Rahoo, A. (2020). An automated system for traffic sign recognition using convolutional neural network. *3C Tecnología. Glosas de innovación aplicadas a la pyme. Edición Especial, Noviembre 2020*, 119-135. <https://doi.org/10.17993/3ctecno.2020.specialissue6.119-135>

## ABSTRACT

TSR (Traffic Sign Recognition) represents an important feature of advanced driver assistance system, contributing to the safety of the drivers, autonomous vehicles as well and to increase driving comfort. In today's world road conditions drastically improved as compared with past decades. Obviously, vehicle's speed increased. So, on driver's point of view there might be chances of neglecting mandatory road signs while driving. This paper explores the system to helps the driver about recognition of road signs to avoid road accidents. TSR is challenging task, while its accuracy depends on two aspects: feature extractor and classifier. Current popular algorithms mainly deploy CNN (Convolutional Neural Network) to execute both feature extraction and classification. In this paper, we implement the traffic sign recognition by using CNN, the CNN will be trained by using the dataset of 43 different classes of traffic signs along with TensorFlow library. The results will show the 95% accuracy.

## KEYWORDS

Convolutional Neural Network, Traffic Sign Recognition, Autonomous Vehicles, Exploratory Data Analysis

# 1. INTRODUCTION

Road and traffic signs must be properly installed in the necessary locations and an inventory of them is ideally needed to help ensure adequate updating and maintenance. Meetings with the highway authorities in both Scotland and Sweden revealed the absence of but a need for an inventory of traffic signs. An automatic means of detecting and recognizing traffic signs can make a significant contribution to this goal by providing a fast method of detecting, classifying and logging signs. This method helps to develop the inventory accurately and consistently. Once this is done, the detection of disfigured or obscured signs becomes easier for human operator. Road and traffic sign recognition is the field of study that can be used to aid the development of an inventory system (for which real-time recognition is not required) or aid the development of an in-car advisory system (when real-time recognition is necessary). Both road sign inventory and road sign recognition are concerned with traffic signs, face similar challenges and use automatic detection and recognition. A road and traffic sign recognition system could in principle be developed as part of an ITS (Intelligent Transport Systems) that continuously monitors the driver, the vehicle, and the road in order, for example, to inform the driver in time about upcoming decision points regarding navigation and potentially risky traffic situations (Fleyeh, 2008).

The aim of intelligent transport systems is to increase transportation efficiency, road safety and to reduce the environmental impact with the use of advanced communication technologies (Sermanet, & LeCun, 2011; De la Escalera, Armingol & Mata, 2003). Automatic TSR, as an important task of Advanced Driver Assistance Systems and ITS has been of great interest in recent years. The road signs are placed on either roadside or above the roads. These signs provide mandatory information regarding to guiding, warning and regulating the behaviors to drivers in order to make driving safer and easier.

There are several different TSR like speed limits, no entry, traffic signals, turn left or right, children crossing, no passing of heavy vehicles, etc. Traffic sign classification/recognition is the process of identifying the, which class traffic sign belongs to. TSR has a direct impact on the safety of drivers, and damages can be easily produced due to their ignorance. Automatic systems are developed to assist the drivers, based on detection and recognition of signs which corrects the most unsafe driving behaviors.

The main purpose of advanced driver assistance systems is to collect significant information for drivers in order to reduce their effort in safe driving. Because drivers must pay attention to various conditions, including vehicle speed and orientation, passing cars and to many more. So, if driver assistance systems collect such information, it will greatly reduce the burden of drivers. Thus, road signs are designed in such a way that attracts a driver's attention with colors and simple geometric shapes.

The research work available on recognition of traffic signs for local roads is quite sparse and still at the preliminary stage. Mostly it is focused on recognition of traffic signs for local roads and they are also still at the preliminary stage and focused on recognition of traffic signs through static images. In this work, algorithms were developed in “Google Colab” environment to recognize traffic signs while vehicles in motion. Project is mainly focused on automatic recognition of warning signs placed in local roads captured by image clips. Traffic signs were recognized based on its geometrical characteristics and color information (Gunawardana 2010). In this project, we develop a deep NN (Neural Network) model that that can classify the traffic signs present in the image into different categories. With this model, we can read and understand traffic signs which are very important task for autonomous vehicles.

## 2. LITERATURE SURVEY

There are many researches in the literature dealing with Road TSR problem. According to Kale and Mahajan (2015), the road sign recognition system is to be divided into two parts, the first part is detection stage which is used to detect the signs from a whole image, and the second part is classification stage that classifies the detected sign in the first part into one of the reference signs which are presents in the dataset. They used PCA (Principle Component Analysis) and ANN (Artificial Neural Network) techniques for detection and recognition with the dataset of different road signs from Maharashtra RTO (Regional Transport Office). Tool used by them was MATLAB. For TSR, mostly the preferable model for image classification is CNN. The recognition system is implanted into autonomous vehicle ‘Eurecar’. The system was followed by HSV (Herpes Simplex Viruses) and Hough transform algorithms for extracting ROI (Return on Investment) of traffic signs. Gaussian blurring was also applied as canny edge detectors. Then extracted area is given to CNN

model. They used dataset of 6 types of (Korean-Version) traffic signs to train the CNN model. The obtained results demonstrated low accuracy; it shows overlapping results when several proposal regions point to a same traffic sign. Development of clustering algorithm is considered as a future work for robust recognition system (Jung et. al. 2016). Most of the research used color segmentation technique with C-CNN with GERMAN traffic signs dataset for detection. The C-CNN method consists of selecting a set of ROIs by applying a color thresholding on the input image, thus reducing the search space. Then, a trained CNN is used to classify the ROI (whether it contains a traffic sign or not), followed by another CNN with the same architecture, that is used to recognize the detected traffic signs. Therefore, 2 datasets are selected, one for detection and another one, to recognize the traffic sign. Therefore, CNN was trained to recognize two classes: traffic sign/no traffic sign. It was concluded that C-CNN is slow and sensitive to weather conditions (Boujemaa *et al.*, 2017).

Researchers presented a three-stage real-time TSR system, consisting of a segmentation, a detection and a classification phase. They combine the color enhancement with an adaptive threshold to extract red regions in the image. The detection is performed using an efficient linear SVM (Support Vector Machine) with HOG (Histogram of Oriented Gradients) features. The tree classifiers, K-d tree and Random Forest, identify the content of the traffic signs found. A spatial weighting approach is proposed to improve the performance of the K-d tree. The Random Forest and Fisher's Criterion are used to reduce the feature space and accelerate the classification. They presented that only a subset of about one third of the features is enough to attain a high classification accuracy on the GTSRB (German Traffic Sign Recognition Benchmark (Zaklouta & Stanculescu 2014). The paper proposed a method for Traffic Sign Detection and Recognition using image processing for the detection of a sign and an ensemble of CNN for the recognition of the sign. TensorFlow is used for the implementation of the CNN. They have achieved higher than 99% recognition accuracies for circular signs on the Belgium and German data sets (Vennelakanti *et al.*, 2019). Research based on TSR methods proposed mechanism for real time TSR using CNN. The training database was established by field sample collection, with which the neural network model was trained. SGD (Stochastic Gradient Descent) optimizer is utilized during training to improve the learning efficiency. The test results show that the proposed

method achieves good performance in speed, accuracy and robustness for real time TSR (Xu *et al.*, 2018).

R-CNN was the first to use this strategy, but it is very slow for two reasons (Girshick *et al.*, 2014). Firstly, generating category-independent object proposals is costly; it takes about 3s to generate 1000 proposals for the Pascal VOC 2007 images (Simonyan & Zisserman 2014). Secondly, it applies a whole deep CNN to every candidate proposal calculated, which is obviously very inefficient and time consuming. To improve efficiency, the SPP-Net (Spatial Pyramid-Pooling Network). Girshick *et al.* (2015) calculated a convolutional feature map for the entire image and extracts feature vectors from the shared feature map for each proposal. This speed up the R-CNN approach about 100 times. They have proposed the Fast R-CNN model, which is a faster version of the R-CNN approach. He *et al.* (2015) proposed RPNs (Region Proposal Networks), which generate object proposals using convolutional feature maps. This allows the generator of the object proposal to share the convolutional features of the whole image with the detection network. With this technique detection system can achieve a frame rate of 5 fps on a powerful GPU (Graphics Processing Unit). Szegedy *et al.* (2016) improved the network architecture, to achieve a frame rate of 50 fps in testing, with competitive detection performance.

In current traffic management systems, there is high probability that driver may miss some of the traffic signs on the road because of overcrowding due to neighboring vehicles. So, we have introduced the TSR system with an aim of detecting and recognizing all the emerging traffic signs.

### 3. METHODOLOGY

Initially, we opted for the data collection. We applied some techniques on the data for exploration and then visualized the data through EDA techniques. And finally, we build in this study a classification model based on the CNN. Afterwards, model is trained and validated and then based on the validated model, we attempted a test. And afterwards, we deployed our classifier. As we mentioned earlier that for classification, we have used CNN model, it is based on convolution of filters and images or raw inputs.



In this section, we will describe the CNN based approach. A flowchart of the main phases is shown in Figure 1.

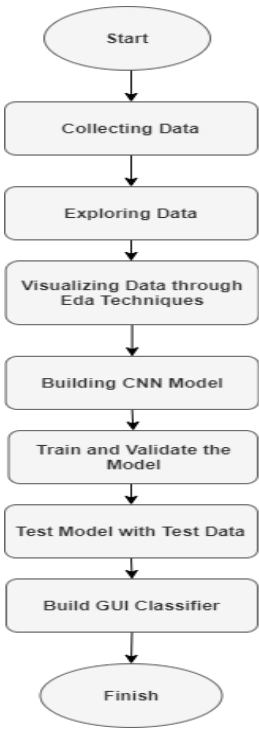


**Figure 1.** Flowchart of methodology.

In NNs, CNN is one of the main categories to do images recognition, images classifications. CNN image classifications take an input image, process it and classify it under certain categories (Eg, Dog, Cat, Tiger, Lion).

Technically, deep learning CNN models to train and test, each input image will pass it through a series of convolution layers with filters (Kernels), Pooling, fully connected layers (FC) and apply Softmax function to classify an object with probabilistic values between 0 and 1. The calculation of the convolutional layer can be simplified as shown in Equation (1):

$$a^k = f \left( \sum_{i,j=1}^3 w_{ij}^k \times x_{ij} + b^k \right) \quad (1)$$

Where,  $k_{w_{ij}}$  is the weight value of the convolution kernel;  $i_j$  x the input pixel value corresponding to the weight of the convolution kernel; the offset corresponding to the first convolution kernel;  $k$  b is the bias;  $f()$  x is the activation function. CNN commonly used activation functions as an RLU (Rectified Linear Unit).

The Figure 2 is a complete flow of CNN to process an input image and classifies the objects based on values.

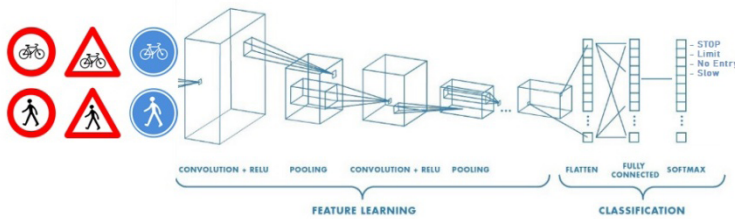


**Figure 2.** Neural network with many convolutional layers.

Convolution Layer is the first layer to extract features from an input image. Convolution preserves the relationship between pixels by learning image features using small squares of input data. It is a mathematical operation that takes two inputs such as image matrix and a filter or kernel.

In Non-Linearity (ReLU): ReLU stands for RLU for a non-linear operation. Its purpose is to introduce non-linearity in our ConvNet. Since, the real-world data would want our ConvNet to learn would be non-negative linear values.

The Pooling Layer would reduce the number of parameters when the images are too large. Spatial pooling also called sub-sampling or down-sampling which reduces the dimensionality of each map but retains important information. Spatial pooling can be of different types:

- Max Pooling
- Average Pooling
- Sum Pooling

Max pooling takes the largest element from the rectified feature map. Taking the largest element could also take the average pooling. Sum of all elements in the feature map call as sum pooling.

Fully Connected Layer is attached flattened the matrix into vector and feed it into a fully connected layer like a NN. The feature map matrix will be converted as vector ( $x_1, x_2, x_3, \dots$ ). With the fully connected layers, we combined these features together to create a model. Finally, we have an activation function such as SoftMax or sigmoid to classify the outputs as cat, dog, car, truck etc.

In the subsequent sections, we present the detailed steps of our methodology.

## 4. DATA PREPROCESSING

For this project, we have selected the publicly available dataset from Kaggle. The dataset contains more than 50,000 images of different traffic signs. It is further classified into 43 different classes. Few of them are shown in Figure 3. Prior to training a NN, data is divided in training and test sets.



**Figure 3.** Dataset of traffic signs.

The ‘train’ folder contains 43 folders each representing a different class. The range of the folder is from 0-42. With the help of OS module, we must iterate overall the classes and append images and their respective labels in the data and label list.

An image is made up of pixels and each pixel has 3 values to specify its color i.e. RGB (Red, Green Blue). In order for machines to understand the image, we converted the image into numbers. For this purpose, we use the PIL (Python Imaging Library) that can perform many image manipulations tasks. The subsequent step was of resizing the images into some uniform criteria. Therefore, we resize all the images to a fixed size, such as, 30x30. Let's traverse through all the classes, open the image using PIL and also resize the image to 30x30 dimensions. Then we will append the data and label in the X and Y list respectively. After storing all the images and their labels into lists (data and labels), the list was further transformed into NumPy arrays for feeding the model. Nevertheless, finally the shape of

data is (39209, 30, 30, 3) which means that there are 39,209 images of size 30x30 pixels and the last 3 means the data contains colored images (RGB Value).

4.1. APPLYING EDA TECHNIQUES

In order to apply the EDA techniques, we have divided the process in three steps. Initially, we have focused on in-depth understanding for the dataset. Subsequently, some data cleaning is applied. EDA is the practice of using visual and quantitative methods to understand and summarize a dataset without making any assumptions about its contents. It is a crucial step to take before diving into machine learning or statistical modeling because it provides the context needed to develop an appropriate model for the problem at hand and to correctly interpret its results. Afterwards, we have attempted to find some correlations available in the dataset.

**Step-1: Understanding the Data:** Tables 1-2 present the details of data set by summarizing the first and last 5 rows respectively, its attributes and associated values. The dataset contains 12630 rows and 8 columns. This indicates that the data is enough to be used for any Deep learning architecture.

Table 1. Showing head function.

Data No.	Width	Height	ROI.X1	ROI.Y1	ROI.X2	ROI.Y2	Class Id	Path
12625	42	41	5	6	37	36	12	Test/12625.png
12626	50	51	6	5	45	46	33	Test/12626.png
12627	29	29	6	6	24	24	6	Test/12627.png
12628	48	49	5	6	43	44	7	Test/12628.png
12629	32	31	6	5	27	26	10	Test/12629.png

Table 2. Showing tail function.

Data No.	Width	Height	ROI.X1	ROI.Y1	ROI.X2	ROI.Y2	Class Id	Path
0	53	54	6	5	48	49	16	Test/00000.png
1	42	45	5	5	36	40	1	Test/00001.png
2	48	52	6	6	43	47	38	Test/00002.png
3	27	29	5	5	22	24	33	Test/00003.png
4	60	57	5	5	55	52	11	Test/00004.png

**Step-2: Cleaning the Data:** After understanding the data it was further examined null or missing values. Data set is free from missing values as depicted in Table 3.

**Table 3.** Showing cleaning process.

Width	0
Height	0
RoiX1	0
RoiY1	0
RoiX2	0
RoiY2	0
ClassId	0
Path	0
dtype	Int64

**Step-3: Analyzing the Relationship:** Correlation matrix is used to summarize the data as an input into more advanced analysis. We get visual representation of correlation matrix by heatmap. The heatmap is a way of representing the data in a 2D (Two-Dimensional) form. The data values are represented as colors in the graph. The goal of the heatmap is to provide a colored visual summary of information. It is a graphical representation of data where the individual values contained in a matrix are represented as colors. It is a bit like looking a data table from above. It is useful to display a general view of numerical data, not to extract specific data point. Figure 4 shows heatmap.



**Figure 4.** Heatmap.

A bar chart or bar graph is a chart or graph that presents categorical data with rectangular bars with heights or lengths proportional to the values that they represent. The bars can be plotted vertically or horizontally. A vertical bar chart is sometimes called a column chart.

We used bar to plot graphs for any column's visual representation. Here we used width and height column of dataset with bar plot function. Figure 5 shows bar plot for input.

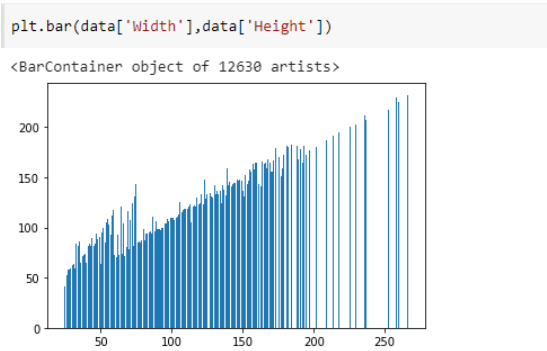


**Figure 5.** Bar plot.

## 5. EXPERIMENTAL SETUP FOR CNN

To classify the images into their respective categories, we developed and trained. The CNN have proved the state of the art in image classification tasks and this is what we will be using for our model. A CNN is made up of convolutional and pooling layers. At each layer, the features from the image are extracted that helps in classifying the image.

Apart from this, a dropout layer is also added, which is used to handle the over fitting of the model. The dropout layer drops some of the neurons while training. Finally, the model is compiled with cross entropy measures, because the dataset has multi classes to be classified. The Table 4 shows layers in details of CNN model along with parameters.

**Table 4.** Architecture of CNN model.

Layer Number	Layer Type
L1	Conv2D (32x5x5), ReLU
L2	Conv2D (32x5x5), ReLU
L3	MaxPool2Dlayer(pool_size=(2,2))
L4	Dropout layer (rate=0.25)
L5	Conv2D (64x5x5), ReLU
L6	Conv2D (64x5x5), ReLU
L7	Flatten Layer (1 Dimension)
L8	DenseFullyconnected layer (256 nodes,ReLU)
L9	Dropout layer (rate=0.5)
L10	Dense Layer (43 nodes, softmax)

### 5.1. TRAIN AND VALIDATE THE MODEL

After building the architecture of model. The model is defined, and the data is ready. To start the training of our model we initialize the training set, validation set, batch size and no of epochs.

So, for classifier, we opted for multiple architectures of CNN model. We experimented with various number of batch sizes and activation functions. The Table 5 shows the details of all our implemented models.

**Table 5.** CNN trained model summary.

CNN Model No.	Batch Size	Epochs	Test Accuracy (%)
1	32	100	82.00
2	32	110	91.00
3	64	100	94.00
4	64	110	95.00

However, as we find out that CNN4 has outperformed to the rest of other models. Therefore, we used this model to further demonstrations associated with it.

Therefore, this model is trained with batch size 64. And after 110 epochs, the accuracy was stable. Our model got 95% accuracy on the training dataset. We plot the graph for accuracy and loss. Figures 6-7 showing accuracy and loss respectively.

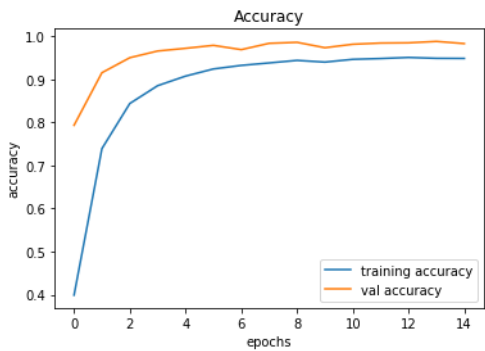


**Figure 6.** Accuracy of trained model CNN4.

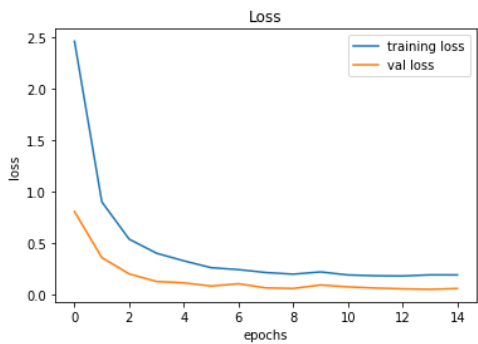


**Figure 7.** Loss of trained model CNN 4.

Finally, we build a graphical user interface for our traffic signs classifier. The GUI (Graphical User Interface) is built for uploading the image and to predict the traffic sign we must provide the same dimension we have used when building the model. A GUI will save a lot of time in testing and seeing the results of our model prediction.

From the interface of the GUI application, we will ask the user for an image and extract the file path of the image. Then we use the trained model that will take the image data as input and provide us the class our image belongs to.

## 6. RESULTS

This section presents the series of experiments carried out to validate the CNN approach for recognition of road signs. To get the road images, we use camera of 16 megapixels, to get the good distribution of images at different angles and positions. The images in each class are randomly chosen.

By observing Figures 8-9, we got an understanding of how autonomous vehicles can take advantage of CV (Computer Vision) and Deep Learning techniques to automatically recognize and classify from multiple classes.



**Figure 8.** Showing results of speed Limit(30km/hr).



**Figure 9.** Showing results of turn right ahead.

## 7. CONCLUSION

In this research work, we demonstrated and developed an efficient alert traffic sign detection and recognition system. Both color information and the geometric property of the road signs are used to classify the detected traffic signs. The experiment shows that the system can achieve a high detection rate of 95%. System is giving accurate results under different illumination conditions, weather conditions, day light conditions and different speed levels of the vehicle. We have successfully classified the traffic signs classifier with 95% accuracy and visualized how our accuracy and loss changes with time, which is pretty good from a



simple CNN model. The techniques implemented in this research can be used as a basis for developing general purpose, advanced intelligent traffic surveillance systems.

## ACKNOWLEDGEMENT

We are thankful to the Department of Computer Systems Engineering, Mehran University of Engineering & Technology, Jamshoro, Pakistan, for providing facilities to conduct this research work.

## REFERENCES

- Boujemaa, K.S., Berrada, I., Bouhoute, A., & Boubouh, K. (2017).** Traffic Sign Recognition Using Convolutional Neural Networks. In *2017 International Conference on Wireless Networks and Mobile Communications (WINCOM)*, pp. 1-6. <https://doi.org/10.1109/WINCOM.2017.8238205>
- De la Escalera, A., Armingol, J. M., & Mata, M. (2003).** Traffic Sign Recognition and Analysis for Intelligent Vehicles. *Image and Vision Computing*, 21(3), 247-258. [https://e-archivo.uc3m.es/bitstream/handle/10016/7089/traffic\\_escalera\\_IVC\\_2003\\_ps.pdf](https://e-archivo.uc3m.es/bitstream/handle/10016/7089/traffic_escalera_IVC_2003_ps.pdf)
- Fleyeh, H. (2008).** *Traffic and Road Sign Recognition* (Doctoral Dissertation). Napier University. <https://www.diva-portal.org/smash/get/diva2:523372/FULLTEXT01.pdf>
- Girshick, R., Donahue, J., Darrell, T., & Malik, J. (2014).** Rich Feature Hierarchies for Accurate Object Detection and Semantic Segmentation. In *2014 IEEE Conference on Computer Vision and Pattern Recognition*, pp. 580-587. <https://doi.org/10.1109/CVPR.2014.81>
- Girshick, R., Donahue, J., Darrell, T., & Malik, J. (2015).** Region-Based Convolutional Networks for Accurate Object Detection and Segmentation. *IEEE Transactions on Pattern Analysis and Machine Intelligence*, 38(1), 142-158. <https://doi.org/10.1109/TPAMI.2015.2437384>

- Gunawardana, P.M. (2010).** *Automatic Detection and Recognition of Traffic Signs* (Doctoral Dissertation). University of Colombo, Sri Lanka.
- He, K., Zhang, X., Ren, S., & Sun, J. (2015).** Spatial Pyramid Pooling in Deep Convolutional Networks for Visual Recognition. *IEEE Transactions on Pattern Analysis and Machine Intelligence*, 37(9), 1904-1916. <https://doi.org/10.1109/TPAMI.2015.2389824>
- Jung, S., Lee, U., Jung, J., & Shim, D.H. (2016).** Real-Time Traffic Sign Recognition System with Deep Convolutional Neural Network. In *IEEE 13th International Conference on Ubiquitous Robots and Ambient Intelligence (URAI)*, pp. 31-34 <https://www.semanticscholar.org/paper/Real-time-Traffic-Sign-Recognition-system-with-deep-Jung-Lee/17a608865ba3c6b2c27fcb18973c27139560954a>
- Kale, A.J., & Mahajan, R.C. (2015).** A Road Sign Detection and the Recognition for Driver Assistance Systems. *IEEE International Conference on Energy Systems and Applications*, pp. 69-74.
- Sermanet, P., & LeCun, Y. (2011).** Traffic Sign Recognition with Multi-Scale Convolutional Networks. In *The 2011 International Joint Conference on Neural Networks*, pp. 2809-2813. <https://doi.org/10.1109/IJCNN.2011.6033589>
- Simonyan, K., & Zisserman, A. (2014).** Very Deep Convolutional Networks for Large-Scale Image Recognition. *arXiv preprint*. <https://arxiv.org/abs/1409.1556>
- Szegedy, C., Ioffe, S., Vanhoucke, V., & Alemi, A. (2016).** Inception-V4, Inception-Resnet and the Impact of Residual Connections on Learning. *arXiv Preprint*. <https://arxiv.org/abs/1602.07261>
- Vennelakanti, A., Shreya, S., Rajendran, R., Sarkar, D., Muddegowda, D., & Hanagal, P. (2019).** Traffic Sign Detection and Recognition Using a CNN Ensemble. In *2019 IEEE International Conference on Consumer Electronics (ICCE)*, pp. 1-4. <https://doi.org/10.1109/ICCE.2019.8662019>

**Xu, S., Niu, D., Tao, B., & Li, G. (2018).** Convolutional Neural Network Based Traffic Sign Recognition System. *IEEE 5th International Conference on Systems and Informatics (ICSAI)*, pp. 957-961.

**Zaklouta, F., & Stanciulescu, B. (2014).** Real-Time Traffic Sign Recognition in Three Stages. *Robotics and Autonomous Systems*, 62(1), 16-24. <https://doi.org/10.1016/j.robot.2012.07.019>

/08/

# ACCEPTABILITY IN THE OPTIMAL FORMULATION OF CHRYSIN WITH PARTIAL REPLACEMENT OF PITUCA FLOUR

---

**Pervis Paredes**

National University Federico Villarreal, (Peru).

E-mail: [pparedes@unfv.edu.pe](mailto:pparedes@unfv.edu.pe) ORCID: <https://orcid.org/0000-0002-7186-9614>

**Doris Esenarro**

National University Federico Villarreal, (Peru).

E-mail: [desenarro@unfv.edu.pe](mailto:desenarro@unfv.edu.pe) ORCID: <https://orcid.org/0000-0002-7186-9614>

**Jannina J. Bernabe**

National University Federico Villarreal, (Peru).

E-mail: [jbernabe@unfv.edu.pe](mailto:jbernabe@unfv.edu.pe) ORCID: <https://orcid.org/0000-0002-7186-9614>

**Wilber Quispe**

National University Federico Villarreal, (Peru).

E-mail: [wquispe@unfv.edu.pe](mailto:wquispe@unfv.edu.pe) ORCID: <https://orcid.org/0000-0002-7186-9614>

**Recepción:** 10/09/2020 **Aceptación:** 30/10/2020 **Publicación:** 13/11/2020

## **Citación sugerida Suggested citation**

Paredes, P., Esenarro, D., Bernabe, J. J., y Quispe, W. (2020). Acceptability in the optimal formulation of chrysin with partial replacement of pituca flour. *3C Tecnología. Glosas de innovación aplicadas a la pyme. Edición Especial, Noviembre 2020*, 137-147. <https://doi.org/10.17993/3ctecno.2020.specialissue6.137-147>

## ABSTRACT

The aim of this research is to determine the acceptability of chrysin with the partial replacement of pituca flour by protein intake. The methodology applied was based on a quasi-experimental design and the ingredients used for the research were foods with a high nutritional percentage that are pituca flour (16.36%) and wheat flour (47.27%), margarine (5.45%), white sugar (5.45%), water (25%) and yeast (0.09%). The results obtained through the descriptive test in which the results of 20 panelists were collected, the data were evaluated through the MINITAB and SPSS programs. The number of formulations and at the same time the prognosis of ingredient behaviour was determined by a Taguchi chart. The acceptability of chrysin was determined by microbiological studies and physicochemical analyses obtained, which resulted in no differences from the product, but if they are within the parameters required by the standard, the percentage of proteins was also checked.

## KEYWORDS

Chrysin, Pituca, Quinoa, Descriptive test, Yeast, Optimal, Variation, Texture, Range.

# 1. INTRODUCTION

The advance of scientific knowledge confirms every day that the correct nutrition, fruit of an adequate nutrition, is one of the determining factors in health. A healthy diet, which maintains constant the composition of the tissues, which allows the functioning of devices and systems, which guarantees the reproduction and which gives the individual a state of well-being that leads him to the activity, is the one that fulfills four fundamental laws; that is: the law of quantity, quality, harmony and adequacy (Bustos & Marapara, 2016). However, the nutritional recommendations, the progress of technology, the availability and access to food, do not allow by themselves, the population to adopt adequate forms of life and food. The food of today's society is highly influenced by the daily habits that are implemented in many occasions as a result of the pace of life it imposes. In Peru due to biological diversity, there are many varieties of fruits with many properties for health care, that is why this fruit called pituca has been chosen, for its physical and chemical characteristics, the dietary patterns incorporated mainly in urban areas condition the choice of processed foods with low nutritional value, low fiber content, high percentages of saturated fats, refined sugars, additives, preservatives (predominantly sodium) and high caloric value. This situation predisposes to the development of certain diseases that arise as a result of an unhealthy diet: obesity (Alvarado *et al.*, 2020), malnutrition, dyslipidemia, high blood pressure and cardiovascular disease, among others. This research aims to develop a change in bakery products, the replacement of wheat flour (traditional in the preparation of bread) by pituca flour (*colocasia esculenta*) in the chrysin is considered, since *colocasia esculenta* has greater nutritional properties wheat and its composition manages to adapt to heat treatment to extract flour from it (Cerón *et al.*, 2011) .

Chrysin becomes one of the preferred options and can be considered a food for mass consumption. The pituca would play an important role in food, rich in minerals and carbohydrates beneficial to health. (Torres & Montero, 2014). In our country it can be found profusely in areas of the jungle, although its consumption at a local level is only observed in Amazonian populations, especially in native populations or those who have knowledge of its digestive use, but the rest of the country, unknown this tuber, its properties and uses (Quispe *et al.*, 2020).

## 2. METHODOLOGY

This research was carried out at the Federico Villarreal National University physicochemical and microbiology laboratory, where the drying process of the pituca was carried out in order to extract the flour that would be used to produce the croutons de aljonjolí. For the preparation of chrysins, the laboratory of the company Exandal S.A.C. where innovations in flour products were previously developed from germ, tare, etc. The quantity in percentage of ingredients to be used is detailed.

**Table 1.** Control chrysin ingredients, chrysin with partial replacement.

Ingredients (g/100g)	Chrysine control (0%)	Optimum chrysin (30%)	Percentage average
Water	27.50	27.50	25.00%
White Sugar	6.00	6.00	5.45%
Margarine	6.00	6.00	5.45%
Yeast	0.10	0.10	0.09%
Sesame	0.40	0.40	0.09%
Pituca Flour	12.00	18.00	16.36%
Wheat flour	58.00	52.00	47.27%

Table 1 shows the inputs for the preparation with their respective portions and their percentage of participation for the preparation.

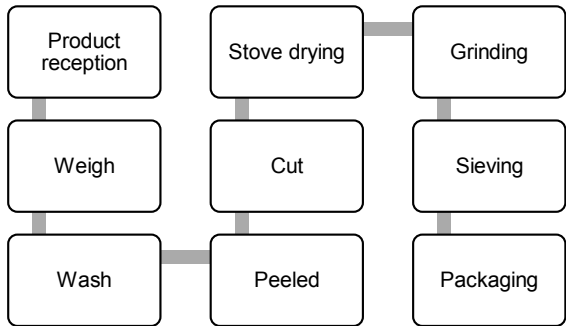


**Figure 1.** Flow chart for obtaining pituca flour.

In the Figure 1 It can see the sequence First stage: Obtaining pituca flour (*colocasia esculenta*), as well as the processes established in each stage.



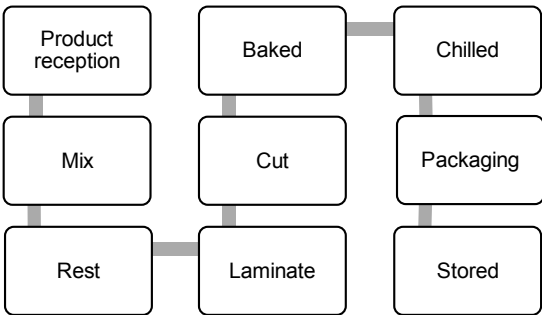


**Figure 2.** Flow chart for obtaining chrysin with pituca flour replacement.

In the Figure 2 It the second stage: Preparation of sesame seeds with the optimal formulation (colocasia esculenta).

Third stage: Sensory evaluation of the chrysin with optimal formulation.

It was carried out with 20 panelists in a 5-level Hedonic scale. Fourth stage: Physical-chemical and microbiological analysis of the chrysin with optimal formulation.

The optimal formulation will be analyzed from NTS N to 071-minsa / digesa-v.0.1.

The instrument used for data collection was Groove & Alvarado’s (2016) thesis to apply for the title of food engineer.

### 3. RESULTS

The results obtained from the development of the tests carried out during the elaboration of the product in the laboratory carried out are detailed below.

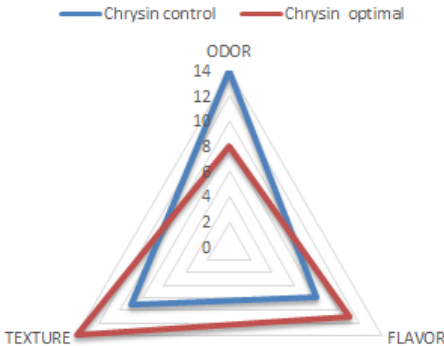


**Figure 3.** Sensory analysis results with panelists.

The Figure 3 shows a graph with their respective characteristics such as texture, odor, flavor obtained from elaborated tests.

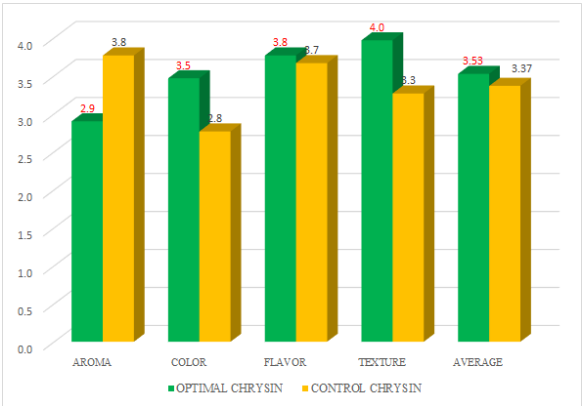


Figure 4. Sensory analysis results with panelists.

As can be seen in Figure 3 the optimum chrysinum compared to the chrysinum control has a better taste, colour and texture than the average control or chrysinum control (in this case based on wheat flour only).

3.1. RESULTS OF THE PHYSICO-CHEMICAL ANALYSIS

Table 3. pH analysis results.

	Test value = 7,45					
	t	gl	Sig. (bilateral)	Difference of means	95% confidence interval of difference	
					lower	higher
pH	-,736	4	,503	-,17000	-,8116	,4716

In the pH analysis, Table 3 statistically it turns out that the results obtained do not differ significantly from the parameter in which  $p > 0.05$ , therefore, the null hypothesis is rejected for having obtained results within the limits.

Table 4. Protein analysis results.

	Test value = 12					
	t	gl	Sig. (bilateral)	Difference of means	95% confidence interval of difference	
					lower	higher
Protein	-1,125	4	,323	-,05600	-,1942	,0822

In the analysis of the proteins Table 4 statistically it turns out that the results obtained to the parameter do not differ significantly, therefore the null hypothesis is rejected for having obtained results within the limits.

**Table 5.** Results of ash analysis.

	Test value = 3					
	t	gl	Sig.(bilateral)	Difference of means	95% confidence interval of difference	
					lower	higher
Ash	-122,275	4	,000	-1,16000	-1,1863	-1,1337

In the analysis of the ash Table 5 statistically it turns out that there are significant differences the results obtained to the parameter in which  $<0.05$ , therefore the null hypothesis is accepted since it is not in the primitive limits.

### 3.2. RESULTS OF THE MICROBIOLOGICAL ANALYSIS

**Table 6.** Results of the microbiological analyzes.

Essays	Optimal formulation	Limits ntp 206.001:2016	
		Min.	Max.
Moulds (UFC/g)	59x10	10x2	10x3
Escherichia coli (UFC/g)	< 3	3	20
Salmonella sp.	Absence /25g	Absence /25g	
Mesophilic aerobes (CFU/g)	24x10-2	10x4	10x5

In Table 6 you can see the results obtained from the microbial analyzes, having as the optimal results required as shown by the data.

## 4. DISCUSSION

The results of the acceptability of the chrysins are comparable to other non-traditional products (Cerón *et al.*, 2011) since in the production of cookies with pituca flour it indicates that in the flavor, the odor is not demonstrated differentiation, being accepted by the panelists.

The reports of the Lima-Metropolitan Association (Hleap-Zapata, Burbano-Portillo, & Mora-Vera, 2017) show that snacks (corn sticks, chips, sweet potatoes, etc.) in Lima are

highly consumed, which means that there is a 30% excess of consumption of these, being the main cause of obesity (Carranza *et al.*, 2020).

Although most of the baby foods in the lunch box are cookies, crackers and some bakery products, within the first 10 consumptions of regular diet, this study was conducted to bring a not new product, but with changes in its ingredients by enriching it with pituca and wheat flour, and encourage the production of these in various bakery products (Meng *et al.*, 2017; Correia, Soares & Brites, 2017).

## 5. CONCLUSIONS

Pituca fruit as an excellent food for athletes or people who do some physical work, because it provides a lot of energy, but above all, it is vital as food for children, especially babies in their bone and dental stage, so its use is important (Umo & Alabi, 2016).

The partial formulation of optimal chrysin is accepted, with the results of the sensory, physicochemical and microbiological analysis it is concluded that the product is adequate and has the quality characteristics to perform its commercialization.

Finally, another study obtained as a result in the sensory analysis performed on extruded snacks (quinoa flour, sweet potato flour, and tarwi flour) coated with a 50 ° Brix honey solution, determined that there is no significant difference between the level to please the 16 formulations (Pérez, Elías, & Delgado, 2017).

The incorporation of a new drink with healthy characteristics and with a unique product on the market, makes it more likely that consumers can have alternatives to choose from their diet for their charity (Quispe *et al.*, 2020).

The addition of quinoa flour if it affects the sensory acceptability of the product according to the S / R determines that the higher the amount of quinoa flour shows lower the acceptability of the product.

## REFERENCES

- Alvarado, K., Esenarro, D., Rodriguez, C., & Vasquez, W.** (2020). Lemna minor influence in the treatment of organic pollution of the industrial effluents. *3C Tecnología. Glosas de innovación aplicadas a la pyme*, 9(3), 77-97. <https://doi.org/10.17993/3ctecno/2020.v9n3e35.77-97>
- Bustos, G. C., & Marapara, J. L.** (2016). *Parámetros de secado en bandeja de colocasia esculenta (pituca) para la producción de harina y su uso en galletas*. <http://repositorio.unapiquitos.edu.pe/handle/UNAP/4902>
- Carranza, K., Rodriguez, C., Esenarro, D., Veliz, M., & Arteaga, J.** (2020). Sensory evaluation of a perfume made of orange essential oil. *International Journal of Chemical Engineering and Applications*, 11(4). <http://www.ijcea.org/vol11/786-H3021.pdf>
- Cerón, A. F., Hurtado, A., Osorio, O., & Buchelly, M.** (2011). Estudio de la formulación de harina de patata de la variedad marrón pardúnque (*solanum tuberosum*) como un sustituto parcial de la harina de trigo en la panadería. *Biotechnología en el sector agropecuario y agroindustrial*, 9(1), 105-111. <http://www.scielo.org.co/pdf/bsaa/v9n1/v9n1a13.pdf>
- Correia, P. M. R., Soares, A. M., & Brites, C.** (2016). Quality Characteristics of Maize Flours and Breads. *International Journal of Food Engineering*, 2(2), 113-118. <https://doi.org/10.18178/ijfe.2.2.113-118>
- Groove, A., & Alvarado, K.** (2016). Estudios estadísticos de pruebas sensoriales de la harina compuesta para hornear. *Revista Boliviana de Estadísticas Químicas*, 3(2).
- Hleap-Zapata, J. I., Burbano-Portillo, M. Y., & Mora-Vera, J. M.** (2017). Evaluación fisicoquímica y sensorial de salchichas incluyendo harina de quinoa (*Chenopodium quinoa* W.). *Biotechnología en el Sector Agrícola y Agroindustrial*, 15(2), 61-71. <http://www.scielo.org.co/pdf/bsaa/v15nspe2/1692-3561-bsaa-15-spe2-00061.pdf>
- Meng, Q., Fan, H., Ji, S., Li, J., & Zhang, L.** (2017). Effects of Different Drying Methods on Physico-Chemical Properties of *Dendrobium Officinale*. *International Journal of Food Engineering*, 3(1), 35-41. <https://doi.org/10.18178/ijfe.3.1.35-41>

**Pérez, K., Elías, C., & Delgado, V.** (2017). High-protein snack: an extruded from quinoa (*Chenopodium quinoa* Willd.), tarwi (*Lupinus mutabilis* Sweet), and sweet potato (*Ipomoea batatas* L.). *Scientia Agropecuaria*, 8(4). <https://revistas.unitru.edu.pe/index.php/scientiaagrop/article/view/1641>

**Quspe, W., Esenarro, E., Rodriguez, C., Alvarado, K., Ruiz, C., & Alvarez, W.** (2020). Physicochemical quality of honey bee (*Apis mellifera*) in three bioclimatic zones in Apurimac Perú. *International Journal of Advanced Science and Technology*, 29(7), 268 - 275. <http://sersec.org/journals/index.php/IJAST/article/view/13219>

**Torres, A., & Montero, P. M.** (2014). Utilización de almidón de malanga (*colocasia esculenta* L.) en la elaboración de salchichas tipo Frankfurt. *Biotecnología en el Sector Agropecuario y Agroindustrial*, 12(2), 97-105. <https://dialnet.unirioja.es/servlet/articulo?codigo=6117735>

**Umo, A. M., & Alabi, S. B.** (2016). Advances in Super-Saturation Measurement and Estimation Methods for Sugar Crystallisation Process. *International Journal of Food Engineering*, 2(2), 108-112. <https://doi.org/10.18178/ijfe.2.2.108-112>



/09/



# YIELD OF TOCOSH FLOUR IN TWO POTATO VARIETIES (SOLANUM TUBEROSUM) AND THEIR CHARACTERISTICS

---

**Jorge Jave Nakayo**

Universidad Nacional Mayor de San Marcos - UNMSM, Lima, (Perú).

E-mail: [jorge.jave@unmsm.edu.pe](mailto:jorge.jave@unmsm.edu.pe) ORCID: <https://orcid.org/0000-0003-3536-881X>

**Verónica Espinel Pino**

Universidad Técnica de Manabí, Manabí, (Ecuador)

E-mail: [vespinel@utm.edu.ec](mailto:vespinel@utm.edu.ec) ORCID: <https://orcid.org/0000-0002-7604-7599>

**Jorge Luis López Bulnes**

Universidad Nacional Mayor de San Marcos - UNMSM, Lima, (Perú).

E-mail: [jlopezb@unmsm.edu.pe](mailto:jlopezb@unmsm.edu.pe) ORCID: <https://orcid.org/0000-0002-9583-1143>

**Violeta Vega Ventosilla**

Universidad Nacional Federico Villarreal – UNFV, Lima, (Perú).

E-mail: [vvega@unfv.edu.pe](mailto:vvega@unfv.edu.pe) ORCID: <https://orcid.org/0000-0002-7763-6993>

**Recepción:** 13/11/2020 **Aceptación:** 13/11/2020 **Publicación:** 13/11/2020

## **Citación sugerida Suggested citation**

Jave, J., Espinel, V., López, J. L., y Vega, V. (2020). Yield of tocosh flour in two potato varieties (solanum tuberosum) and their characteristics. *3C Tecnología. Glosas de innovación aplicadas a la pyme. Edición Especial, Noviembre 2020*, 149-159. <https://doi.org/10.17993/3ctecno.2020.specialissue6.149-159>

## ABSTRACT

In the present investigation it allows to demonstrate the yield of the flour of tocosh of two varieties of potato (*solanum tuberosum*) canchán and native variety of “calamarca The raw material was acquired in the district of Paucartambo province of Pasco department of Pasco, to 2880 msnm. For the experimental study the two varieties of potatoes were placed using as technique a pool with a water current with varied times, where the microorganisms act and increase their activity related to the acidity. The evaluation was made using the tukey trial to compare the two varieties, obtaining results for the native variety “calamarca” which had a fermentation time of 45 days to have all the conditions to be tocosh with a flour yield of 59.6% compared to the variety of canchán whose fermentation time was 31 days with a yield of 45%.

## KEYWORDS

Tocosh, Yield, *Solanum tuberosum*, Potato, Calamarca, Flour.

# 1. INTRODUCTION

Potato is undoubtedly one of the most important crops in the country Peru has more than 5,000 potato varieties in terms of area planted (260,000 ha/year), number of producers who depend on it (600,000), contribution to the national economy (11.3% of agricultural GDP) and to the human diet (average consumption of 68.4 kg/inhabitant/year). Potato tocosh is a naturally processed potato for nutritional and healing purposes of traditional Peruvian medicine (Velasco-Chong, *et al.*, 2020). The potato is produced in 19 of Peru's 24 departments, which demonstrates its plasticity in terms of adaptation. As the centre of origin of the potato, Peru maintains a culture of diversity; for this reason, in the mountains, it is common today to find mixed agriculture with native and improved varieties (Velasco-Chong, *et al.*, 2020).

Straw or "ichu" and pressed mechanically with stones under a stream of water from a spring. This treatment gives products nutritional and therapeutic properties used only by those who know and consume them and which could be a natural alternative to alleviate, prevent or cure some diseases (Sandoval *et al.*, 2015), a product obtained thanks to butyric fermentation, while this product has an unpleasant smell, which is a limitation for its consumption in most of the population, this product offers a diversity of health benefits, which is why it is reason to study to find the solution for which this limitation should be a problem in consumer acceptance (Quispe *et al.*, 2020).

We will use two varieties, which will be placed, in a well with a stream of water in a varied time, in which microorganisms act that in turn will increase the activity related to acidity. It seeks to extend the life of a product, transforming it into another as is tocosh flour; evaluate the sensory and physicochemical properties. To make the comparison between two varieties that will produce results that can show us which of them has better properties; better yield and that ferments in less time (Carranza *et al.*, 2020).

We will determine the results based on tocosh in the varieties of potatoes Yungay and Conchán that come from the district of Paucartambo (Agricultural and Hydroelectric Valley) with an altitude of 2880 meters above sea level, province of Pasco in the department of Pasco.

## 2. METHODOLOGY

The raw material for this study was acquired from the district of Paucartambo province of Pasco department of Pasco, at 2880 meters above sea level the varieties of potato *solanum tuberosum* used are Canchan and native Calamarca.

For the experimental study were placed the two varieties of potatoes in a pool with a water current with varied times in order that the microorganisms act and increase their activity related to the acidity.

The parameters considered for the elaboration of the tocosh were: ambient temperature between 10 and 18 °C Water temperature between 5 and 15 °C average storage time 30 days  $H\ 6.0 \pm 2.0$  (Alvarado *et al.*, 2020).

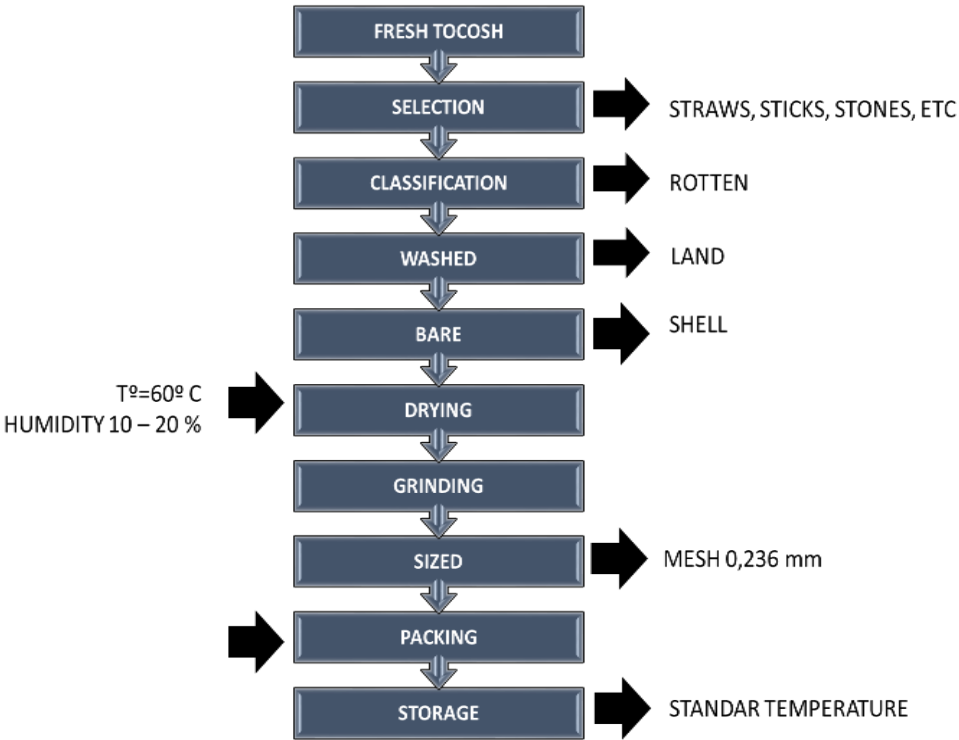


**Figure 1.** Flowchart of tocosh flour processing (self-made source).

Figure 1 shows the unit operations for the processing of tocosh of the two varieties under study by which the results for the present study will be obtained.

### 3. RESULTS

The yield in the production of tocosh flour obtained with the flow of tocosh flour processing figure 1 for each variety of potato in the study was: 59.60%, for the native variety 45%, variety of canchan.

The fermentation time for the native variety was 45 days and for the canchan variety was 45 days.

**Table 1.** Evaluation of physicochemical characteristics during fermentation (Canchan variety).

Control		General appearance	Smell	Ph	T
1	14/04/2019	Smooth shell with hard consistency, characteristic of the potato.	Characteristic of the potato	6.56	9°C
2	21/04/2019	Soft shell of soft consistency	Strong fermentation odor	6.40	9°C
3	28/04/2019	Soft shell with soft consistency	Strong fermentation odor	80	9°C
4	05/05/2019	Soft shell with soft consistency	Strong fermentation odor	5.20	9°C
5	12/05/2019	Robust housing with soft consistency, tocosh feature	Tocosh feature	4.70	9°C

Table 1 shows the evaluation of the physicochemical characteristics during fermentation (Canchan variety), the dates of the controls of its structural changes and its odours, the pH and the temperatures of each sample.

The fermentation of the Canchan potato variety in the production of tocosh flour begins at a pH of 6.56 and ends at a pH of 4.70.

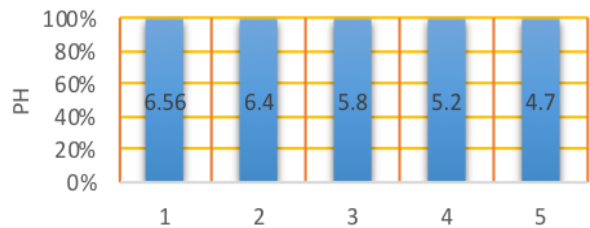


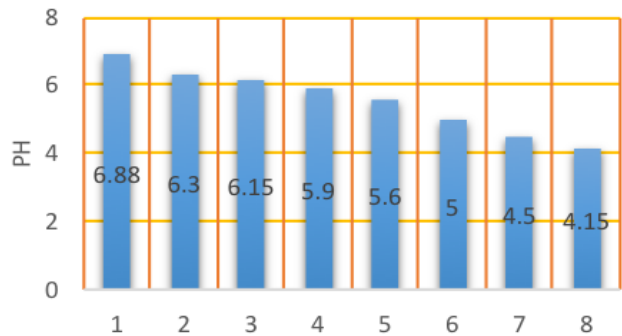
**Figure 2.** PH variation at 9°C - PAPA CANCHAN.

In Figure 2, the general appearance and smell of the potato changes during the fermentation process; starting the fermentation of the potato in study with smooth skin, hard consistency and characteristic smell of fresh and finished potato.

**Table 2.** Evaluation of physicochemical characteristics during fermentation (native variety).

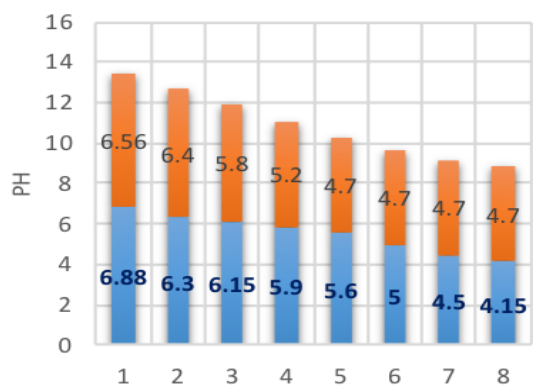
Control		General appearance	Smell	Ph	T
1	14/04/2019	Smooth shell with hard consistency, characteristic of the potato	Characteristic of the potato	6.88	9 °C
2	21/04/2019	Characteristic of the smooth potato peel of soft consistency	Strong fermentation odor	6.30	9 °C
3	28/04/2019	Smooth, hard consistency shell	Strong fermentation odor	6.15	9 °C
4	05/05/2019	Smooth, hard consistency shell	Strong fermentation odor	5.90	9 °C
5	12/05/2019	Soft rough skin.	Strong fermentation odor	5.60	9 °C
6	19/05/2019	Rough shell with a soft consistency.	Strong fermentation odor	5.00	9 °C
7	25/05/2019	Rough shell of soft consistency.	Strong fermentation odor	4.50	9 °C
8	01/06/2019	Roughened shell of soft consistency.	Tocosh feature	4.15	9 °C

Table 2 shows the evaluation of the physicochemical characteristics during fermentation (Nativa variety), the dates of controls of its structural changes and odours, the pH and temperatures of each sample.



**Figure 3.** PH variation at 9°C - NATIVE POTATO.

Figure 3 shows that the general appearance and odour of the potato changes during the fermentation process; the two varieties of potatoes under study with smooth skin, hard consistency and odour characteristic of fresh and finished potatoes start to ferment.



**Figure 4.** PH comparison PAPA NATIVA vs. CANCHAN.

In Figure 4 we can see the comparison of the two varieties of parasites used in the experiment, also seeing the values between the two varieties there is a significant difference.

**Table 3.** Analysis of variance, Tukey “flavour attribute”.

SOURCE	GI	SC AJUST.	MC AJUST.	VALUE F	PROBABILITY VALUE	VALUE P
Factor	1	3.125	3.1250	4.52	7,1043E-19	0.042
Error	30	20.750	0.6917			
Total	31	23.875				

In Table 3, the comparison of the treatments of the two potato varieties by Tukey’s taste attribute test, it is observed that the T2 treatment (tocosh - made from the native potato) statistically has a difference with the T1 treatment (tocosh made from the canchan potato), which means that the T2 treatment has better organoleptic attributes on average than the T1 treatment.

**Table 4.** Analysis of Variance, Tukey “consistency attribute”.

SOURCE	GI	SC AJUST.	MC AJUST.	VALUE F	PROBABILITY VALUE	VALUE P
Factor	1	6.125	6.1250	7.86	7,1043E-19	0.009
Error	30	23.375	0.7792			
Total	31	29.500				

Table 4 shows the comparison of the treatments of the two potato varieties by Tukey’s consistency attribute test. It is observed that the T2 treatment (tocosh made from native

potato) has a statistical difference with the T1 treatment (tocosh made from canchan potato). This means that the T2 treatment has better organoleptic attributes on average than the T1 treatment.

**Table 5.** Analysis of Variance, Tukey “appearance attribute.

SOURCE	GI	SC AJUST.	MC AJUST.	VALUE F	PROBABILITY VALUE	VALUE P
Factor	1	2.531	2.5312	4.48	7,1043E-19	0.043
Error	30	16.938	0.5646			
<b>Total</b>	<b>31</b>	<b>19.469</b>				

In Table 5 the comparison of the treatments of the two varieties of potatoes by Tukey’s test of the general appearance attribute, it can be seen that the T2 treatment (tocosh made from native potato) has a statistical difference with the T1 treatment (tocosh made from canchan potato), which means that the T2 treatment has better organoleptic attributes on average than the T1 treatment.

The result obtained from the organoleptic attributes of the two potato varieties applying the tukey test statistic found that the T2 treatment corresponding to the native potato variety presents on average better organoleptic attributes than the T1 treatment (tocosh made from canchan potato).

## 4. DISCUSSION

### 4.1. FROM THE STUDY OF THE FERMENTATION OF EACH POTATO

Variety of physicochemical characteristics. In this sense, the potato experiences a decrease in pH until it obtains the tocosh and therefore an increase in acidity (Machaca & Mamani, 2020). Tocosh comes from a fermentation process (Andean technique), which is suitable for distribution and consumption in the different markets of Peru as flour or in its raw form. On the other hand, the amount of glycoalkaloids are related to the cultivation method, storage and temperature, depending overall on the Andean techniques destined for its production and can be distributed in different rates in *Solanum tuberosum* tubers, they have been found in the tuber (smaller quantity), leaves and peel (greater quantity), and some



analysis showed quantities such as 300–600 mg/kg in peel, 2000–4000 mg/kg in buds, and 3000–5000 mg/kg in flowers.

As for changes during the fermentation process of the general appearance and smell of the potato. The phenomenon of transformation of the potato Tocosha loses water and its volume is reduced by about half with the exception of the skin, therefore the Tocosha skin is rough “wrinkled” and the consistency soft; on the other hand, after the fermentation process, it achieves a very peculiar smell that is unpleasant, being less pronounced at the end of fermentation (Velasco-Chong, *et al.*, 2020).

## 4.2. FERMENTATION TIME FOR EACH POTATO VARIETY

The fermentation of the potato in the production of tocosha should last from 30 to 90 days depending on the variety, size of the potato and the temperature of the water (Bustos, 2018).

Considering that the potatoes of each variety studied had uniform sizes and fermented in continuous pools with the same conditions in terms of water temperature. You could “make sure that the difference in fermentation time is due to the particular characteristics of each potato variety used in the study (Barrera *et al.*, 2018).

## 4.3. YIELD OF FRESH TOCOSH AND TOCOSH FLOUR BY POTATO VARIETIES UNDER STUDY

Machaca and Mamani (2020) mentions that the yield in tocosha production is 30 to 45%, depending on these values of the potato variety used. The variety with the highest solids, including the highest amount of starch, will have a higher yield in obtaining tocosha.

On the other hand, indicates that the yield per process in obtaining tocosha flour is 35 to 60% depending on the humidity of the flour desired. Tocosha flour, like other flours, must contain a maximum of 12% humidity to guarantee its conservation.

According to the above, we can say that the yield of the process in the production of tocosha for each variety of potato in study is 33.80 to 53.00%. While the yield per process in the

production of tocosh flour is 42.80 to 60.00%; which are within the range established by the mentioned authors (Sandoval *et al.*, 2015).

The tocosh flour did not present toxicity at the repeated dose for 28 days in the highest dose corresponding to 1000 mg/kg BW. There were no deaths at up to 5000 mg/kg BW, therefore, the oral LD50 was greater than 5000 mg/kg (Velasco-Chong, *et al.*, 2020).

## 5. CONCLUSIONS

The fermentation time of each variety of potato was: in the court 30, native 45 days. And the tocosh obtained from the native potato variety has better sensory characteristics than the other treatments under study (taste, smell, consistency and overall appearance), obtaining the qualitative qualifier I am very pleased according to the qualification of the panelists.

The potato variety with the highest process yield in obtaining tocosh is the native variety with 53.3%, followed by the canchan variety with 50.1%

The potato variety with the highest process yield in the production of tocosh flour is the native variety with 59.6%, followed by the variety Canchan 45.00%.

## REFERENCES

- Alvarado, K., Esenarro, D., Rodriguez, C., & Vasquez, W.** (2020). Lemna minor influence in the treatment of organic pollution of the industrial effluents. *3C Tecnología. Glosas de innovación aplicadas a la pyme*, 9(3), 77-97. <https://doi.org/10.17993/3ctecno/2020.v9n3e35.77-97>
- Barrera, C. M., Blas, J. S., Landa, M. V., & Sánchez, L. S.** (2018). Tocoshana. Universidad Peruana de Ciencias Aplicadas (UPC). Universidad Peruana de Ciencias Aplicadas (UPC), Lima, Perú. <https://repositorioacademico.upc.edu.pe/handle/10757/625145>

- Bustos, S. K.** (2018). *Exportación de yogurt de tocosh al mercado mexicano para mejorar la salud gastrointestinal, 2018* [Tesis de licenciatura]. Facultad De Ingeniería Y Negocios Escuela Académico Profesional De Negocios Y Competitividad. <http://repositorio.uwienner.edu.pe/bitstream/handle/123456789/2478/TESIS%20Bustos%20Stefany.pdf?sequence=1&isAllowed=y>
- Carranza, K., Rodriguez, C., Esenarro, D., Veliz, M., & Arteaga, J.** (2020). Sensory evaluation of a perfume made of orange essential oil. *International Journal of Chemical Engineering and Applications*, 11(4). <http://www.ijcea.org/vol11/786-H3021.pdf>
- Córdova, A., Amaya, P., Esenarro, D., & Rodriguez, C.** (2020). Vegetable Contamination by Heavy Metal Contained in Effluents from Wastewater. Plant in the Totora Community, Ayacucho –Peru. *Journal of Green Engineering*, 10(7), 3484–3497.
- Machaca, S. C., & Mamani, R. V.** (2020). *Estudio comparativo del efecto antibacteriano de tres marcas del tocosh (Solanum tuberosum) frente a staphylococcus aureus ATCC 25923 Arequipa-2019.* <https://www.semanticscholar.org/paper/Estudio-comparativo-del-efecto-antibacteriano-de-a-Machaca-Mamani/82c1f081f7665e512dd737c60f69514cb8105250>
- Quispe, W., Esenarro, D., Rodríguez, C., Alvarado, K., Ruiz, C., & Alvarez, W.** (2020). Physicochemical quality of honey bee (*Apis mellifera*) in three bioclimatic zones in Apurímac Perú. *International Journal of Advanced Science and Technology*, 29(7), 268-275. <http://serisc.org/journals/index.php/IJAST/article/view/13219>
- Sandoval, M. H., Tenorio, J., Tinco, A., Ponce, R. A. L., & Calderón, S.** (2015). Efectos antioxidantes y citoprotectores de *Solanum tuberosum* ‘papa’ tocosh en mucosa gástrica en animales de experimentación. *Anales de la Facultad de Medicina*, 76(1), 15-20. <https://doi.org/10.15381/anales.v76i1.11070>
- Velasco-Chong, J. R., Herrera-Calderón, O., Rojas-Armas, J. P., Hañari-Quispe, R. D., Figueroa-Salvador, L., Peña-Rojas, G., Andía-Ayme, V., Yuli-Posadas, R. Á., Yepes-Perez, A. F., & Aguilar, C.** (2020). TOCOSH FLOUR (*Solanum tuberosum* L.): A Toxicological Assessment of Traditional Peruvian Fermented Potatoes. *Foods*, 9(6), 719. <https://doi.org/10.3390/foods9060719>

/10/

# VULNERABILITY OF THE SOILS OF METROPOLITAN LIMA AND THEIR RELATIONSHIP WITH URBAN SUSTAINABILITY

---

**Raúl Méndez Gutiérrez**

National University Federico Villarreal, (Peru).

E-mail: [rmendez@unfv.edu.pe](mailto:rmendez@unfv.edu.pe) ORCID: <https://orcid.org/0000-0001-5644-483X>

**Doris Esenarro Vargas**

National University Federico Villarreal, (Peru).

E-mail: [desenarro@unfv.edu.pe](mailto:desenarro@unfv.edu.pe) ORCID: <https://orcid.org/0000-0002-7186-9614>

**Pedro Amaya Pingo**

National University Federico Villarreal, (Peru).

E-mail: [pamaya@unfv.edu.pe](mailto:pamaya@unfv.edu.pe) ORCID: <https://orcid.org/0000-0001-9123-0124>

**Ciro Rodriguez Rodriguez**

National University Mayor de San Marcos, (Peru).

E-mail: [crodriguezro@unmsm.edu.pe](mailto:crodriguezro@unmsm.edu.pe) ORCID: <https://orcid.org/0000-0003-2112-1349>

**Recepción:** 13/11/2020 **Aceptación:** 13/11/2020 **Publicación:** 13/11/2020

## **Citación sugerida Suggested citation**

Méndez, R., Esenarro, D., Amaya, P., y Rodriguez, C. (2020). Vulnerability of the soils of Metropolitan Lima and their relationship with urban sustainability. *3C Tecnología. Glosas de innovación aplicadas a la pyme. Edición Especial, Noviembre 2020*, 161-177. <https://doi.org/10.17993/3ctecno.2020.specialissue6.161-177>

## ABSTRACT

This research work has a great influence on the physical security of the urban infrastructure and the citizens of our capital city, that is why it is necessary to apply prevention strategies since our city is located in a very vulnerable area to seismic events, mainly huaycos, floods and landslides, settlements, landslides and other superficial mass movements, so it is necessary to have knowledge of the causes and effects of these phenomena, the different types and carrying capacity of soils in the districts of Metropolitan Lima, in order to contribute to the knowledge of the degree of vulnerability in which urban areas, marginal urban areas, human settlements are exposed. In conclusion, surveys of public servants allowed us to determine that only 55% of them know the meaning of risk and vulnerability, so 45% are totally unaware of these terms. Likewise, surveys of the general public on the lack of a prevention culture, 83% indicated that they did, hence the need to apply a course or training on disaster risk management issues at all educational levels.

## KEYWORDS

Metropolitan Lima, Urban sustainability, Bearing capacity, Soil vulnerability.

# 1. INTRODUCTION

The present work called “Management of the Vulnerability of the Soils of Metropolitan Lima and its Relationship with Urban Sustainability” has been developed considering the importance of providing real theoretical, practical and statistical knowledge of the risks of disasters resulting from the vulnerability of soils and the latent threats or hazards in our community, which due to the lack of knowledge and implementation of preventive measures have caused a high rate of deaths and injuries, affecting the physical infrastructure works and socioeconomic activities of our capital city.

Metropolitan Lima is a city that is immersed in a process of urbanization having as factors the economic, social and environmental aspects, without considering a true urban planning that allows its integral development. The process of disorderly growth conditions the factors of vulnerability in the urban space which gives rise to a risk of disasters due to the dangers of earthquakes, floods, huaycos, etc., which threatens the physical safety of the population, urban infrastructure and the socio-economic development of the city (Alvarado *et al.*, 2020).

It is important to consider an integral approach that contemplates the factors of vulnerability of our city considering the studies of grounds where the buildings are founded (Hospitals, schools, residential buildings, houses, etc), road infrastructure, water and drainage networks, electrical and gas installations, reservoirs, etc., because it allows us to design the foundations where the civil works are going to be built considering the aspects of seismicity and others that allow a capacity of response before a seismic event of great magnitude. Knowing the vulnerability of the soils in our capital city will allow us to have a better knowledge of the risk levels in which it is found and thus give greater importance to soil studies in accordance with the National Building Regulations (Centro Nacional de Estimación, Prevención y Reducción del Riesgo de Desastres (CENEPRED), 2015).

The study of Soil Mechanics becomes a necessary and essential element through which it allows us to know the bearing capacity of soils, settlements, etc., for the purpose of building foundations in areas of urban expansion as well as in places of building renovation. In the developed work, it has been taken into account the analysis of the causes that originate the vulnerability of the soils, for which field works (Trial pits), laboratory and office are indicated, as well as statistical data of the last years, conceptualizations referring to risk,

vulnerability and danger are discussed, for the obtaining of results taking into consideration the stratigraphic profiles, Results of the calculations of bearing capacity and settlement of soils, as well as the chemical analysis of soils in most districts of Metropolitan Lima, whose significant results show the importance of soil studies to know the resistance and response to mainly seismic and other hazards, which will allow the reduction of vulnerability and therefore mitigate the risk of future disaster events. Surveys have also been carried out in various districts of the capital in which the current situation of soil knowledge and its relationship with urban sustainability is analyzed. The main objective is to establish how the management of soil vulnerability in Metropolitan Lima and its relationship with urban sustainability will implement physical safety in our capital city, to finally reach conclusions and recommendations for a better culture of prevention against future disaster risks in Metropolitan Lima (Ramos, Esenarro *et al.*, 2020).

## 2. MATERIALS Y METHOD

Due to the proposal to apply, verify and test the effectiveness of a Training Program on Disaster Risk Management Issues, which involves vulnerability, a “quasi-experimental” research design was applied, which corresponds to what is known as “design before and after with a non-randomized control group”.

Both the Pre Test and the Post Test will be applied to the Experimental Group as well as to the Control Group, however the application of the Disaster Risk Management Training Program only to the Experimental Group, which will allow us to verify the effectiveness of the program directed to central government officials and municipalities to know the degree of knowledge and in this way to contribute to the reduction of the levels of the disaster risk according to the vulnerability of the soils of the capital city. Initially the Pre Test has the purpose of determining that both groups are similar or equivalent at the beginning of the application of the program. The Independent Variable, that is to say, the Training in Disaster Risk Management, will be applied only to the Experimental Group, therefore the Control Group will not be applied to this Program (Rodriguez *et al.*, 2020).

The objective of the Post Test is to establish if there are significant differences between both groups at the end of the training program. If the Disaster Risk Management Training



Program has been effective, there must be statistically significant differences between both groups in the Post-Test, which obviously must favour the experimental group. At the end of the application of the training program the Experimental Group will have to present a greater knowledge of the levels of risk, danger, vulnerability, resilience and environmental impact, related to the vulnerability of the soils of Lima. Finally, it is tried to determine, that if the Training Program in Disaster Risk Management is effective to obtain a reduction of the level of vulnerability of the soils of Lima and the relation with the urban sustainability. For the population where 180 people will be considered among officials and servants of the Metropolitan Municipality of Lima, of the districts of greater vulnerability of their soils and institutions of the central government that have to do with the vulnerability of our country.

**Table 1.** The distribution of the study population.

N°	Entities	N° de Servers
1	Central Government	100
2	Metropolitan Municipality of Lima and District	80
	<b>Total</b>	<b>180</b>

It will be formed by workers whose ages fluctuate between 25 and 55 years, being 55 % of the masculine sex and 45% feminine (see Table 1) (Esenarro *et al.*, 2020).

Considering a non-probabilistic sampling of the criterion type, it is determined by applying criteria who will make up the experimental group and who will make up the control group.

**Table 2.** The distribution of the research design.

Group	Central government	MM de Lima y Distritos	Total
Experimental	30	30	60
Control	30	30	60
		<b>Total</b>	<b>120</b>

Therefore, 120 workers from both the central and local governments are considered for the research sample, where 60 will belong to the experimental group and 60 to the control group, which is equivalent to 66.67% of the total population considered. (See Table 2).

## 2.1. RESEARCH TECHNIQUES

The main technique considered for this work are the surveys that were carried out in the state entities as well as to the general public. The same applies to the data on soil bearing capacities that are the subject of the research.

## 2.2. DATA COLLECTION INSTRUMENTS

The main instrument applied is a training program in disaster risk management aimed at workers of the Central Government and Regional Governments, which will be applied to the Experimental Group and will not be applied to the Control Group under consideration. (Esenarro *et al.*, 2020).

As a contribution for greater knowledge in training topics related to vulnerability, the ones carried out by CENEPRED (2015).

## 2.3. DATA PROCESSING AND ANALYSIS

- It is considered an orderly sequence for obtaining the expected results.
- Collection of updated documentary and statistical information.
- Critical analysis of the documentation.
- Application of the Training on the National System of Disaster Risk Management (SINAGERD).
- Analysis of the results of the application of the SINAGERD training.
- Appropriate corrective measures.
- Approach of alternatives tending to improve the Risk Prevention Culture.
- Analysis of the results of the surveys
- Analysis of the results of soil bearing capacities.
- Regarding the statistical technique, descriptive statistics are applied considering measures of central tendency such as
- Mean, dispersion measures such as variance and standard deviation, use of tables and statistical histograms, among others.

Trial pits:

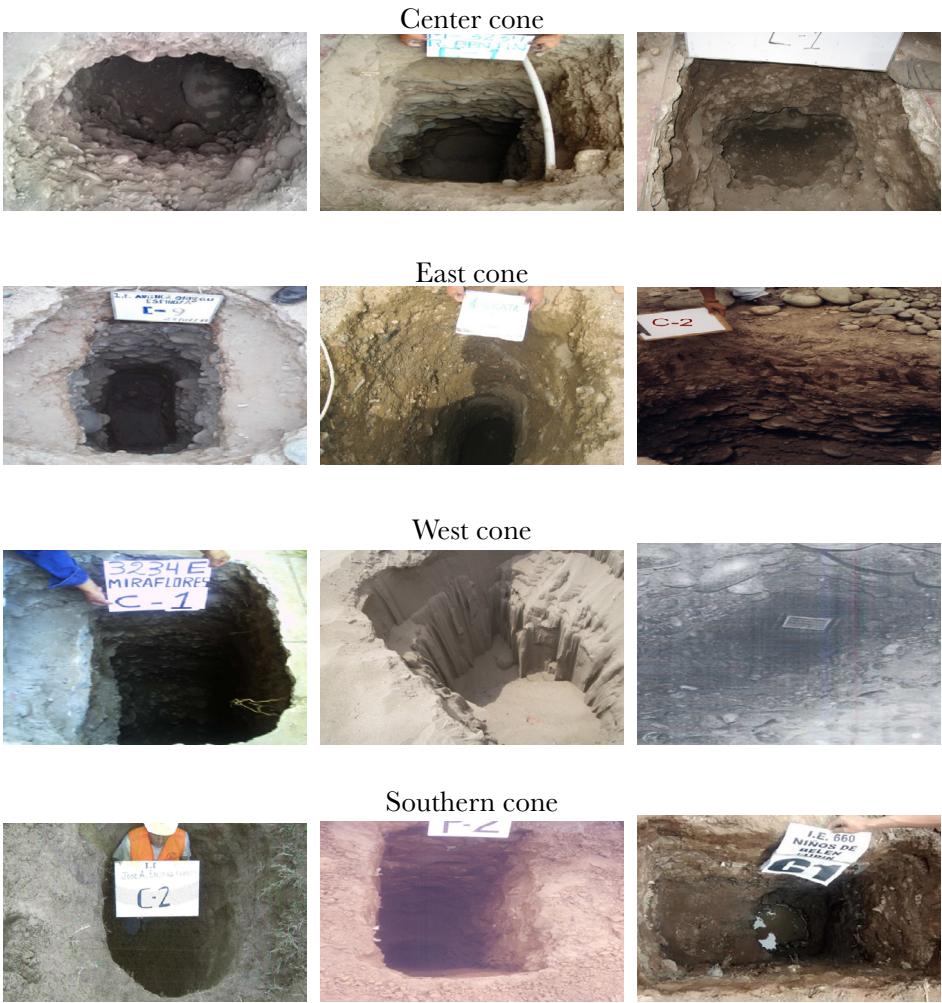


**Figure 1.** Trial pits of Metropolitan Lima.

In the Figure 1 it can see the photos with the different types of soil, which are found in the Lima cones.

### 3. RESULTS

Elaboration of cartography of the study of the ground of Metropolitan Lima and its relationship with the urban sustainability (Guerra *et al.*, 2020).

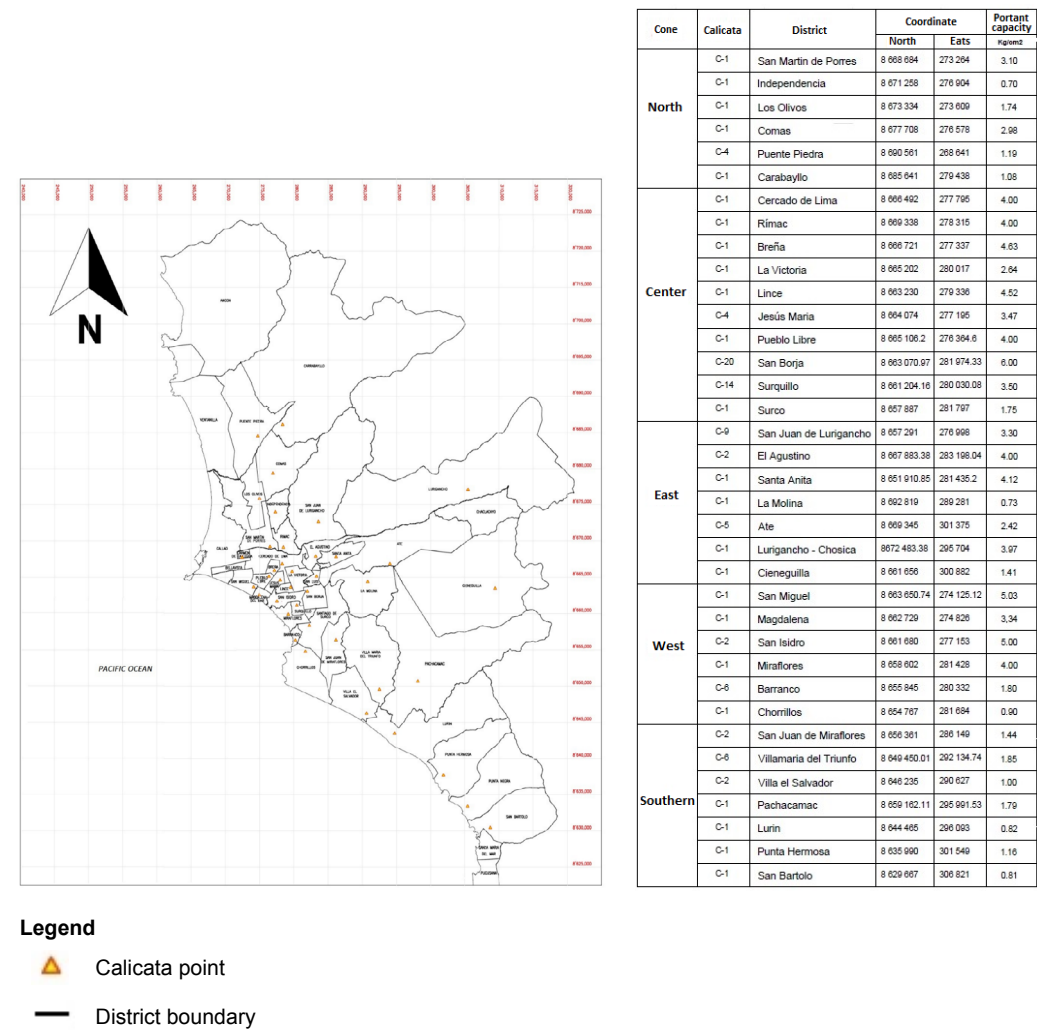
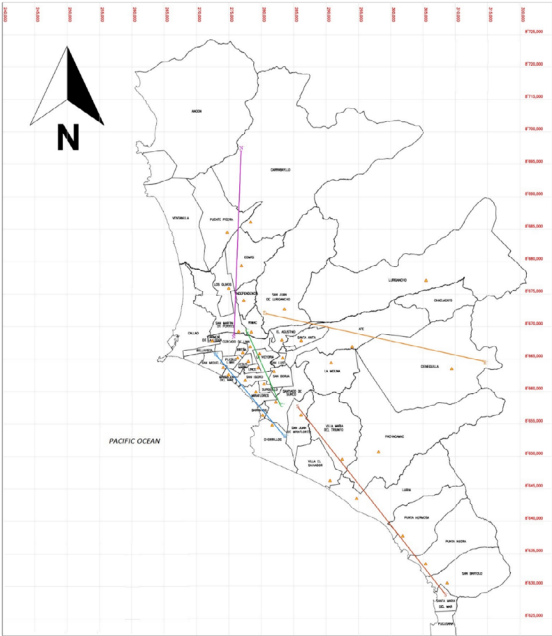


**Figure 2.** Trial pit location in Metropolitan Lima.

Figure 2 shows the location of the pits that have been taken as study points, the points are also observed on the map.



Cone	Calicata	District	Coordinate		Portant capacity
			North	Eats	
North	C-1	San Martín de Porres	8 068 684	273 204	3.10
	C-1	Independencia	8 071 258	276 904	0.70
	C-1	Los Olivos	8 073 334	273 609	1.74
	C-1	Comas	8 077 708	276 578	2.98
	C-4	Puente Piedra	8 080 581	268 641	1.19
	C-1	Carabaylo	8 085 641	279 438	1.08
Center	C-1	Cercado de Lima	8 086 492	277 765	4.00
	C-1	Rímac	8 089 338	278 315	4.00
	C-1	Breña	8 086 721	277 337	4.63
	C-1	La Victoria	8 085 202	280 017	2.84
	C-1	Lince	8 063 230	279 336	4.52
	C-4	Jesús María	8 064 074	277 195	3.47
	C-1	Pueblo Libre	8 065 106.2	276 364.6	4.00
	C-20	San Borja	8 063 070.97	281 974.33	6.00
	C-14	Surquillo	8 061 204.16	280 030.08	3.50
	C-1	Surco	8 057 887	281 797	1.75
East	C-9	San Juan de Lurigancho	8 057 291	276 998	3.30
	C-2	El Agustino	8 067 883.38	283 198.04	4.00
	C-1	Santa Anita	8 051 910.85	281 435.2	4.12
	C-1	La Molina	8 052 819	289 281	0.73
	C-5	Ate	8 069 345	301 375	2.42
	C-1	Lurigancho - Chosica	8072 483.38	295 704	3.97
	C-1	Cieneguilla	8 061 656	300 882	1.41
	C-1	San Miguel	8 063 650.74	274 125.12	5.03
West	C-1	Magdalena	8 062 729	274 826	3.34
	C-2	San Isidro	8 061 680	277 153	5.00
	C-1	Miraflores	8 058 602	281 428	4.00
	C-6	Barranco	8 055 845	280 332	1.80
	C-1	Chorrillos	8 054 767	281 694	0.90
	C-2	San Juan de Miraflores	8 056 361	286 149	1.44
Southern	C-6	Villamaria del Triunfo	8 049 450.01	292 134.74	1.85
	C-2	Villa el Salvador	8 046 235	290 627	1.00
	C-1	Pachacamac	8 059 162.11	295 991.53	1.79
	C-1	Lurin	8 044 465	299 093	0.82
	C-1	Punta Hermosa	8 035 990	301 549	1.16
	C-1	San Bartolo	8 029 867	306 821	0.81

Legend








-  Calicata point
-  District boundary
-  North cone section line
-  Center cone section line
-  East cone section line
-  Center west cone section line
-  Southern cone section line

Figure 3. Cross section of Trial pits in Metropolitan Lima opia.

Figure 3 shows the location of the holes identified with their respective colors and reference points as well as north, east, south and west, as can be seen in the graph, Zoning according to soil bearing capacity of Metropolitan Lima.

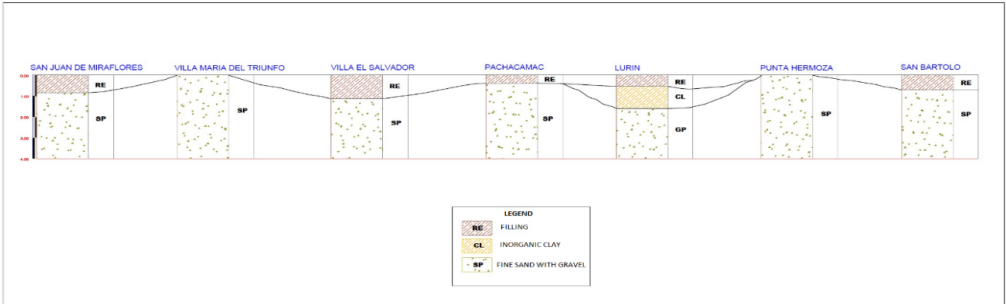


Figure 4. Soil profile south cone N-N'.

The Figure 4 shows the profile of the soil in the area of the south cono N-N.

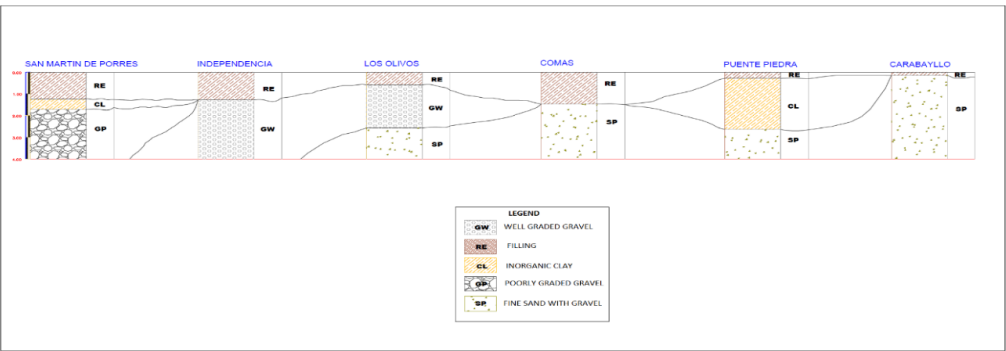


Figure 5. Soil profile north cone N-N'.

The Figure 5 shows the profile of the soil in the area of the north cono N-N.

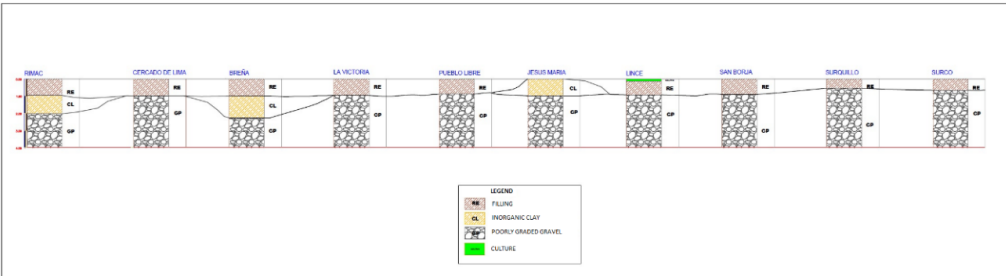


Figure 6. Soil profile cone C-C' Center.

The Figure 6 shows the profile of the soil in the area of the center cono C-C.

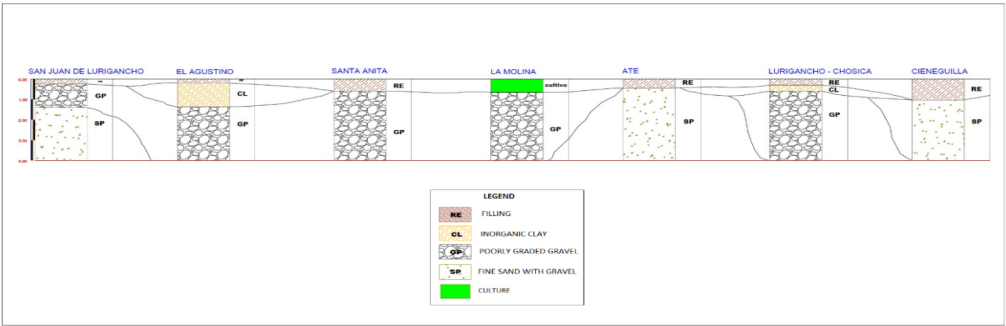


Figure 7. W-W' West Cone Soil Profile.

The Figure 7 shows the profile of the soil in the area of the West Soil profile.

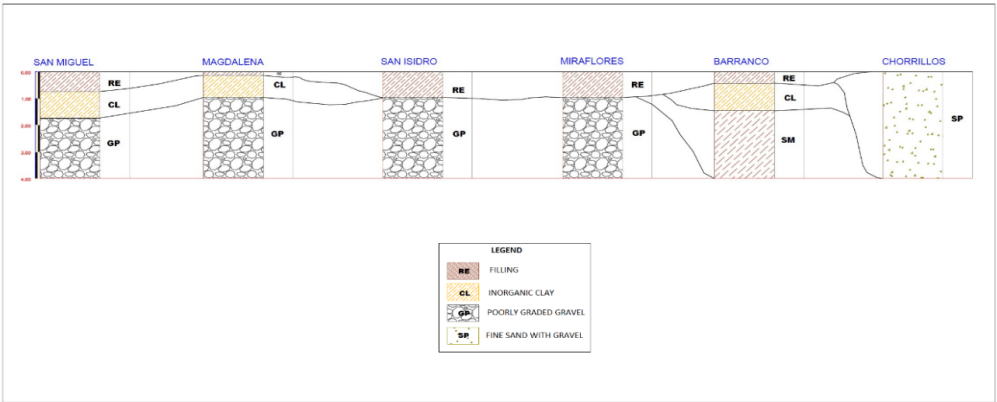


Figure 8. Soil profile north cone N-N'.

The Figure 8 shows the profile of the soil in the area of the north cono N-N.

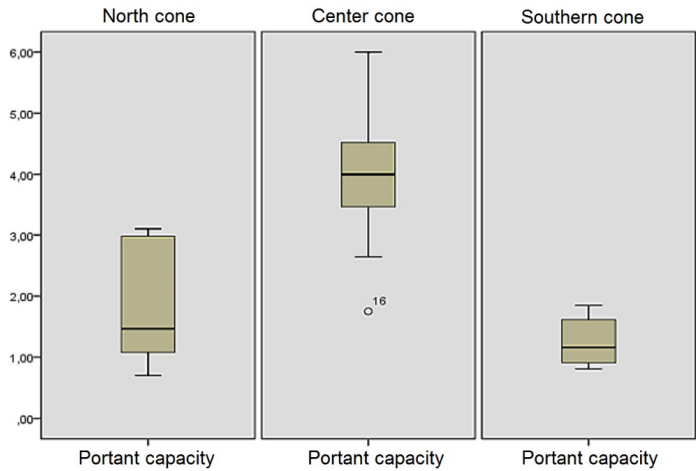


Figure 9. Anova test. (Bearing capacity = Kg/cm²).



In the Figure 9 The anova test (statistical) was used to compare the means of the bearing capacity of the soils of the northern, central and southern cone. it is the one that concludes that the means of the north and south cone are statistically equal. on the contrary, the mean of the center cone turned out to be significantly higher, which is observed in the bar graph.

With the results obtained with the studies of Mechanics of Soils, the Map of Zoning of Soils according to Bearing Capacity has been elaborated - Metropolitan Lima, where districts have been grouped by cones and considered a general classification of the soils that are included from very good, good, regular, bad and very bad, according to the average values of bearing capacity obtained of the districts matter of the investigation. For the purpose of preparing the Zoning Map, Table 4 has been considered, which presents a range of referential values of Soil Bearing Capacity.

**Table 4.** Comparison of the level of knowledge in the control group and the experimental group at the beginning of the experiment (pre-test) for resilience Test of independent samples.

Pre-test	F	Sig.	t	Test T gl	Sig. (bilateral)
Equal variance has been assumed	,006	,938	-,119	118	,905
Equal variance has not been assumed	0	0	-,119	117,604	,905

The results of soil profiles grouped at the level of 5 cones, after their interpretation, show us the stratigraphic sequence, being the districts of the central cone those that have mostly gravelly soils which indicate us to be good soils for foundation purposes, with respect to the northern cone and the southern cone that have mostly sandy soils of less stability.

#### 4. DISCUSSION

The present research, in accordance with the application of the Training Program in DRM, which involves vulnerability, seeks to contribute to the knowledge in matters of risk prevention culture, and to promote the active participation of the organizations involved in safety issues in the face of events that cause disasters in our capital city, which, despite some not being predictable, can be mitigated and reduce the risks of disasters. In order to face the problem, it is necessary to have an integral and multidisciplinary coordination and participation of all the sectors of the state and private institutions (Chu *et al.*, 2020).



At present, there are several institutions that carry out research studies related to vulnerability, hazards and risks, whose information is widely dispersed and there is no specific data bank that articulates them, which is considered a future task to incorporate research sources to an institution or central entity where information is available to all stakeholders. Likewise, there are institutions whose specific function is disaster preparedness and rapid response with the main task of saving lives. Therefore, the importance of political will and commitment of those who lead the institutions must be kept in mind. In addition, they are necessary for the implementation and enforcement of regulations in an effective and timely manner since citizens living not only in Metropolitan Lima. But throughout our territory, have the peace of mind and security that we are prepared to respond to a future disaster (Ascue *et al.*, 2020).

The research shows very important results with respect to vulnerability, where the value can be observed ( $\text{Sig} = 0.00 < 0.05$ ) and it can be said that the Experimental Group (to which the training program was applied), showed a higher level of knowledge in vulnerability than the control group (to which the training program was not applied), those before and after the experiment remain statistically the same. That is, after two years of applying the training program to the experimental group, they are better prepared in knowledge. The significant difference allows us to reject the Null Hypothesis  $H_0$ , therefore the Alternative Hypothesis  $H_1$  is accepted, with a confidence level of 95%, considered in the proposed research (Lohani *et al.*, 2020).

The surveys to the general population of our capital city have determined the little knowledge in risk, danger and vulnerability issues, so 83% responded that a greater education is required from the institutions and organisms responsible in the fulfillment of the norms of the Law of the National System of Management of the Disaster Risk, since these do not fulfill their functions, at the moment there is very little progress in training on these subjects being a main problem of security in our city the lack of conscience and culture of prevention to face the future events that cause disasters in our city.

In 2010 the Geophysical Institute of Peru - IGP, conducted the study “Seismotectonic Zoning for 7 districts of Metropolitan Lima” (Pucusana, Santa Maria, San Bartolo, Punta Negra, Punta Hermosa, Santa Rosa and El Agustino), in order to obtain results from the dynamic behavior of the soil for the seismic part and the soil analysis for the geotechnical

part, following the procedure provided by CISMID in the “Study of Vulnerability and Earthquake Risk in 42 districts of Lima and Callao”. Making the comparison with the present research work, 36 districts are being considered from which their soil analysis and the consequent classification and bearing capacity of the soils for foundation purposes have been made, in order to determine the level of vulnerability of the soils of the districts, grouping them by cones according to their geographical location and better approach for their interpretation, which allows to indicate that in spite of the existing risks, the central cone of Lima is the one with the lowest degree of vulnerability according to the results of soil bearing capacity.

## 5. CONCLUSIONS

The results of the application of the training program in disaster risk management, to public officials, show us a Sig in the experimental group is 0.00, less than 0.05, and it can be concluded that the risk in terms of the score in the experimental group is directly and significantly related to urban sustainability in terms of knowledge.

To compare the means of soil bearing capacity in the northern, central and southern cones, we used the ANOVA test and as a complement the Tukey test, which allowed us to conclude that the means in the northern and southern cones are statistically equal. On the contrary, the mean for the central cone was significantly higher than the other two cones, which can be seen in Figure 10. Therefore, it can also be concluded that the soils of the central cone are better than the soils of the northern and southern cones, which are from regular too bad, respectively.

Surveys of public servants allowed us to determine that only 55% of them are aware of the meaning of risk and vulnerability, therefore 45% are totally unaware of these terms. Likewise, surveys to the general public about the lack of prevention culture, 83% indicated that yes, hence the need to apply a course or training on disaster risk management issues at all levels of education.

The dangers or hazards in Metropolitan Lima are extremely complex, mainly earthquakes, huaycos, floods and others, which affect the physical, social and economic environment of our capital city according to the degree of vulnerability. Therefore, in order to achieve a

resilient capital and to face adverse events, a greater knowledge of the physical reality of our city is required. This allows us to respond in a timely manner to the occurrence of any disaster or emergency.

## REFERENCES

- Alvarado, K., Esenarro, D., Rodriguez, C., & Vasquez, W.** (2020). Lemna minor influence in the treatment of organic pollution of the industrial effluents. *3C Tecnología. Glosas de innovación aplicadas a la pyme*, 9(3), 77-97. <https://www.3ciencias.com/wp-content/uploads/2020/09/art-4-3c-tecno-ed.-35-vol.-9-n.-3-1.pdf>
- Ascue, J. C., Esenarro, D., Rodriguez, C., Tafur, I., & Vázquez, W.** (2020). Geological Vulnerability of the Fragile Ecosystem Case: Huancaro-District of Santiago Micro-Basin – Cusco. *Journal of Green Engineering*, 10(6), 2746–2761. <http://www.jgenng.com/volume10-issue6.php>
- Centro Nacional de Estimación, Prevención y Reducción del Riesgo de Desastres (CENEPRED).** (2015). *Manual para la evaluación de riesgos originados por fenómenos naturales. 02 Versión.* [http://www.cenepred.gob.pe/web/wp-content/uploads/Guia\\_Manuales/Manual-Evaluacion-de-Riesgos\\_v2.pdf](http://www.cenepred.gob.pe/web/wp-content/uploads/Guia_Manuales/Manual-Evaluacion-de-Riesgos_v2.pdf)
- Chu, H., Gao, G.-F., Ma, Y., Fan, K., & Delgado-Baquerizo, M.** (2020). Soil Microbial Biogeography in a Changing World: Recent Advances and Future Perspectives. *mSystems*, 5(2). <https://doi.org/10.1128/mSystems.00803-19>
- Esenarro, D., Escate, I., Anco, L., Tassara, C., & Rodriguez, C.** (2020). Proposal for an Ecological Research Center for the Recovery and Revaluation of Biodiversity in the Town of Quichas-Lima, Peru. *International Journal of Environmental Science and Development*, 11(4), 212-216. <https://doi.org/10.18178>
- Esenarro, D., Rodriguez, C., Huachaca, K., Cachay, B., & Aylas, C.** (2020). Classification and Characterization of the Sustainable Wetland Bello Horizonte *Test Engineering & Management*, 13453 – 13458.

**Guerra, C. A., Rosa, I. M. D., Valentini, E., Wolf, F., Filipponi, F., Karger, D. N., & Xuan, A.** (2020). Global vulnerability of soil ecosystems to erosion. *Landscape Ecology*, 35, 823–842. <https://doi.org/10.1007/s10980-020-00984-z>

**Lohani, S., Baffaut, C., Thompson, A. L., Aryal, N., Bingner, R., Bjorneberg, D. L., Bosch, D., Bryant, R., Buda, A., Dabney, S. M., Davis, A. R., Duriancik, L. F., James, D., King, K., Kleinman, P., Locke, M., McCarty, G. W., Pease, L., Reba, M., ... & Yasarer, L.** (2020). Performance of the Soil Vulnerability Index with respect to slope, digital elevation model resolution, and hydrologic soil group. *Journal of Soil and Water Conservation*, 75(1), 12-27. <https://doi.org/10.2489/jswc.75.1.12>

**Ramos, L., Esenarro, D., Rodriguez, C., & Lagos, J.** (2020). Recovery of public spaces for the conservation of green areas in Tablada Lurin. In *IOP Conference Series: Materials Science and Engineering, Volume 910, 3rd International Conference on Civil Engineering and Architecture (ICCEA 2020)*. Compiègne, France. <https://doi.org/10.1088/1757-899X/910/1/012020>

**Rodriguez, C., Esenarro, D., Corimanya, P., Flores, F., Aylas, C., & Lagos, J.** (2020). Proposal for a Sustainable Infrastructure Design (Ecolodge) in Quichas Town, Perú. *Test Engineering & Management*, 9250 - 9256.



/11/

# MICROBIAL BIODEGRADATION OF POLYETHYLENE OF LOW DENSITY, UNDER CONTROLLED THERMAL CONDITIONS IN AIR LIFT BIO-REACTOR

---

**Alexandra Milagros Hermoza Rojas**

University Cesar Vallejo, (Perú).

E-mail: [alexandrah@gmail.com](mailto:alexandrah@gmail.com) ORCID: <https://orcid.org/0000-0001-7468-8969>

**Jorge Jave Nakayo**

Universidad Nacional Mayor de San Marcos - UNMSM, Lima, (Perú).

E-mail: [jorge.jave@unmsm.edu.pe](mailto:jorge.jave@unmsm.edu.pe) ORCID: <https://orcid.org/0000-0003-3536-881X>

**Jorge Luis López Bulnes**

Universidad Nacional Mayor de San Marcos - UNMSM, Lima, (Perú).

E-mail: [jlopezb@unmsm.edu.pe](mailto:jlopezb@unmsm.edu.pe) ORCID: <https://orcid.org/0000-0002-9583-1143>

**Vicenta Irene Tafur Anzualdo**

National University Federico Villarreal, (Perú).

E-mail: [itafur@unfv.edu.pe](mailto:itafur@unfv.edu.pe) ORCID: <https://orcid.org/0000-0002-1888-7848>

**Recepción:** 18/09/2020 **Aceptación:** 02/11/2020 **Publicación:** 13/11/2020

## **Citación sugerida Suggested citation**

Hermoza, A. M., Jave, J., López, J. L., y Tafur, V. I. (2020). Microbial biodegradation of polyethylene of low density, under controlled thermal conditions in air lift bio-reactor. *3C Tecnología. Glosas de innovación aplicadas a la pyme. Edición Especial, Noviembre 2020*, 179-189. <https://doi.org/10.17993/3ctecno.2020.specialissue6.179-189>

## ABSTRACT

The present investigation seeks to identify new mechanisms that serve as tools for the mitigation of plastic contamination through the biodegradation of low density polyethylene using microorganisms of the species *Pseudomona aeruginosa* (bacteria) and *Aspergillus brasilensis* (fungus) under controlled thermal conditions in an airlift bioreactor. The methods used were 2 samples of low density polyethylene with concentrations of 50 mg/L and 2 samples of 100 mg/L deposited in an airlift bioreactor under controlled thermal conditions with a duration of 7 days. As a result it was obtained that the species *Pseudomona aeruginosa* (bacteria) reduced the low density polyethylene sample by 2% with a concentration of 49 mg/L at a temperature of 21.8°C with a pH of 6.5 and dissolved oxygen (OD) of 6.8 mg/L, likewise the species *Aspergillus brasilensis* (fungus) reduced the low density polyethylene sample by 7% reaching a concentration of 93 mg/L at 22.1°C of temperature, 7.14 of pH and 7.45 of dissolved oxygen (OD).

## KEYWORDS

Air lift bioreactor, Biodegradation, Thermal conditions, Low density polyethylene (LDPE).



# 1. INTRODUCTION

As we know, plastics are a big problem nowadays, since we live in a world where people do not have an adequate environmental conscience, unfortunately this generates a very negative impact to our planet. Plastics have a low economic value in the market and are the most used, therefore, the amount of plastic waste increases. In addition, he tells us that “In 2010, 8.07% of plastic waste was generated in our country and in 2011 9.85%, this indicates that every year there is an increase in plastic waste. Plastic bags (low-density polyethylene) take 150 years to degrade, which is why we have been looking for alternatives to reduce the life span of plastic, such as incineration, which causes health problems because it generates the famous greenhouse gases (GHGs), in addition to the release of dioxins and furans (POPs) that are highly carcinogenic according to the World Health Organization (WHO) (Barlow *et al.*, 2019).

Plastic waste is a worldwide problem since people use the bags only once, throw them away and buy others again without realizing it; this is how pollution begins, causing damage mainly to marine ecosystems, since fauna often confuses them with food. A study conducted for MINAM in June 2012 indicates that Peruvians generate approximately 23,260 tons of solid waste, which gives us a per capita production of 800 grams (Córdova *et al.*, 2020).

A study released in 2015 tells us that sea turtles have been ingesting 52% of garbage, with plastic waste such as bags being the most common (Inforegion, 2015).

Finally, according to the Peruvian newspaper El Comercio (2018), 79% of plastic waste globally is found in dumps or thrown on the roads; only 9% is recycled and 12% is incinerated.

## 2. MATERIALS AND METHODS

### 2.1. PLACE OF STUDY AND SAMPLING

In this stage the place to work was selected and was an informal dump located in the town center of Santa Clara in the district of Ate in Lima in April, which presented a large amount of plastic in an apparent state of degradation (Catto *et al.*, 2016).

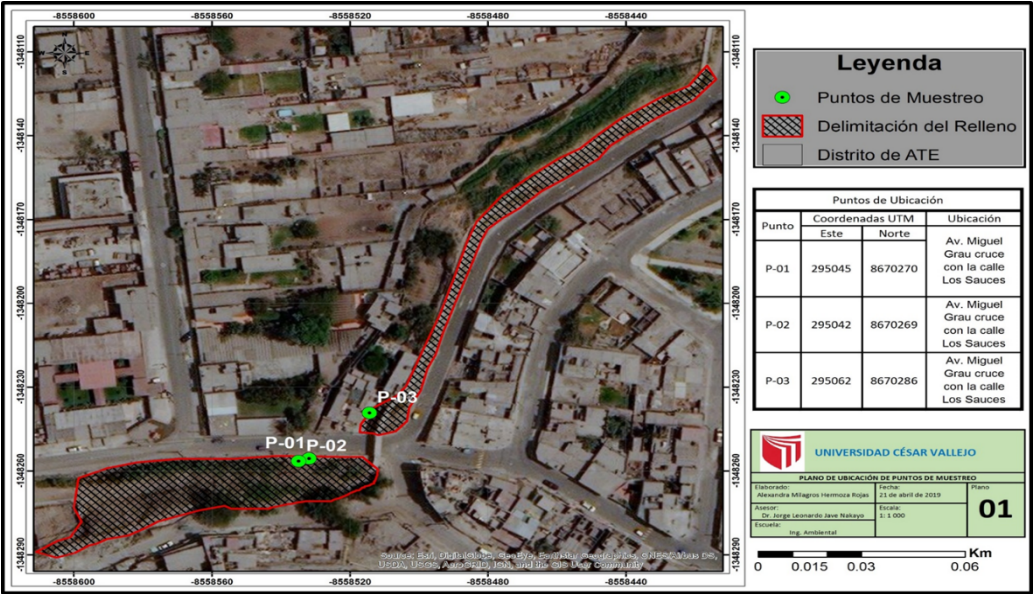


Figure 1. Map of sampling points

## 2.2. ELABORATION OF AIR LIFT BIOREACTORS

The bioreactors are made in the laboratory, they have a cylindrical glass culture chamber of 100 mm diameter by 200 mm height with a small pipe to take the samples, a deflector tube or central distribution of 80 by 28 mm, a venting filter attached to a regulating valve for air output, control valves for air input/output and air flow connectors attached to the tank pumps; which are the main source of oxygen for the bioreactor (Paço *et al.*, 2017). The culture chamber and deflector tube, the bioreactor accessories such as the top cover (airtight lid), air inlet/outlet control valves and air flow connectors are sterilized by immersion in 70% medicinal alcohol for 15 minutes and rinsed with purified water.

## 2.3. SOWING OF MICROBIAL CULTURES

The microorganisms chosen for the biodegradation process were a bacterium (*seudomona aeruginosa*) which was seeded on Trypticase Soy agar and incubated for 24 hours at a temperature of 30oc to 35oc and a fungus (*Aspergillus brasiliensis*) grown on Saburo Dextrose agar, incubated for 48 hours at a temperature of 20oc to 25oc (Giacomucci *et al.*, 2019).

It should be considered that for the process to be more effective, the strains should be used within the first two hours after leaving the incubator.

2.4. BIOREACTOR OPERATION OF THE CULTURES

The microbial colonies kept inactive in refrigeration are reactivated in new plates with half Trypticase Soy and Saburo Dextrose forming in seed inocula for the bioreactors. The proportion is 15% of the total volume (1000ml). The operation starts with the ignition of the air pumps, the total opening of the vent valve for a period of at least 7 days (Soto, 2016).

2.5. CONCENTRATION OF LOW DENSITY POLYETHYLENE BAGS

The degradation of the low density polyethylene (LDPE) is determined with the decrease of concentrations placed in the bioreactor, for which we work with 50mg/L for the type A bags, 100 mg/L for the type B bags, as concentrations for the beginning of operation, these samples are measured again after three days. To find the final concentration, the whole culture medium is autoclaved for 15 minutes, then the low density polyethylene (LDPE) samples are extracted, rinsed with purified water and taken to the oven for 12 to 24 hours at 80°c. Finally, the weighing is done in the analytical balance.

Table 1. Table of concentrations of low density polyethylene (LDPE) type A.

Bioreactors	Concentrations of LDPE type A (mg/L)		
	DAY 0	DAY 3	DAY 7
pseudomonas 1	50	49.000623	49
aspergillus 2	50	45.000023	45

2.6. DETERMINATION OF TEMPERATURE, DISSOLVED OXYGEN AND PH

The determination of the internal temperature was obtained at the beginning, after three days and at the end after 7 days by means of a thermometer, for dissolved oxygen in the same time interval it will be determined by an oximeter in the unit's mg/L and finally for the determination of the pH in the same time interval it was obtained by means of a potentiometer (Janczak *et al.*, 2019).

2.7. STATISTICAL ANALYSIS

The statistical test Anova was used to compare the low density polyethylene (LDPE) groups in a quantitative variable where  $p < \alpha$ ,  $p\text{-value} = 0.04$  to  $\alpha = 0.05$ , T for the samples in the different groups, since the group of individuals sampled is less than 30.

2.8. RESULTS AND DISCUSSION

The results obtained in low density polyethylene (LDPE) type A using the concentration of 50 mg/L in relation to the determination of concentrations had a decrease of 1% for pseudomonas and 5% for aspergillus, taking into account the higher efficiency of the latter, according to the variation of the temperature of 1°C. influenced in the efficiency due to the fact that these temperatures are within the environmental thermal conditions. However, the concentrations of dissolved oxygen increased by 4% pseudomonas and 20% for aspergillus during the days of experimentation, as opposed to a reduction of pH by 17% for pseudomonas and 13% for aspergillus (Sadhukhan *et al.*, 2019).

Table 2. Table of concentrations of PEBD type B.

Biorreactors	Concentrations of PEBD type B (mg/L)		
	DAY 0	DAY 3	DAY 7
pseudomonas 1	100	98.001246	98
aspergillus 1	100	93.000064	93

The results obtained in low density polyethylene (LDPE) type B using the concentration of 100 mg/L in relation to the determination of concentrations had a decrease of 2% for pseudomonas and 7% for aspergillus, taking into account the higher efficiency of the latter, according to the variation of the temperature of 1°C. influenced in the efficiency due to the fact that these temperatures are within the environmental thermal conditions. However, the concentrations of dissolved oxygen increased by 8% pseudomonas and 4% for aspergillus during the days of experimentation, as opposed to a reduction of pH by 19% for pseudomonas and 11% for aspergillus.

### 3. DISCUSSION

Microorganisms are capable of biodegrading low density polyethylene (LDPE) under certain controlled thermal conditions. On day zero, two samples of low density polyethylene (type A) with concentrations of 50 mg/L and two samples with 100mg/L of low density polyethylene with biodegradable additives (type B) were taken. On the last day of the process, sample 1 of type A had a final concentration of 49mg/L and sample 2 reached a concentration of 45mg/L. The first type B sample reached a concentration of 98mg/L and the second one a concentration of 93mg/L, which was the sample where the highest degradation was obtained with a temperature of 22.1°C.

For an efficient degradation by microorganisms, a favorable thermal condition is needed. Native bacteria present in worm, horse and chicken humus biodegraded polyethylene terephthalate and oxo-polyethylene efficiently at a temperature of 22°C in 35 days. For this research, an average temperature of 22.1°C was obtained on the last day of the process, this being the most efficient temperature for the biodegradation of low-density polyethylene with *Aspergillus brasiliensis* (Perpetuo *et al.*, 2020).

The chemical conditions are important for microbial biodegradation, the pH of the samples was determined during the process. The most efficient pH for the sample with *Pseudomona aeruginosa* was 6.49 and for the sample with *Aspergillus brasiliensis* was 7.14. This value was the most efficient for the whole process. For the optimum pH for the polyethylene sample with bacteria such as *Pseudomonas* sp was 5.5 and for the sample with fungi (unidentified yeast) was 7 (Alvarado *et al.*, 2020).

Finally, a percentage of 1% of degradation was obtained with *Pseudomona aeruginosa* for sample 1 of polyethylene type A and for the degradation with *Aspergillus brasiliensis* for sample 2 of the same type of polyethylene a percentage of 5% was obtained. For sample 1 of polyethylene type B with *Pseudomona aeruginosa* a percentage of 2% was obtained and for sample 2 of the same type of polyethylene with *Aspergillus brasiliensis* a result of 7% of degradation was obtained. For NOVOTNÝ, C (2015) in a period of six weeks and with a temperature of 28°C the samples of PETP/LA with *Pseudomona aeruginosa* had mass reductions of up to 5-10%.

## 4. CONCLUSIONS

Microbial biodegradation of low-density polyethylene was evaluated in Santa Clara in an air lift type bioreactor and the results were 1% and 2% for low density polyethylene (LDPE) type A and B samples with *Pseudomona aeruginosa* bacteria under controlled thermal conditions.

For the low density polyethylene (LDPE) type A and B sample with *Aspergillus brasilensis* fungus are 5% and 7% respectively at controlled thermal conditions. The thermal condition favorable for microorganisms to degrade the low density polyethylene (LDPE) efficiently is 22.1°C since a degradation of 7% was obtained for the sample of low density polyethylene (LDPE) type B with *Aspergillus brasilensis*.

The chemical conditions necessary for the microorganisms to degrade the low density polyethylene (LDPE) efficiently were pH and dissolved oxygen (OD), being the most efficient pH value for biodegradation 7.14 in 7 days of duration of the process and the most efficient dissolved oxygen (OD) value is 7.45mg/L for the sample 2 type B with *Aspergillus brasilensis*.

## REFERENCES

- Alvarado, K., Esenarro, D., Rodriguez, C., & Vasquez, W.** (2020). Lemna minor influence in the treatment of organic pollution of the industrial effluents. *3C Tecnología. Glosas de innovación aplicadas a la pyme*, 9(3), 77-97. <https://www.3ciencias.com/wp-content/uploads/2020/09/art-4-3c-tecno-ed.-35-vol.-9-n.-3-1.pdf>
- Catto, A. L., Montagna, L. S., Almeida, S. H., Silveira, R. M. B., & Santana, R. M. C.** (2016). Wood plastic composites weathering: Effects of compatibilization on biodegradation in soil and fungal decay. *International Biodeterioration & Biodegradation*, 109, 11-22. <https://doi.org/10.1016/j.ibiod.2015.12.026>
- Córdova, A., Amaya, P., Esenarro, D., & Rodriguez, C.** (2020). Vegetable Contamination by Heavy Metal Contained in Effluents from Wastewater Plant in the Totorá Community, Ayacucho –Peru. *Journal of Green Engineering*, 10(7), 3484–3497. <http://www.jgenng.com/volume10-issue7.php>

- Giacomucci, L., Raddadi, N., Soccio, M., Lotti, N., & Fava, F.** (2019). Polyvinyl chloride biodegradation by *Pseudomonas citronellolis* and *Bacillus flexus*. *New Biotechnology*, 52, 35-41. <https://doi.org/10.1016/j.nbt.2019.04.005>
- Hung, C.-S., Barlow, D. E., Varaljay, V. A., Drake, C. A., Crouch, A. L., Russell, J. N., Nadeau, L. J., Crookes-Goodson, W. J., & Biffinger, J. C.** (2019). The biodegradation of polyester and polyester polyurethane coatings using *Papiliotrema laurentii*. *International Biodeterioration & Biodegradation*, 139, 34-43. <https://doi.org/10.1016/j.ibiod.2019.02.002>
- Inforegión.** (2015, January 25). *El 46% de los residuos sólidos en playas del Perú son plásticos*. <http://www.inforegion.pe/196519/el-46-de-los-residuos-solidos-en-playas-del-peru-son-plasticos/>
- Janczak, K., Hryniewicz, K., Znajewska, Z., & Dąbrowska, G.** (2019). Use of rhizosphere microorganisms in the biodegradation of PLA and PET polymers in compost soil. *International Biodeterioration & Biodegradation*, 130, 65-75. <https://doi.org/10.1016/j.ibiod.2018.03.017>
- Novotný, C., Erbanová, P., Sezimová, H., Malachová, K., Rybková, Z., Malinová, L., Prokopová, I., & Brožek, J.** (2015). Biodegradation of aromatic-aliphatic copolyesters and polyesteramides by esterase activity-producing microorganisms. *International Biodeterioration & Biodegradation*, 97, 25-30. <https://doi.org/10.1016/j.ibiod.2014.10.010>
- Paço, A., Duarte, K., da Costa, J. P., Santos, P. S. M., Pereira, R., Pereira, M. E., Freitas, A. C., Duarte, A. C., & Rocha-Santos, T. A. P.** (2017). Biodegradation of polyethylene microplastics by the marine fungus *Zalerion maritimum*. *Science of The Total Environment*, 586, 10-15. <https://doi.org/10.1016/j.scitotenv.2017.02.017>
- Perpetuo, E. A., da Silva, E. C. N., Karolski, B., & Oller, C. A.** (2020). Biodegradation of diethyl-phthalate (DEP) by halotolerant bacteria isolated from an estuarine PERPETUO, environment. *Biodegradation*. <https://doi.org/10.1007/s10532-020-09913-y>

- Sadhukhan, J., Martinez-Hernandez, E., Amezcua-Allieri, M. A., Aburto, & Honorato, J. A.** (2019). Economic and environmental impact evaluation of various biomass feedstock for bioethanol production and correlations to lignocellulosic composition. *Bioresource Technology Reports*, 7, 100230. <https://doi.org/10.1016/j.biteb.2019.100230>
- Soto, M.** (2016, June 3). *Contaminación por plástico es nuevo reto ambiental del país*. Diario La Nación. [http://www.nacion.com/vivir/ambiente/Contaminacion-plastico-nuevo-ambiental-pais\\_0\\_1564643544.html](http://www.nacion.com/vivir/ambiente/Contaminacion-plastico-nuevo-ambiental-pais_0_1564643544.html)





